Aspects of neutrino mass models in the light of recent oscillation data

Thesis submitted to the
University of Calcutta
for the degree of Doctor of Philosophy (Science)

by

Soumita Pramanick

Department of Physics
University of Calcutta

2017

– To the journey of life –

Acknowledgements

I find this section extremely hard to write as I feel I can never complete writing this. Neither the list of people to be thanked can be completed nor their contributions in my life can be acknowledged in words. No matter how vividly I express my gratitude towards them I must admit I really do not have words to acknowledge their contribution and support. "Thank you" really is too small a word. Whatever I say will only be a fraction of my gratefulness.

It is a bright summer afternoon in May 2017, when I am writing this note and some M.Sc students busy in cheerful chat drags my attention in the University corridor. It seems just like yesterday when I entered this department after completing my B.Sc in Physics (Honours) from Scottish Church College, Kolkata. To be a part of this highly esteemed department of C.V. Raman, Meghnad Saha, Satyendranath Bose happened to be a dream since childhood and with the M.Sc admission a journey of close association with the department started. All my teachers from the department had been extremely student friendly in their interactions, always keen to help us in issues be it academic or administrative. Days went by and a beautiful bond resulted between the teachers and the student and unknowingly this place gradually became a home away from home and the department became an academic family. After successful completion of M.Sc examination it was a time to get parted from this integral part of my existence. I can vividly recollect the memory of the last M.Sc lecture in particle physics specialization course when a feeling of sadness prevailed in my heart as a very dear association with the Physics department of Rajabazar Science College (that is what we call informally the University of Calcutta, Rajabazar Campus where the Department of Physics is located) was about to end. I am immensely thankful to all my teachers including Dr. Sudipta Bandyopadhyay, Prof. Abhijit Bhattacharyya, Prof. Subinay Dasgupta, Dr. Anindya Datta, Prof. Gautam Gangopadhyay, Prof. Debnarayan Jana, Prof. Anirban Kundu, Prof. Indrajit Mitra, Dr. Jayashree Saha, Prof. Parongama Sen and Dr. Jayalakshmi Shamanna for their kind support and guidance in moments of need from the bottom of my heart.

Then came another chance of getting associated with the department as a Ph.D. student of Prof. Amitava Raychaudhuri and work in particle physics when a new journey started. Working with Prof. Raychaudhuri was like a dream come true. He has not only taught me about the physics research problem but also has inspired me as a human being. I am thankful to Prof. Raychaudhuri from the core of my heart for making me cognizant of various branches of particle physics including neutrinos. It was the educative discussions with him that has developed my interests in diverse fields of particle physics research. I owe all my research activities in particle physics now and in future to the interest in this fascinating branch of physics that Prof. Raychaudhuri introduced me to through his discussions and guidance. His valuable advice has guided me to handle several administrative issues from time to time during the research. He has encouraged me to attend several schools and workshops in India and abroad. His extreme patience, inspiration and

mental support throughout was very conducive to research. Altogether it had been fantastic learning experience. My heartfelt gratitude to Prof. Raychaudhuri for his kind support and wonderful guidance. No matter what I write, it will always remain insufficient to convey my regards and deep respect for Prof. Raychaudhuri.

The academic bond with the department strengthened more during my Ph.D. research. I am indebted to the other particle physics research group members − Prof. Amitava Datta, Dr. Anindya Datta and Prof. Anirban Kundu for their discussions and help in matters academic and administrative. I wish to thank specially Dr. Sudipta Bandyopadhyay and Prof. Subinay Dasgupta for checking my office so as to ensure I am safe during my stays in University working till late in the evenings. My colleagues, the other Ph.D. students of the department, had been extremely friendly in their interactions making this period very memorable. Apart from being a constant source of inspirations, they have gifted me several moments of happiness to be cherished throughout my life. I wish to express my sincere regards to Prof. Gautam Bhattacharyya of the Saha Institute of Nuclear Physics, India. I am also thankful to the non-teaching staff of the department who had always been ready to help in administrative matters with a smile on their face.

On the domestic front, my journey till date had been completely a result of someone working very hard behind the scenes, my mother. My father had been a constant source of inspiration for me. I wish to thank my sister, friends and family for their help and support to handle various practical situations.

I wish to thank everyone I mentioned here for bestowing on me the wealth of good memories.

This entire research was funded by CSIR (NET) Junior Research Fellowship later on upgraded to CSIR (NET) Senior Research Fellowship for which I wish to acknowledge the financial support under Sanction No. 09/028(0890)/2012-EMR-I of Council of Scientific and Industrial Research (CSIR), Government of India.

Department of Physics,
University of Calcutta, India.

Soumita Pramanick
May 2017.

Abstract

Neutrinos are massive and they oscillate. The three-neutrino oscillation paradigm is characterized by the three mixing angles $(\theta_{12}, \theta_{13}, \theta_{23})$; two mass square splittings $(\Delta m^2_{solar}, \Delta m^2_{atmos})$ and one complex phase (δ) responsible for CP violation. It is noteworthy that $\Delta m^2_{solar}/\Delta m^2_{atmos} \sim 10^{-2}$. Earlier the experimental observations were roughly consistent with popular lepton mixing patterns like the Tribimaximal (TBM), Bimaximal (BM) and Golden Ratio (GR) mixing as they give $\theta_{13} = 0$ and maximal mixing in the atmospheric sector $(\theta_{23} = \pi/4)$ by construction. In 2012 short-baseline reactor anti-neutrino experiments observed non-zero θ_{13} which is small compared to the other two mixing angles i.e., $\theta_{13} \sim 9^\circ$. A running theme of my research work is to consider a two-component Lagrangian, one of which is dominant and the other one smaller. The dominant constituent offers any of the popular lepton mixings or a scenario where all the mixing angles are either 0 or maximal $(\pi/4)$ to start with accompanied by $\Delta m^2_{solar} = 0$, while the sub-dominant component amends the dominant part so as to generate non-zero θ_{13} and Δm^2_{solar} and brings the other mixing angles in concord with the experimental data while predicting the CP violation phase δ.

We began with an introduction which reviews the essentials of neutrino properties and the Standard Model that were used throughout the thesis. Then we have analysed the two-component scenario in the context of different mixing patterns in a model independent fashion. Next we examined the possibility that the sub-dominant contribution could originate from a Type I seesaw mechanism. The theories result in interesting interrelationships between different oscillation parameters making it testable. In particular, the CP phase δ, octant of θ_{23}, ordering of neutrino masses and the lightest neutrino mass get correlated.

We have also explored the possibility of such models arising from discrete flavour symmetries such as $A4$ and $S3$. We have identified the quantum numbers of the leptons such that the Type II seesaw mechanism gives rise to the dominant part of the neutrino mass matrix while the smaller Type I seesaw contribution attributes corrections which bring the mixing angles and masses into the measured range. The Lagrangian includes all terms allowed by the symmetries and no soft symmetry breaking term is introduced. Symmetries are broken spontaneously. The models predict the octant of θ_{23} as well as the effective mass for neutrinoless double beta decay in terms of the lightest neutrino mass and are therefore testable. It was inferred that normal ordering is always associated with the first octant of θ_{23} whereas the second octant with inverted ordering. The models have rich scalar sectors which are carefully studied in terms of the local minimization of the scalar potential and the necessary conditions specific to them are obtained.

Aspects of neutrino mass models in the light of recent oscillation data

Soumita Pramanick

Department of Physics, University of Calcutta

Abstract

Three-neutrino oscillations are characterised by the mixing angles $(\theta_{12}, \theta_{13}, \theta_{23})$, mass square splittings $(\Delta m^2_{solar}, \Delta m^2_{atmos})$ and a Dirac CP phase (δ). Experiments indicate that $\Delta m^2_{solar}/|\Delta m^2_{atmos}| \sim 10^{-2}$. Prior to the observation of $\theta_{13} \neq 0$ in 2012, lepton mixings of the Tribimaximal, Bimaximal, and Golden Ratio forms were constructed with $\theta_{13} = 0$ and $\theta_{23} = \pi/4$. Their sharp contrast with the experimental observations accentuates the necessity of amendment. A two-component formalism is the motif of the thesis. The dominant contribution corresponded to $\Delta m^2_{solar} = 0$ along with any of the popular mixings or NSM (no solar mixing i.e., $\theta_{23} = \pi/4$, $\theta_{13}, \theta_{12} = 0$). The sub-dominant constituent nudged these parameters into the observed range. Predictions for the CP phase δ were obtained.

Preceded by an overview of neutrino physics and the Standard Model in Chapter 1, in Chapter 2 a model independent realization of the strategy for the four mixings is presented. In Chapter 3 viability of the scheme was explored for NSM with the dominant and sub-dominant contributions generated by Type II and Type I seesaw respectively. In Chapters 4 and 5, we employed discrete flavour symmetries $A4$ and $S3$ to yield the mass matrices conducive to our scheme. All four mixings were considered in Chapter 5. Our endeavours were restricted to only the NSM case in Chapter 4. The octant of θ_{23}, δ and $|m_{\nu_e\nu_e}|$ were predicted in terms of the lightest neutrino mass thereby interrelating them. In all the cases, the first octant of θ_{23} got associated with normal ordering, the second octant with inverted ordering. Both models had opulent scalar content studied to the extent of local minimization of scalar potential. Symmetries were broken spontaneously to render *vev* to the scalars leading to lepton masses. No soft symmetry breaking was allowed. The models have several testable predictions.

Contents

List of Figures

List of Tables

Chapter 1

Introduction

Neutrinos are one of the most fascinating entities of the particle kingdom. These chargeless spin $\frac{1}{2}$ fermions were first proposed by Wolfgang Pauli [1] in 1930 to explain the missing energy of beta decay. Neutrinos are the second most abundant particles in the universe but are extremely feebly interacting and therefore very hard to detect. They interact only through weak interactions. Clyde Cowan and Frederick Reines [2] jointly reported the first detection of the anti-neutrinos (the antiparticles of neutrinos) in 1956 for which Reines was awarded Nobel Prize in 1995. The elusive neutrinos can serve as ideal messengers for transporting information from distant cosmic sources such as supernovae. They may play a pivotal role in the evolution of the early universe, in particular in generating the dominance of matter over antimatter by providing a source of lepton number violation as well as CP violation.

Another interesting property of the neutrino is its surprisingly tiny mass (it could be about 500000 times lighter than the electron). This along with neutrino oscillations circumscribes the periphery of my thesis. This chapter comprises of a detailed discussion of neutrino oscillation (Sec. 1.1.1) and its interrelationship with the neutrino masses which is indispensable for oscillations to occur. This is succeeded by a general discussion (Sec. 1.2) of the Standard Model (SM) in the context of its signature mass generating principle thereby identifying the limitations which forbid it from providing masses to the neutrinos. Thus the experimental observation of neutrino oscillation was one of the pioneering evidences of physics Beyond the Standard Model (BSM). In Sec. 1.3 some BSM scenarios for neutrino mass generation technically known as the seesaw mechanism will be discussed. Finally, having discussed in detail the inducements that propelled my doctoral research, we will conclude this chapter by presenting a schematic layout of the thesis in Sec. 1.4.

1.1 Nuances of Neutrinos

Neutrinos occur in three flavour eigenstates (ν_e, ν_μ, ν_τ) named after the charged lepton counterparts (e^-, μ^-, τ^-) whose left-handed component constitute doublets of $SU(2)_L$ along with left-handed neutrinos[1] of the same flavour. These flavour eigenstates (ν_α where $\alpha \equiv e, \mu, \tau$) participate in weak interactions and are therefore also often termed as the weak basis in which the neutrino mass matrix is not necessarily diagonal. Thus it is worth defining the mass eigenstates (ν_i, $i = 1, 2, 3$), a basis in which the neutrino mass matrix is diagonal that is different from the weak eigenstates. The weak basis and the mass basis of the neutrinos are connected by a unitary basis transformation matrix (U_ν),

$$|\nu_\alpha\rangle = \sum_{i=1}^{N} (U_\nu)_{\alpha i} |\nu_i\rangle. \tag{1.1}$$

where N is the number of generic species of light neutrinos taking part in weak interactions[2]. Similarly one can define a flavour basis for the charged leptons (l_β, $\beta = e^-, \mu^-, \tau^-$) in which the charged lepton mass matrix is not diagonal and a mass basis (l_j, $j = 1, 2, 3$) for the same designated by a diagonal charged lepton mass matrix. If the unitary basis transformation matrix relating these two bases for the charged leptons be U_l then one can define the unitary lepton mixing matrix called the Pontecorvo Maki Nakagawa Sakata (PMNS) [3] matrix[3] (U_{PMNS}) as:

$$U_{PMNS} = U_l^\dagger U_\nu. \tag{1.2}$$

Now if we can choose a basis for writing down the mass matrices such that the charged lepton mass matrix is diagonal in that basis then it is crucial to note that the lepton mixing matrix for that case is given by:

$$U_{PMNS} = U_\nu \quad \text{for} \quad U_l = \mathbb{I} \tag{1.3}$$

simply[4]. Neutrinos are capable of oscillating from one flavour eigenstate to another by virtue of their mass in course of their propagation from one point to the other by a purely quantum mechanical phenomenon known as neutrino oscillation (to be discussed in detail in the following sections) which in its turn dictates the U_{PMNS}.

For an $N \times N$ unitary matrix, there are $N(N-1)/2$ angles and $N(N+1)/2$ phases among which $(2N-1)$ phases can be absorbed by appropriate re-phasing of the

[1] Needless to mention that the SM is an $SU(3)_C \times SU(2)_L \times U_1(Y)$ theory that will be discussed in detail in Sec. 1.2.

[2] From $Z^0 \longrightarrow$ *invisible* decay width it is well known that $N = 3$.

[3] This can be thought to be an analogue of the Cabibbo Kobayashi Maskawa (CKM) mixing matrix in the quark sector.

[4] In all the chapters of my thesis except Chapter 5 this choice of the flavour basis has been adopted in which the charged lepton mass matrix is diagonal and the entire mixing resides in the neutrino sector. In Chapter 5 we performed our analysis in the mass basis of the neutrinos and the entire mixing was generated by the charged leptons.

left-handed Dirac fields. Thus $(N-1)(N-2)/2$ physical phases remain, which are responsible for CP violation. Needless to point out that CP violation can therefore occur only if the number of generations for the neutrinos $N \geq 3$. Thus for a simple case of 2 flavour oscillation, CP violation cannot take place. If the neutrinos are of Majorana nature[5], then the phases associated with them cannot be absorbed by re-phasing. Only N phases associated with the left-handed charged lepton Dirac fields can be re-phased and absorbed and $N(N-1)/2$ physical phases persist among which $(N-1)(N-2)/2$ are the usual Dirac phases whereas the $N-1$ phases are of Majorana kind. Thus for a three-flavour oscillation ($N = 3$) there are three mixing angles (namely $\theta_{12}, \theta_{13}, \theta_{23}$) and one Dirac phase ($\delta$) responsible for CP violation and a couple of Majorana phases. Neutrino oscillations are immune from the effects of Majorana phases and the latter are therefore of no consequences for our discussion henceforth.

1.1.1 Neutrino Oscillations

Pontecorvo coined the concept of neutrino oscillation based on a two-level quantum mechanical system [4] in 1957. For a quantum mechanical two-level system characterized by the stationary state $|\Psi_n\rangle$ with energy eigenvalue E_n, the time evolved ket after a time t i.e., $|\Psi_n(t)\rangle$ is given by[6]

$$|\Psi_n(t)\rangle = e^{-iE_n t}|\Psi_n(0)\rangle. \tag{1.4}$$

Thus the stationary state will continue to be an eigenstate of the Hamiltonian after the time t with just a phase modification. But in case of a non-stationary state (for example, some arbitrary superposition of the stationary states $|\Psi_1\rangle$ and $|\Psi_2\rangle$ with eigenvalues E_1 and E_2 respectively), it is evident that the probability of remaining in the initial state after time evolution will instead be an oscillatory function of time having frequency $(E_2 - E_1)$.

One can immediately map this knowledge to neutrinos by identifying the neutrino flavour eigenstates $|\nu_\alpha\rangle$ (non-stationary states) as a linear combination of the mass eigenstates $|\nu_i\rangle$ with $(U_\nu)_{\alpha i}$ as the co-efficients of the linear expansion as implied by Eq. (1.1) to fetch an explanation to the phenomenon of neutrino oscillations. In other words, the probability a neutrino flavour eigenstate $|\nu_\alpha\rangle$ to be in the same flavour eigenstate will also oscillate with time. If a neutrino flavour eigenstate $|\nu_\alpha\rangle$ is produced at $x, t = 0$ by a source, then after time t it will evolve in accordance to

$$|\nu_\alpha(t)\rangle = \sum_{i=1}^{N} U_{\alpha i}|\nu_i(t)\rangle = \sum_{i=1}^{N}(U_\nu)_{\alpha i}e^{-iE_i t}|\nu_i(0)\rangle, \tag{1.5}$$

and will travel as a superposition of the mass eigenstates $|\nu_i\rangle$. The probability of a neutrino flavour eigenstate $|\nu_\alpha\rangle$ to migrate into another flavour eigenstate $|\nu_\beta\rangle$

[5]A property yet to be confirmed by neutrinoless double beta decay ($0\nu2\beta$) experiments.
[6]Throughout the thesis we will be using natural units, $\hbar = c = 1$.

after time t in which it travels a distance $L(=t)$ in vacuum[7], i.e., precisely the neutrino oscillation probability[8], is given by

$$P_{\nu_\alpha\nu_\beta} = |\langle\nu_\beta|\nu_\alpha(t)\rangle|^2 = |\sum_{i=1}^{N}\sum_{j=1}^{N}(U_\nu)_{\alpha i}(U_\nu^*)_{\beta j}\langle\nu_j|\nu_i(t)\rangle|^2\,. \tag{1.6}$$

In the ultra-relativistic regime for tiny masses of the neutrinos we can approximate $p_i \simeq p_j \equiv p \simeq E$ and $E_i = \sqrt{p_i^2 + m_i^2} \simeq p + \frac{m_i^2}{2E}$ where m_i and E_i are the mass and energy of $|\nu_i\rangle$. Using this and the orthogonality of the mass eigenstates we get

$$\begin{aligned} P_{\nu_\alpha\nu_\beta} = \delta_{\alpha\beta} \quad &- \quad 4\sum_{i<j}^{N}\mathrm{Re}[(U_\nu)_{\alpha i}(U_\nu)_{\beta j}(U_\nu^*)_{\beta i}(U_\nu^*)_{\alpha j}]\sin^2\chi_{ij}^{osc} \\ &+ \quad 2\sum_{i<j}^{N}\mathrm{Im}[(U_\nu)_{\alpha i}(U_\nu)_{\beta j}(U_\nu^*)_{\beta i}(U_\nu^*)_{\alpha j}]\sin 2\chi_{ij}^{osc}\,, \end{aligned} \tag{1.7}$$

where

$$\chi_{ij}^{osc} = \frac{(m_i^2 - m_j^2)L}{4E} = 1.27\,\frac{\Delta m_{ij}^2}{\mathrm{eV}^2}\,\frac{L/E}{m/\mathrm{MeV}}\,. \tag{1.8}$$

The oscillation wave-length is given by

$$L_{ij}^{osc} = \frac{4\pi E}{\Delta m_{ij}^2} \;\simeq\; 2.48\;m\,\frac{E\,(\mathrm{MeV})}{\Delta m_{ij}^2\,(\mathrm{eV}^2)} =\; 2.48\;km\,\frac{E\,(\mathrm{GeV})}{\Delta m_{ij}^2\,(\mathrm{eV}^2)} \tag{1.9}$$

It is imperative to note from Eq. (1.7) that for neutrino oscillations to take place, the mass square splittings, $\Delta m_{ij}^2 \equiv m_i^2 - m_j^2$ have to be non-vanishing. Thus the experimental observation of neutrino oscillation tells us that at least there should be a non-zero mass difference between two neutrino mass eigenstates i.e., at least one of the $|\nu_i\rangle$ must be massive. Thus the observation of neutrino oscillation asserted the massive nature of the neutrinos[9]. At this point it is also worth accounting that neutrino oscillation is insensitive to the absolute neutrino mass scale and its measurement can only render information about the mass square splittings. For the three-flavour oscillation there are two such mass square splittings namely the solar splitting, $\Delta m_{solar}^2 \equiv m_2^2 - m_1^2$ and the atmospheric splitting $\Delta m_{atmos}^2 \equiv m_3^2 - m_2^2$. These two mass square splittings along with the three mixing angles $(\theta_{12}, \theta_{13}, \theta_{23})$ and one Dirac CP phase (δ) constitute the spectrum of three-neutrino oscillation.

Let us now in the following section decipher Eq. (1.7) in terms of the mixing angles for a simple toy model of two generations and later on extend it for the three flavour oscillations.

[7]The effects of matter on neutrino oscillation will be discussed in Sec. 1.1.1.C.

[8]For anti-neutrinos the U_ν are to be replaced by U_ν^* and vice versa.

[9]According to the SM neutrinos are devoid of masses (detailed discussion appears in Sec. 1.2). Thus the discovery of neutrino oscillation was the first low energy signature of departure from SM for which Takaaki Kajita and Arthur B. McDonald were awarded the Nobel Prize in 2015.

1.1.1.A Two-flavour oscillations

For a two-flavour oscillation, the neutrino mixing matrix U_ν is a 2×2 matrix delineated by a single[10] mixing angle θ (say) expressed[11] as:

$$U_\nu = \begin{pmatrix} \cos\theta & \sin\theta \\ -\sin\theta & \cos\theta \end{pmatrix} \tag{1.10}$$

A single mass square splitting Δm^2 prevails. Using the form of U_ν featured in Eq. (1.10) in Eq. (1.7) we get:

$$P_{\nu_\alpha \nu_\beta} = \sin^2 2\theta \ \sin^2\left(1.27\Delta m^2 \frac{L}{E}\right), \tag{1.11}$$

and

$$P_{\nu_\alpha \nu_\beta} = 1 - \sin^2 2\theta \ \sin^2\left(1.27\Delta m^2 \frac{L}{E}\right). \tag{1.12}$$

Here the mass square splitting Δm^2 is in eV^2, the distance traversed by the neutrino L is in m (km) and its energy E in MeV (GeV). The oscillation amplitude and frequency are dictated by θ and Δm^2 respectively. Thus to probe a particular Δm^2, the experimental set up has to be devised with $E/L \approx \Delta m^2$ i.e, $L \sim L^{osc}$.

As already mentioned, the above discussion is a warm-up exercise for the three generation case to be explored in the next section.

1.1.1.B Three-flavour oscillations

Since the active light neutrinos occur in three flavours, the study of three-generation oscillation is of paramount importance and this discussion will constitute one of the cardinal quoin on which my thesis is based.

From the closing remarks of Secs. 1.1 and 1.1.1 we have already gained cognizance of the fact that the three-neutrino oscillation paradigm is characterised by the three mixing angles $(\theta_{12}, \theta_{13}, \theta_{23})$, one Dirac CP phase (δ) and the two independent mass square splittings viz. $\Delta m^2_{solar} \equiv m_2^2 - m_1^2$ and $\Delta m^2_{atmos} \equiv m_3^2 - m_2^2$. The solar mixing angle is given by θ_{12}, θ_{23} is the atmospheric mixing angle. As we will see later from Eq. (1.16), all the three mixing angles have to be non-vanishing for CP violation to take place[12]. The splitting $\Delta m^2_{solar} \equiv m_2^2 - m_1^2 = \Delta m^2_{21}$ is responsible for solar neutrino oscillation and is observed to be positive ($\sim 10^{-5}\text{eV}^2$) ensuring $m_2 > m_1$. The atmospheric splitting ($\sim 10^{-3}\text{eV}^2$) is larger i.e., $|\Delta m^2_{31}| \cong |\Delta m^2_{32}| \gg \Delta m^2_{21}$. The sign of the atmospheric splitting is not yet known. For Normal Ordering (NO), $\Delta m^2_{atmos} > 0$ i.e., $m_3 > m_2 > m_1$ whereas $\Delta m^2_{atmos} < 0$ for Inverted Ordering (IO) of neutrino masses[13] i.e., $m_2 > m_1 > m_3$.

[10] Recall, an $N \times N$ unitary matrix is characterised by $N(N-1)/2$ angles.

[11] For two-flavour oscillations CP violation is prohibited.

[12] Thus the experimental observation of non-zero θ_{13} in 2012 paved the way for CP violation.

[13] Note if $\tilde{m}^\pm \equiv m_3 \pm m_1$, then $\tilde{m}^- > 0$ (< 0) for NO (IO). We will come across something similar while discussing our endeavours integrated to compose this thesis from the next chapter.

The neutrino mixing matrix U_ν can be contemplated as a combination of three successive Eulerian rotations in 3 dimensions in the 1-2 plane followed by that in the 1-3 and 2-3 planes for which the rotation[14] matrices are given by R_{12}, V_{13} and R_{23}.

$$U_\nu = R_{23} V_{13} R_{12}, \tag{1.13}$$

where

$$R_{12} = \begin{pmatrix} c_{12} & s_{12} & 0 \\ -s_{12} & c_{12} & 0 \\ 0 & 0 & 1 \end{pmatrix}, V_{13} = \begin{pmatrix} c_{13} & 0 & s_{13}e^{-i\delta} \\ 0 & 1 & 0 \\ -s_{13}e^{i\delta} & 0 & c_{13} \end{pmatrix},$$

$$R_{23} = \begin{pmatrix} 1 & 0 & 0 \\ 0 & c_{23} & s_{23} \\ 0 & -s_{23} & c_{23} \end{pmatrix}. \tag{1.14}$$

Here $c_{ij} \equiv \cos\theta_{ij}$ and $s_{ij} \equiv \sin\theta_{ij}$ and θ_{ij} is the $i-j$ rotation angle. The neutrino mixing matrix[15] so obtained is given by:

$$\begin{aligned} U_\nu &= \begin{pmatrix} c_{12}c_{13} & s_{12}c_{13} & s_{13}e^{-i\delta} \\ -s_{12}c_{23} - c_{12}s_{23}s_{13}e^{i\delta} & c_{12}c_{23} - s_{12}s_{23}s_{13}e^{i\delta} & s_{23}c_{13} \\ s_{12}s_{23} - c_{12}c_{23}s_{13}e^{i\delta} & -c_{12}s_{23} - s_{12}c_{23}s_{13}e^{i\delta} & c_{23}c_{13} \end{pmatrix} \\ &= U_{PMNS} \text{ if } U_l = \mathbb{I}. \end{aligned} \tag{1.15}$$

The three-neutrino oscillation probability is given by Eq. (1.7). It is useful to note that the CP phase δ is always associated with[16] s_{13}. A basis-independent measure of CP violation is given by the leptonic Jarlskog(J) parameter [5]:

$$J = Im[(U_\nu)_{e1}(U_\nu)_{\mu 2}(U_\nu^*)_{e2}(U_\nu^*)_{\mu 1}] = \frac{1}{8}\cos\theta_{13}\,\sin 2\theta_{13}\,\sin 2\theta_{23}\,\sin 2\theta_{12}\,\sin\delta. \tag{1.16}$$

If CP is conserved $J = 0$. Thus it can be be immediately inferred that CP violation transpires if all the mixing angles as well as δ is non-zero.

So far we have discussed the neutrino oscillations in vacuum. Although neutrinos interact weakly with the particles in the medium it still has an impact on its oscillatory behaviour to be surveyed in the succeeding segment.

1.1.1.C Matter effects

Neutrinos while traversing through a medium interact with the medium components through weak interactions that has consequential influences on its oscillation

[14]There is nothing sacred about combining the rotation matrices in this particular order. They can of course be combined in a different order yielding the neutrino mixing matrices of some other form that can be mapped to the U_ν in Eq. (1.15) by a unitary transformation. But neutrino physicists all over the world conventionally follow the standard parametrization of defining U_ν as expressed in Eq. (1.15) that we will also endorse.

[15]By convention the PMNS mixing matrix (U_{PMNS}) is defined with the mixing angles varying between $0 \leq \theta_{ij} \leq \frac{\pi}{2}$ whereas for the CP phase $0 \leq \delta \leq 2\pi$.

[16]If CP is conserved then the oscillation probabilities for neutrinos and anti-neutrinos are identical. Thus roughly speaking the difference between the oscillation probabilities of the neutrinos and anti-neutrinos could provide a measure of CP violation in the lepton sector.

properties. Among these weak interactions (mediated by $W^{\pm}$ and Z^0)[17] some coherent forward elastic scatterings of the neutrinos with the matter particles take place, the amplitude for which is not flavour democratic. This is because ordinary matter does not contains μ^-, τ^- but has e^- with which ν_e can interact through CC interactions (left panel of Fig. 1.1) but $\nu_{\mu,\tau}$ cannot. This gives rise to a flavour dependence for the CC processes whereas the NC processes contribute equally for all the three flavours as can be seen from the right panel of Fig. 1.1 and hence are not relevant for oscillation studies. The CC interactions of ν_e with e^- produces an additional contribution for the ν_e which is absent for $\nu_{\mu,\tau}$ that tweaks the oscillation probability. The necessary tinkering has to be done with an additional matter potential of the following form

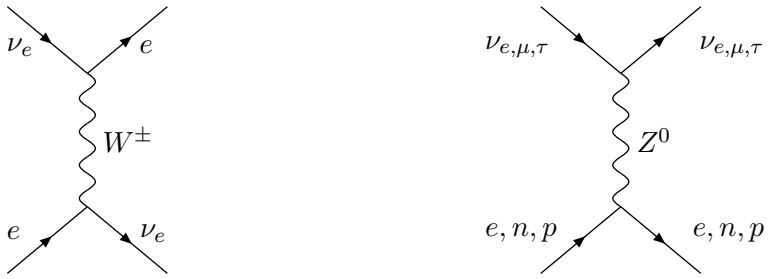

Figure 1.1: Feynman diagrams for CC (NC) interactions of the neutrinos are shown in left (right) panel.

$$V_{eff} = \sqrt{2} G_F N_e \simeq 7.6 Y_e \frac{\rho_{\text{matter}}}{10^{14} \text{g/cm}^3} \text{eV}\,, \tag{1.17}$$

where G_F and ρ_{matter} are the Fermi constant[18] and the matter density of the medium respectively. The relative number density $Y_e \equiv \frac{N_e}{N_p + N_n}$ where N_e, N_p, N_n are the number densities of electron, proton, neutron in the interacting matter.

The Schrödinger equation governing the time evolution of a neutrino flavour eigenstate undergoing matter effects in the two-flavour oscillation scenario is proffered below:

$$i\frac{\partial}{\partial t}\begin{pmatrix}\nu_e \\ \nu_x\end{pmatrix} = \left[C'\mathbb{I} + \frac{\Delta m^2}{p}\begin{pmatrix}-\cos 2\theta & \sin 2\theta \\ \sin 2\theta & \cos 2\theta\end{pmatrix} + \begin{pmatrix}V_{eff} & 0 \\ 0 & 0\end{pmatrix}\right]\begin{pmatrix}\nu_e \\ \nu_x\end{pmatrix}, \tag{1.18}$$

where p, E are the momentum and energy of the neutrino and θ is the mixing angle defined in Eq. (1.10). Here $\nu_x \equiv \nu_\mu$ or ν_τ. Using Eqs. (1.17) and (1.18) one can define:

$$\tilde{A} = \pm A \quad \text{where} \quad A = \frac{2\sqrt{2} E G_F N_e}{\Delta m^2}. \tag{1.19}$$

The positive and negative sign of $\tilde{A}$ in Eq. (1.19) corresponds to neutrinos and antineutrinos respectively. Also the dependence of the sgn(A) on Δm^2, i.e., the mass

[17]The Z^0 boson mediates the neutral current (NC) interactions while charge current (CC) interactions take place by exchange of $W^{\pm}$.

[18]The Fermi constant is related to the weak coupling g by $\frac{G_F}{\sqrt{2}} = \frac{g^2}{8 M_W^2}$ where M_W is the mass of $W^{\pm}$.

ordering, is of far reaching consequence as we will see later. For constant matter density just a simple diagonalisation of the Hamiltonian could yield the results. The two-level case as already pointed out in the vacuum oscillation discussion is completely characterized by a mixing angle (θ) and a mass square splitting (Δm^2) that are modified in presence of matter as:

$$\begin{aligned} (\Delta m^2)^{\text{matter}} &= X\ (\Delta m^2), \\ \sin 2\theta^{\text{matter}} &= \sin 2\theta / X \ \text{ and} \\ \cos 2\theta^{\text{matter}} &= (\cos 2\theta - \tilde{A})/X. \end{aligned} \tag{1.20}$$

where

$$\begin{aligned} X &= \sqrt{(\cos 2\theta - A)^2 + \sin^2 2\theta} \ \text{ for } \ \text{neutrinos}, \\ &= \sqrt{(\cos 2\theta + A)^2 + \sin^2 2\theta} \ \text{ for } \ \text{anti} - \text{neutrinos}. \end{aligned} \tag{1.21}$$

Thus one can immediately conclude that interaction of neutrinos and anti-neutrinos with matter are different. If we study atmospheric neutrino oscillation then the neutrino mass ordering dictates whether $P_{\nu_\mu\nu_\tau} > P_{\bar{\nu}_\mu\bar{\nu}_\tau}$ or $P_{\bar{\nu}_\mu\bar{\nu}_\tau} > P_{\nu_\mu\nu_\tau}$ which in its turn can be exploited to unravel the neutrino mass ordering[19]. Precisely from Eq. (1.21) we can say, if $P_{\nu_\mu\nu_\tau} > P_{\bar{\nu}_\mu\bar{\nu}_\tau}$ then $A > 0$ which implies neutrino masses are ordered in the inverted fashion whereas normally ordered neutrino mass spectrum would lead to $A < 0$ causing $P_{\bar{\nu}_\mu\bar{\nu}_\tau} > P_{\nu_\mu\nu_\tau}$.

In 2002, an experiment was proposed in India, namely the India-Based Neutrino Observatory (INO), to measure the up-down asymmetry for atmospheric neutrinos and anti-neutrinos separately and extract the $P_{\nu_\mu\nu_\tau}$ and $P_{\bar{\nu}_\mu\bar{\nu}_\tau}$ and compare them to specify the neutrino mass ordering. To distinguish between the ν_μ and $\bar{\nu}_\mu$ INO will search for the μ^- and μ^+ coming from processes like:

$$\begin{aligned} \nu_\mu + X &\rightarrow \mu^- + Y \\ \bar{\nu}_\mu + X &\rightarrow \mu^+ + Y' \end{aligned} \tag{1.22}$$

Needless to mention that detection of μ^+ will indicate incoming $\bar{\nu}_\mu$ whereas ν_μ is associated with μ^-. To discriminate between μ^+ and μ^- INO will be using a 50 kt magnetised iron calorimeter (ICAL) functioning with a magnetic field of 1 Tesla for the first time to study atmospheric neutrinos. The charge of the particle can be easily identified in presence of the magnetic field from the curvature direction of their tracks. Thus μ^- and μ^+ and subsequently the associated ν_μ and $\bar{\nu}_\mu$ coming in can be distinguished and the corresponding oscillation probability $P_{\nu_\mu\nu_\tau}$ and $P_{\bar{\nu}_\mu\bar{\nu}_\tau}$ can be measured. This leads to successful determination of neutrino mass ordering[20].

For completeness it is worthy to mention that a resonance can occur when:

$$\Delta m^2 \cos 2\theta = \tilde{A}. \tag{1.23}$$

[19]Recall, from Eq. (1.19) sgn(A)=sgn(Δm^2). A is positive (negative) for NO (IO).

[20]Determination of mass ordering is one of the objectives of INO. Apart from this it is also devised for various other measurements including the CP phase δ [6].

This is the famous MSW resonance[21] effect [7].

Having discussed the mechanism behind the neutrino oscillation both in vacuum and in matter, we will now pay heed to the outcomes of the measurements of this phenomena.

1.1.2 The light of recent oscillation data

Neutrino physics is one of the most dynamic branches of contemporary particle physics research. These mysterious particles are probed by experiments worldwide to procure information about its oscillation parameters including measurement of CP violation (δ) in the lepton sector that might provide an explanation to the matter dominance of the universe over antimatter, to look for indications of lepton number violating BSM physics in $0\nu2\beta$ experiments, etc.[22]. Neutrinos are also used for astrophysical measurements. IceCube Neutrino Observatory located at the South Pole has detected ultra high energy neutrinos ($\sim$PeV), roughly 250 times larger than the energy at which the LHC operates, thereby opening up an alternate avenue for studying high energy events, which although exceedingly interesting is beyond the scope of this thesis. In the following discussion we will restrict ourselves to the neutrino oscillation measurements only.

The current 3σ global fits of the neutrino oscillation parameters as obtained from the NuFIT2.1 of 2016 [8] are:

$$\begin{aligned} \Delta m^2_{21} &= (7.02 - 8.08) \times 10^{-5}\,\mathrm{eV}^2, \;\; \theta_{12} = (31.52 - 36.18)^\circ, \\ |\Delta m^2_{31}| &= (2.351 - 2.618) \times 10^{-3}\,\mathrm{eV}^2, \;\; \theta_{23} = (38.6 - 53.1)^\circ\,, \\ \theta_{13} &= (7.86 - 9.11)^\circ, \;\; \delta = (0 - 360)^\circ \;\; . \end{aligned} \tag{1.24}$$

These neutrino mixing parameters[23] evince certain fascinating features:

1. $\Delta m^2_{solar} \equiv \Delta m^2_{21} = m^2_2 - m^2_1$ and $\Delta m^2_{atmos} \equiv \Delta m^2_{31} = m^2_3 - m^2_1$ differ by two orders of magnitude and it is handy to define $R_{mass} \equiv |\frac{\Delta m^2_{21}}{\Delta m^2_{31}}| \simeq 10^{-2}$.

2. The sign of the atmospheric splitting i.e., $\mathrm{sgn}(\Delta m^2_{31})$ and hence the neutrino mass ordering is yet not known to us.

3. The atmospheric mixing angle θ_{23} which is close to $\frac{\pi}{4}$ can lie in both the octants i.e., whether $\theta_{23} < \frac{\pi}{4}$ (first octant) or $\theta_{23} > \frac{\pi}{4}$ (second octant) remains undetermined.

[21] This was first proposed by L. Wolfenstein and later on applied by S. P. Mikheev and A. Y. Smirnov to observe this effect for the solar neutrinos.

[22] Experimental observation of $0\nu2\beta$ processes will ensure that neutrinos are their own antiparticles (Majorana type), the corresponding mass term for which violates lepton number by 2 units as we will see in Sec. 1.3. There is no such observation yet. Lepton number conservation is an accidental symmetry of the SM and observation of $0\nu2\beta$ will mark evidences of lepton number violating BSM physics.

[23] In Chapter 4 we also use the recent preliminary T2K hints [9] of δ being near -$\pi/2$.

4. The Dirac CP phase δ is not yet a well measured quantity [10, 11].

5. θ_{13} although small compared to the other two mixing angles is non-zero [12], as was observed by the short-baseline reactor anti-neutrino experiments in 2012.

The last in the list i.e., $\theta_{13} \neq 0$ is a comparatively recent result as we can see. Earlier it was not inconsistent with zero and certain popular lepton mixings were fabricated in consonance with $\theta_{13} = 0$ as will be discussed in Sec.1.1.3. Before that let us for completeness have an inventory of the unknowns of the neutrino sector at a glance and the searches going on to unravel them.

1.1.2.A Mysteries that prevail

Despite of intense investigations with proficient experimental set-ups worldwide, the neutrinos continue to allure us with several mysteries in their characteristics as catalogued below:

- The neutrino mass ordering is not ascertained.
- The octant of the atmospheric mixing angle remains unsettled.
- CP phase δ has to be measured.
- The absolute neutrino mass scale has to be determined.
- Whether the neutrinos are Dirac or Majorana particles has to be elucidated.

The first three entries in the list are neutrino oscillation parameters while the rest cannot be obtained by oscillation measurements. Searches for $0\nu2\beta$ can shed light on the Majorana nature of the neutrinos and beta decay end-point spectrum is probed to perceive the absolute neutrino mass scale.

It must also be noted that the SM Higgs boson does not couple to the neutrino to provide them masses[24]. Theorists all over the world are attempting to render an explanation to the origin of neutrino masses that happens to be the prime intent of my doctoral research as well. As will be seen in the following chapters, we have constructed neutrino mass models consistent with the neutrino oscillation parameters already observed and have predictions about the ones yet to be determined[25]. This precisely is the impetus behind the endeavours to be discussed from the next chapter onwards but for the time being let us resume back to the general overview of the subject.

[24]For detail, refer to Sec. 1.2.

[25]In coming days, if the experimental observations about these parameters are found to be in contrast with our model predictions then it can be falsified.

1.1.2.B Searches to unveil

Having gained the acquaintance with the existing puzzles of the neutrino sector, we can now account the proficient experimental pursuits of these parameters conducted across the globe[26]:

1. **Long-Baseline neutrino experiments:** DUNE is the most eminent enterprise in this category. The Deep Underground Neutrino Experiment (DUNE) formerly known as Long-Baseline Neutrino Experiment (LBNE) is the Fermilab international mega-science project. Measurement of CP phase δ, determination of neutrino mass ordering and the octant of θ_{23} are some of the main objectives of the DUNE experiment apart from which it will also search for proton decay and look for the ν_e flux from a core-collapse supernova. Equipped with the supporting infrastructure at Fermilab, DUNE will be supplied with the neutrino beamline from the Long-Baseline Neutrino Facility (LBNF). DUNE is deftly designed with a couple of detectors, one at the Fermi National Accelerator Laboratory in Batavia, Illinois (near detector) and the liquid argon (LAr) far detector at a baseline of 1300 km at the Sanford Underground Research Laboratory in Lead, South Dakota placed more than a kilometre underground. The far detector of fiducial mass 40 kt will be made up of four similar modules, each serving as a liquid argon time-projection chamber (LArTPC). Liquid argon will be used for the first time in a long-baseline neutrino experiment at DUNE which owing to its excellent tracking and calorimetry performance leads to high signal efficiency and effective background discrimination. Further, its excellent reconstruction of the kinematical properties with a high resolution makes it ideal for precise measurement of neutrino events over wide spans of energies. DUNE is expected [13] to be capable of measuring δ up to a precision of 10° to 20° and observing CP violation at 3σ for 67 % values of δ and fathom the neutrino mass ordering up to $\Delta\chi^2 \geq 25$. India is a member of the DUNE collaboration.

   T2K in Japan [10] and Fermilab NOνA [11] are two important ongoing neutrino oscillation experiments of this kind.

2. **Short-Baseline experiments:** Short-baseline anti-neutrino experiments from reactor sources, i.e., Nuclear Power Plants (NPP), measure the survival probability of $\bar{\nu}_e$ at short distances to obtain non-zero θ_{13}. In 2012, Daya Bay [14], a multinational China-based short-baseline experiment, and the RENO [15] (Reactor Experiment for Neutrino Oscillations), located in South Korea, collaborations reported one of the most significant discoveries of contemporary particle physics experiments, namely the non-zero θ_{13} up to 5.2 and 4.9 standard deviations respectively. There are six NPP's operating at 2.9 (2.8 and

[26] We are restricting this discussion to a small sample of the large number of experiments that measure the quantities of immediate interest to us for this thesis. There are several other ongoing and proposed projects searching for diverse aspects of the neutrinos that are uncorrelated to our work and therefore not covered here.

2.66) GW_{th} at Daya Bay (RENO) producing $\bar{\nu}_e$ and detected by eight anti-neutrino detectors, distributed in three groups stretching over a distance of 1.9 km for Daya Bay. RENO has a couple of identical detectors located at 294 m and 1383 m away from the source. Both the experiments use Gadolinium-doped liquid scintillator (Gd-Ls) to identify inverse beta decay i.e., $(\bar{\nu}_e + p \rightarrow e^+ + n)$ as the detection principle.

3. **India-based Neutrino Observatory (INO):** India is embarking on a major neutrino physics programme through the India-based Neutrino Observatory. The flagship experiment will make use of a 50 kt magnetised iron calorimieter (ICAL) for the first time to study atmospheric neutrinos [6]. The main objectives of the experiment are to determine the neutrino mass ordering by studying matter effects[27] and the CP phase (δ).

4. $0\nu2\beta$ **experiments:** $0\nu2\beta$ searches are capable of constraining the effective Majorana neutrino mass and therefore is a riveting branch of neutrino physics worth examining. Lepton number preserving two-neutrino double beta decay (DBD) is allowed by the SM that emits two e^- and two $\bar{\nu}_e$. For $(0\nu2\beta)$ processes lepton number is not conserved and emission of two e^- would take take place sharing the total transition energy. This would lead to a peak in the sum energy spectrum of the two e^-. For the two-neutrino DBD the phase space is smaller compared to that in the $0\nu2\beta$ processes which are however suppressed due to the smallness of the Majorana neutrino mass. Nonetheless, the latter has emerged to be a conducive tool for probing the lepton number violating processes. In fact, this reaction rate is proportional to the square of the effective neutrino mass ($|m_{\nu_e\nu_e}|$) and thus very hard to measure. It is also directly affected by the uncertainties in nuclear matrix element determination. Various dexterous experiments are devised for the search of $(0\nu2\beta)$ among which we discuss CUORE and GERDA here. A detailed account of the present status of such searches can be found in [16].

   The Cryogenic Underground Observatory for Rare Events (CUORE) is at its constructional last phase. Housed at the Gran Sasso Underground Laboratory at a depth of 3400 m.w.e. (meters water equivalent), CUORE [17] will hunt for $(0\nu2\beta)$ using cryogenic bolometers[28] functioning at 10 mK. This temperature is particularly favourable owing to the reduction of the heat capacity of the crystal at this temperature leading to efficient detectability of minute energy depositions from temperature fluctuations that can be yielded by $(0\nu2\beta)$ processes. CUORE made a preliminary search for $(0\nu2\beta)$ with a single string called CUORE-0 that could determine $T_{\frac{1}{2}} > 4.0 \times 10^{24}$ years in TeO_2 with an exposure of 9.8 Kg.year. In future it will attempt to improve it to the extent of 3.5×10^{26} years with reduced background.

   The GERmanium Detector Array (GERDA) uses a new technique of installing an array of 86% enriched HPGe detectors directly in the liquid argon

[27] Some more detail can be found in Sec. 1.1.1.C.

[28] Each bolometer is a $5 \times 5 \times 5$ cm^3 crystal of natural TeO_2. These will be arranged in 19 towers each comprising of 52 crystals containing 200 Kg of ^{130}Te.

(LAr) cryogen that shields external γ rays and supplies the necessary cooling [18]. It started taking data from 2011 and sets $T_{\frac{1}{2}} > 2.1 \times 10^{25}$ years limit for ^{76}Ge with an exposure of 21.6 Kg.year. This combined with the previous experiments puts the best present limit of $T_{\frac{1}{2}} > 3.0 \times 10^{25}$ years.

5. **KATRIN experiment:** The KArlsruhe TRItium Neutrino (KATRIN) experiment at Tritium Laboratory Karlsruhe is designed to measure the absolute neutrino mass scale in a model-independent fashion by measuring the kinematics of electrons coming from beta-decay with ultra-high precision. In order to do so, it employs an adroit high resolution spectrometer, Magnetic Adiabatic Collimation combined with an Electrostatic Filter (MAC-E filter), having 10 m diameter for accurate measurements of the electron energy coming from a Tritium source [19]. Earlier experiments were able to impose an upper bound on the $\bar{\nu}_e$ of about 2.3 eV, whereas KATRIN is expected to measure it by one more order of accuracy.

6. **IceCube/ PINGU experiment:** Located at the South Pole, the IceCube detector was designed to detect the Cherenkov light produced by the interacting neutrinos originating from high energy cosmic rays ($\sim$ PeV) using 1km^3 of transparent Antarctic ice. This unique gigantic ice detector comprises of 5160 optical sensors or digital optical modules (DOM) placed 1.5 km below the geographical South Pole. They are distributed on 86 vertical cables (each holding 60 DOMs) called strings, out of which 78 are placed horizontally 125 m apart in grids of equilateral triangles that form a hexagonal array stretching across a square kilometer of area while the rest of them are more densely organized to constitute the *Deep Core*. Each DOM contains PMT (25 cm long) along with data-acquisition and control electronics. In addition to this 324 DOMs constitute the surface detector called IceTop. After extensive data collection and analysis for three years (2010 - 2013), IceCube detected 37 ultra high energy events.

   Although IceCube was primarily devised and deployed for measurement of very high energy astrophysical neutrinos ($\sim$ PeV), the detector had been made capable of observing low energy neutrinos (10 GeV$\leq E \leq$ 100 GeV), specifically the energy range probed for atmospheric neutrino oscillation studies, by increasing the density of the photodetectors in the ice as well as the efficiency of the PMTs. Thus it is now proficient to measure atmospheric neutrino oscillation parameters like θ_{23} and Δm^2_{32} with efficiency comparable to any other ongoing experiments. As reported in [20], an oscillation analysis conducted with 5174 track-like events measured in 953 days, and binning of data so obtained in logarithm of reconstructed energy ranging between 6 and 56 GeV revealed none of the mass orderings is preferred when θ_{23} and Δm^2_{32} were obtained using binned maximum likelihood technique. For normal ordering $\sin^2\theta_{23} = 0.53^{+0.09}_{-0.12}$ and $\Delta m^2_{32} = 2.72^{+0.19}_{-0.20} \times 10^{-3}\text{eV}^2$ were achieved whereas for inverted ordering the results were $\sin^2\theta_{23} = 0.51^{+0.09}_{-0.11}$ and $\Delta m^2_{32} = -2.72^{+0.18}_{-0.21} \times 10^{-3}\text{eV}^2$. Enhancement in the event reconstruction precision and also the neutrino event number can be procured by increasing

the density of photodetectors in the *Deep Core* volume. Keeping this in mind, the Precision IceCube Next Generation Upgrade (PINGU) has been proposed to achieve better statistics and more precision on the contours of atmospheric neutrino oscillation parameter so as to unravel the neutrino mass ordering upto 3σ after assembling four years of data. Improvisations in the *Deep Core* design is made by reducing the DOM-to-DOM distance from 7 m to 3 m, intensifying the string-to-string spacing from between 40 and 70 m to 22 m and enhancing the number of DOMs per string from 50 to 96 thereby making the detector sensitive to low energy events (≤ 10 GeV).

In the following section the popular lepton mixings will be sketched.

1.1.3 Popular lepton mixings

Let us recall, $\theta_{13} \neq 0$ is a recent observation of 2012. Earlier this mixing angle was consistent with zero. Also from Eq. (1.24), one can readily discern $\theta_{23} = \frac{\pi}{4}$ is allowed by the 3σ data. Prior to the discovery of non-zero θ_{13}, the practice of constructing popular lepton mixings in concurrence with $\theta_{13} = 0$ and $\theta_{23} = \frac{\pi}{4}$ and contriving neutrino mass models that can successfully fit in those mixing structures were in vogue. The PMNS mixing matrix in Eq. (1.15) can be trivially engineered with $\theta_{13} = 0$ and $\theta_{23} = \frac{\pi}{4}$ to obtain a general form for the popular lepton mixings:

$$U^0 = \begin{pmatrix} \cos\theta_{12}^0 & \sin\theta_{12}^0 & 0 \\ -\frac{\sin\theta_{12}^0}{\sqrt{2}} & \frac{\cos\theta_{12}^0}{\sqrt{2}} & \frac{1}{\sqrt{2}} \\ \frac{\sin\theta_{12}^0}{\sqrt{2}} & -\frac{\cos\theta_{12}^0}{\sqrt{2}} & \frac{1}{\sqrt{2}} \end{pmatrix}. \tag{1.25}$$

Tuning the θ_{12}^0 in Eq. (1.25) gives rise to different variants of the popular lepton mixings viz. Tribimaximal [21], Bimaximal [22], Golden Ratio [23] and no solar mixing[29] as shown in Table 1.1.

Mixing name	Tribimaximal	Bimaximal	Golden Ratio	No Solar Mixing
Abbreviation	TBM	BM	GR	NSM
θ_{12}^0	35.3°	45.0°	31.7°	0.0°

Table 1.1: θ_{12}^0 for different popular lepton mixing scenarios.

Hence,

$$U^0 = \begin{pmatrix} \sqrt{\frac{2}{3}} & \sqrt{\frac{1}{3}} & 0 \\ -\sqrt{\frac{1}{6}} & \sqrt{\frac{1}{3}} & \sqrt{\frac{1}{2}} \\ \sqrt{\frac{1}{6}} & -\sqrt{\frac{1}{3}} & \sqrt{\frac{1}{2}} \end{pmatrix} \quad \text{for TBM}, \tag{1.26}$$

[29]The no solar mixing (NSM) was first proposed by us in [24].

$$U^0 = \begin{pmatrix} \sqrt{\frac{1}{2}} & \sqrt{\frac{1}{2}} & 0 \\ -\frac{1}{2} & \frac{1}{2} & \sqrt{\frac{1}{2}} \\ \frac{1}{2} & -\frac{1}{2} & \sqrt{\frac{1}{2}} \end{pmatrix} \quad \text{for BM,} \tag{1.27}$$

$$U^0 = \begin{pmatrix} \sqrt{\frac{\phi}{\sqrt{5}}} & \sqrt{\frac{1}{\sqrt{5}\phi}} & 0 \\ -\frac{1}{\sqrt{2}}\sqrt{\frac{1}{\sqrt{5}\phi}} & \frac{1}{\sqrt{2}}\sqrt{\frac{\phi}{\sqrt{5}}} & \sqrt{\frac{1}{2}} \\ \frac{1}{\sqrt{2}}\sqrt{\frac{1}{\sqrt{5}\phi}} & -\frac{1}{\sqrt{2}}\sqrt{\frac{\phi}{\sqrt{5}}} & \sqrt{\frac{1}{2}} \end{pmatrix} \quad \text{for GR with } \phi = (1+\sqrt{5})/2 \tag{1.28}$$

$$U^0 = \begin{pmatrix} 1 & 0 & 0 \\ 0 & \sqrt{\frac{1}{2}} & \sqrt{\frac{1}{2}} \\ 0 & -\sqrt{\frac{1}{2}} & \sqrt{\frac{1}{2}} \end{pmatrix} \quad \text{for NSM.} \tag{1.29}$$

It is apparent that post non-zero θ_{13} discovery none of the popular lepton mixings accord with the neutrino oscillation data and the necessity of an amendment can be easily comprehended[30]. The neutrino mass models that we will construct will ameliorate this issue for the popular lepton mixings.

In the next section the salient features of the SM are highlighted in the context of the thesis.

1.2 The Standard Model and Neutrinos

The celebrated Standard Model of particle physics is an $SU(3)_C \times SU(2)_L \times U(1)_Y$ theory broken down spontaneously to $SU(3)_C \times U(1)_Q$ by the Higgs mechanism. In this segment we will briefly recollect the essentials implemented in our work. A complete discussion of the Standard Model can be found in any standard particle physics textbook [25]. If g and g' be the couplings for the $SU(2)_L$ and $U(1)_Y$ respectively then the weak mixing angle or the Weinberg angle is given by:

$$\tan\theta_w = \frac{g'}{g}. \tag{1.30}$$

The SM particle content is shown in Table 1.2. It is worth noting that unlike the neutrinos the charged leptons and quarks have both left- and right-handed fields present within the particle spectrum of the SM model. This is of immense consequence as we will see soon. With the fields in hand the charge current (CC) interaction of the neutrinos mediated by the $W^{\pm}$ boson, already discussed in Sec. 1.1.1.C can be interpreted as:

$$-\mathscr{L}_{CC} = \frac{g}{\sqrt{2}} \sum_{\alpha} \bar{\nu}_{L\alpha} \gamma^{\mu} l^{-}_{L\alpha} W^{+}_{\mu} + h.c. \tag{1.31}$$

[30]The solar mixing angle $\theta_{12} = 33.72^{\circ}{}^{+0.79}_{-0.76}$ at 1σ. Thus θ_{12} for each of TBM, BM, GR, and, needless to say, NSM lie outside this range.

Fields	Notations	$SU(2)_L$	Y
Left-handed leptons	$(L_\alpha)_L \equiv \begin{pmatrix} \nu_\alpha \\ l_\alpha^- \end{pmatrix}_L$	2	-1
Right-handed leptons	$(l_\alpha^-)_R$	1	-2
Left-handed quarks	$(q_\alpha)_L \equiv \begin{pmatrix} u_\alpha \\ d_\alpha \end{pmatrix}_L$	2	1/3
Right-handed quarks	$(u_\alpha)_R$	1	4/3
	$(d_\alpha)_R$	1	-2/3
Scalar Higgs Boson	$\Phi \equiv \begin{pmatrix} \phi^+ \\ \phi^0 \end{pmatrix}$	2	+1

Table 1.2: The SM particle content. Only the first generation of fermions is shown, $\alpha = 1, 2, 3$ for the three generations. The last in the list is a the scalar Higgs doublet of $SU(2)_L$ whereas the rest are fermions. Lepton number $L = 1$ for the leptons and 0 otherwise. The electromagnetic charge $Q = T_3 + \frac{Y}{2}$. For upper (lower) members of the $SU(2)_L$ doublets T_3 is $\frac{1}{2}$ (-$\frac{1}{2}$) whereas it is 0 for singlets of $SU(2)_L$. Thus for $SU(2)_L$ singlets, $Q = \frac{Y}{2}$ simply. Under $SU(3)_C$ quarks are triplets and leptons are singlets. The gauge bosons are not mentioned in the list here.

Similarly the Z^0 mediated neutral (NC) interaction of the neutrinos is given by:

$$-\mathscr{L}_{NC} = \frac{g}{2\cos\theta_w} \sum_\alpha \bar{\nu}_{L\alpha} \gamma^\mu \nu_{L\alpha} Z^0_\mu. \tag{1.32}$$

In order to give masses to the gauge bosons in the SM, spontaneous symmetry breaking (SSB) through the Higgs mechanism has to be invoked[31] that we will discuss in Sec. 1.2. The corresponding terms in the Lagrangian are given by

$$\mathscr{L}_{Higgs} = (D_\mu \Phi)^\dagger (D^\mu \Phi) - V(\Phi). \tag{1.33}$$

We will discuss the potential in detail in Sec. 1.2. The covariant derivative in the kinetic term of the Lagrangian is expressed as:

$$D_\mu \Phi = \left(\partial_\mu + ig \sum_{a=1}^{3} T_a W_\mu^a + ig' \frac{Y}{2} B_\mu \right) \Phi, \tag{1.34}$$

[31] Alternate arguments about the existence of the Higgs doublet in the SM from unitarity using $2 \to 2$ scattering of the W boson like $W^+W^- \to W^+W^-$ are also available in literature [26].

where $T_a = \frac{\sigma_a}{2}$ (σ_a being the Pauli matrices) are the generators of $SU(2)_L$ and Y is the hypercharge. Using Eqs. (1.33) and (1.34) one can compute the gauge boson masses to be

$$M_W = \frac{1}{2}gv \quad \text{and} \quad M_Z = \frac{1}{2}\sqrt{g^2 + g'^2} \quad v, \tag{1.35}$$

where v is the vacuum expectation value[32] (vev) of Φ. This leads to the famous "ρ" parameter:

$$\rho = \frac{M_W}{M_Z \cos\theta_w}. \tag{1.36}$$

For a doublet of $SU(2)_L$ this $\rho = 1$. Introduction of other scalar multiplets can lead to departure from unity[33].

Having provided masses to the gauge bosons, we consider the lepton number conserving Dirac mass term[34] for the fermions:

$$\mathscr{L}_{mass} = -m(\bar{\psi}_L\psi_R + \bar{\psi}_R\psi_L). \tag{1.37}$$

Note that this term as it stands is not gauge invariant. This issue is also addressed by the Higgs field[35]. Since right-handed neutrinos are not present in SM, such a mass term cannot be written for them. As a result the neutrinos are massless within the SM framework.

In terms of the scalar Higgs doublet Φ, we can write down the Yukawa terms as:

$$\mathscr{L}_{Yukawa} = -y^\alpha(\bar{L}_{\alpha L}\Phi l_{\alpha R} + \bar{l}_{\alpha R}\Phi^\dagger L_{\alpha L}). \tag{1.38}$$

After SSB, one can readily identify the mass of the charged lepton as

$$m^\alpha = \frac{y^\alpha v}{\sqrt{2}}. \tag{1.39}$$

Similar mass terms can be written for the quarks. Note that since $U(1)_Q$ is conserved, only the neutral scalar can acquire vev. Because of the T_3 and Y assignments the Φ can give mass only to the down-type quarks and for the up-type quarks one has to use $\tilde{\Phi} = i\sigma_2\Phi^*$ for that purpose. Although our models are confined to the lepton sector only, it is worth commenting here that the mass matrices for the quarks so obtained in general, may not be diagonal. The diagonalization of the up and down-type mass matrices can be separately performed by deploying unitary matrices. A combination of these diagonalizing matrices is defined as the Cabibbo Kobayashi Maskawa (CKM) mixing matrix for the quarks.

[32] After spontaneous symmetry breaking the scalar acquires its vev given by $\langle\Phi\rangle = \frac{v}{\sqrt{2}}$ described in Sec. 1.2.1.

[33] $\rho = \frac{M_W}{M_Z \cos\theta_w} = 1$ is a consequence of a *custodial symmetry* [27].

[34] Recall, $\psi = \psi_L + \psi_R$ and $\psi_{L,R} = P_{L,R}\psi$, where the projection operators are given by $P_{R,L} = \frac{(1\pm\gamma_5)}{2}$.

[35] The gauge boson masses are protected by the gauge symmetry and the fermion masses are protected by the chiral symmetry.

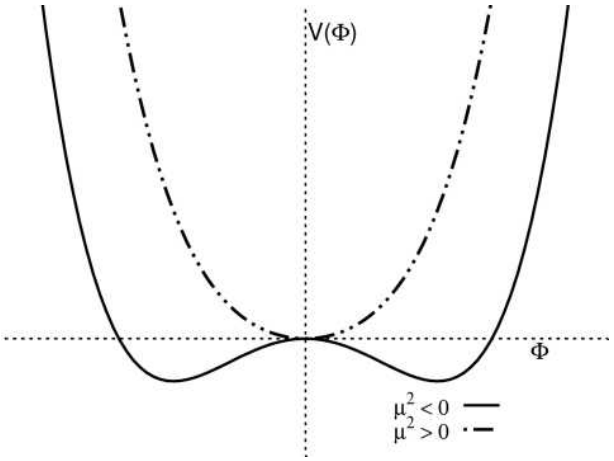

Figure 1.2: Functional behaviour of $V(\Phi)$. Solid curve is for $\mu^2 < 0$, dot-dashed curve is for $\mu^2 > 0$. In case of $\mu^2 < 0$ spontaneous symmetry breaking occurs.

1.2.1 Sponatneous Symmetry Breaking for one scalar doublet

If a Lagrangian conserves a certain symmetry but the vacuum breaks it [28], then spontaneous symmetry breaking is said to have occurred [29]. Let us consider a symmetry operation generated by τ^b and θ_b be the corresponding parameter. For SSB to take place, the symmetry transformation $e^{-i\tau^b.\theta_b}$ shall not keep the vacuum unchanged i.e.,

$$e^{-i\tau^b.\theta_b}|0\rangle \neq |0\rangle \quad \Rightarrow \quad \tau^b|0\rangle \neq 0 \ \text{ for some } \ b. \tag{1.40}$$

Thus for a system, SSB eventuate if the symmetry transformation conserved by the Lagrangian comprises of at least one generator that does not annihilate the vacuum.

The SM Lagrangian is symmetric under $SU(2)_L \times U(1)_Y$. The scalar potential in Eq. (1.33) containing all the terms allowed by the gauge symmetry is written as:

$$V(\Phi) = \mu^2(\Phi^\dagger\Phi) + \lambda(\Phi^\dagger\Phi)^2 \tag{1.41}$$

λ and μ are the quartic and quadratic couplings respectively[36]. When minimized this leads to[37]

$$\frac{\partial V(\Phi)}{\partial v} = \mu^2 v + \lambda v^3 = 0 \tag{1.42}$$

For the potential to be bounded from below $\lambda > 0$. μ^2 can be both positive or negative.

[36]To keep the potential renormalizable only the terms involving fields with mass dimension up to 4 are included.

[37]For simplicity we are assuming real *vev*.

For $\mu^2 > 0$, $V(\Phi)$ is minimum at $\langle\Phi\rangle = 0$ plotted as the dot-dashed curve in Fig. 1.2. It can be readily inferred from the plot $\langle\Phi\rangle = 0$ is the only minimum of $V(\Phi)$ and for this case the vacuum preserves the original symmetry obeyed by the Lagrangian and hence SSB cannot take place. Since the Lagrangian symmetry is kept intact by the ground state both the complex scalar fields, namely ϕ^+ and ϕ^0 constituting Φ endure degeneracy in their masses.

The $\mu^2 < 0$ case, plotted by the solid line in Fig. 1.2, is devoid of any "true minimum" at $\langle\Phi\rangle = 0$. Alternatively now a continuum of minima is available for $V(\Phi)$ at $|\langle\Phi\rangle| = \frac{v}{\sqrt{2}}$ where $v = \sqrt{\frac{-\mu^2}{\lambda}}$. The degenerate minima can be clearly identified in Fig. 1.2, all of them are equally probable and the system can choose to be in any one of them. Since the ground state does not preserve the symmetry of the original Lagrangian the SSB takes place. The occurrence of the SSB is irrespective of the preference of the system to lie on any point of the circle with radius $\frac{v}{\sqrt{2}}$ in the complex plane spanned by $\mathrm{Re}(\Phi)$ and $\mathrm{Im}(\Phi)$. Let us say, the system chooses $\langle\mathrm{Re}(\phi^0)\rangle = \frac{v}{\sqrt{2}}$ then this can be written as:

$$\Phi = \begin{pmatrix} \phi^+ \\ \phi^0 \end{pmatrix} \quad \longrightarrow \quad \Phi = \begin{pmatrix} \chi^+ \\ \frac{(\phi+v)+i\chi}{\sqrt{2}} \end{pmatrix} \tag{1.43}$$

Here the two real scalar fields χ and ϕ have vanishing *vev*. Using Eqs. (1.41) and (1.43) we obtain the mass of the physical Higgs field (ϕ):

$$m_\phi^2 = 2\lambda v^2. \tag{1.44}$$

The other scalars $\chi^\pm$ and χ are left massless. Thus spontaneous breaking of the Lagrangian symmetry gives rise to massless modes in the theory in accordance to the Goldstone theorem. After SSB, there are three massless Nambu-Goldstone bosons ($\chi^\pm$ and χ) and one massive physical real scalar field (ϕ).

Thus before symmetry breaking there were four massless gauge bosons (three corresponding to $SU(2)_L$ and one for $U(1)_Y$)[38] each having 2 transverse degrees of freedom (dof) contributing[39] $4 \times 2 = 8$ dof and the scalar Φ is composed of two complex scalar fields leading to additional four scalar dof. Thus before SSB there are total 12 dof. After SSB, the $W^\pm$ and Z^0 gains mass (3 dof each, a total 9 dof) while the photon remains massless (2 dof) and there exists only one massive real physical scalar field (ϕ) with 1 dof summing to a total 12 dof. Thus the total dof remains conserved before and after SSB as expected. It is often said that the 3 massless scalar dof were "eaten up" to provide longitudinal components to the $W^\pm$ and Z^0 gauge bosons[40]. On July 4, 2012 both the ATLAS [30] and the CMS [31] collaborations declared the observation of a Higgs-like boson of mass ~ 125GeV marking the triumph of this theory.

[38] $SU(2)_L$ has three generators thus has three gauge bosons whereas $U(1)_Y$ has only 1 generator and therefore one gauge boson.

[39] There are two transverse dof for massless gauge fields whereas for massive ones an additional longitudinal dof is added leading to a total three dof.

[40] After SSB, the Lagrangian in the unitary gauge lacks any term consisting of the Goldstones $\chi^\pm$ and χ, as if the gauge bosons "eat up" the Goldstones to acquire mass.

Here we have studied the Higgs mechanism for one scalar field. The models we have constructed have a rich scalar sector with different transformation properties under $SU(2)_L$ that were studied[41] in the context of local minimization of the scalar potential inclusive of all the gauge invariant terms simultaneously allowed by the additional discrete symmetry under consideration.

Let us now address the problem of providing masses to the neutrino, forbidden within the periphery of the Standard Model, by some alternate mass generating mechanism i.e., the seesaw mechanism.

1.3 Neutrino masses and Seesaw

Within the purview of SM, the neutrino Dirac mass term is forbidden owing to the absence of the right-handed neutrino field (ν_R) while the Majorana mass term is prohibited as as it violates the $(B-L)$ symmetry by 2 units. Thus the SM needs to be extended to bestow tiny masses to the neutrinos.

For Type I seesaw mechanism to be operational, the SM field content has to be appended with right-handed neutrino fields ν_R, singlets under $SU(2)_L \times U(1)_Y$.

Allowing violation of lepton number the relevant Majorana mass term is furnished below:

$$\mathscr{L}_{mass} = \frac{1}{2} \begin{pmatrix} \nu_L^T & (\nu_R^c)^T \end{pmatrix} \begin{pmatrix} 0 & M_D^T \\ M_D & M_R \end{pmatrix} \begin{pmatrix} \nu_L^c \\ \nu_R \end{pmatrix} + h.c. \tag{1.45}$$

where: $\nu_{R,L}^c \equiv (\nu_{L,R})^C = C\bar{\nu}_{L,R}^T$ and

$$M_{D+M} \equiv \begin{pmatrix} 0 & M_D^T \\ M_D & M_R \end{pmatrix}. \tag{1.46}$$

Here m_D and m_R are the mass scales of M_D and M_R respectively. m_R is not protected by electroweak gauge symmetry as ν_R is an electroweak singlet and therefore can be large. Masses of M_D, on the other hand, owing to its origin from the *vev* of Higgs field Φ introduced in Sec. 1.2, is comparable to the electroweak scale. Further, it is assumed that $m_D \ll m_R$. In other words, the greatest eigenvalue of $\sqrt{M_D^\dagger M_D}$ is assumed to be much less than the smallest eigenvalue of $\sqrt{M_R^\dagger M_R}$. Moreover, M_R is assumed to be invertible. Needless to accentuate its symmetric nature.

In order to decouple the heavy and light neutrino fields, a basis transformation is employed leading to:

$$W^T M_{D+M} W = \begin{pmatrix} M_\nu^{light} & 0 \\ 0 & M_\nu^{heavy} \end{pmatrix} \tag{1.47}$$

[41] Additional discrete symmetries were imposed to obtain the neutrino mass matrices of desired form.

and

$$\begin{pmatrix} \nu_L \\ \nu_R^c \end{pmatrix} = W \begin{pmatrix} \nu_{light} \\ \nu_{heavy} \end{pmatrix}. \tag{1.48}$$

The terms of leading order corresponding to the light neutrino mass matrix results into the famous *seesaw formula*

$$M_\nu^{light} = -M_D^T M_R^{-1} M_D. \tag{1.49}$$

The leading terms of the heavy neutrino mass matrix can be used to yield,

$$M_\nu^{heavy} = M_R. \tag{1.50}$$

It must be commented that the corrections to M_ν^{light} and M_ν^{heavy} are suppressed by $(m_D/m_R)^2$. Our discussions so far is confined to the Type I seesaw mechanism. The Type II and Type III seesaw mechanisms are mediated by scalars and fermions transforming as triplets under $SU(2)_L$ respectively.

For the Type II seesaw, the scalar sector of the SM has to be extended with a triplet of $SU(2)_L$ denoted by Δ_L. The lepton number violating mass term for this case used in our model is given by:

$$\mathscr{L}_{\text{mass}} = \frac{1}{2}(y^l \nu_L^T C^{-1} \nu_L \Delta_L) + h.c. \tag{1.51}$$

The *vev* of this triplet scalar Δ_L, given by v_L, is assumed to be very small[42] compared to v. This ensures that the parameter ρ remains close to unity. y^l is the Yukawa coupling and the Majorana mass of the neutrino $m_\nu \propto y^l v_L$. In our work, we have used Type I and Type II seesaw only[43].

So far our discussion was intended to recapitulate some fundamental ideas that we make use of in our analysis. In the next section we deduce the motivations that impelled our explorations and present a glimpse of the latter in a nutshell.

1.4 Modus Operandi of the thesis

Summing up, the highlights of our discussion till now:

- Neutrinos are massive and they oscillate by virtue of their mass.
- The particle content of the SM model is insufficient to provide masses to the neutrinos.

[42] In the literature models can be found where the spirit of the nomenclature *seesaw* is captured by attributing the smallness of the *vev* of this triplet to the largeness of the *vev* of some other scalar in the model.

[43] Type III seesaw is somewhat close to the Type I seesaw scenario in the sense both of them are mediated by fermions but their $SU(2)_L$ behaviour is the discriminating feature between the two viz. singlet for Type I seesaw and triplet for the Type III case. In our work we have not used Type III seesaw, hence will not pursue its description here.

- Alternate BSM mechanisms like the seesaw had to be devised to generate neutrino masses.
- Popular lepton mixings and the neutrino oscillation data are not in harmony with each other and an amendment is necessary.
- Δm^2_{solar} is smaller than Δm^2_{atmos} by two orders of magnitude. Also the mixing angle θ_{13} is smaller than the other two mixing angles θ_{23} and θ_{12}.

This entire package will be addressed in our works. The operational concept behind this enterprise was to construct models for realistic neutrino masses and mixings using a two-component Lagrangian one of the dominant kind, other of the sub-dominant nature. The dominant contribution was characterised by observed values Δm^2_{atmos} and vanishing Δm^2_{solar} in all the cases we have analysed. The mixing in the neutrino sector for this contribution varied from project to project but our choices were limited to the popular lepton mixings viz. TBM, BM, GR or NSM. Needless to mention such a dominant scenario is not in consonance with the experimental observations. The role of the sub-dominant component was to tinker the values of the mass square splittings and mixings so as to concord with the oscillation data.

Guided by the last observation in the list of highlights, in Chapter 2 we did a model independent investigation of the viability of this scheme [24, 32] for the dominant contribution with all the four mixing patters which was specified by $\Delta m^2_{solar} = 0, \;\; \theta_{13} = 0$ and a sub-dominant correction could yield non-zero values of these two oscillation parameters allowed by the data. Being derived from the same source i.e., the sub-dominant contribution, the solar splitting and θ_{13} get interrelated which in its turn put bounds on the parameters comprising this contribution leading to interesting consequences and observable predictions of δ for all the four mixing patterns (Fig. 2.5).

In Chapter 3 we have considered a dominant contribution of NSM kind i.e., in addition to $\Delta m^2_{solar} = 0, \;\; \theta_{13} = 0$, we had $\theta_{12} = 0$ and $\theta_{23} = \frac{\pi}{4}$. Again a sub-dominant contribution was capable of nudging these values of the oscillation paramerters into the ranges allowed by the oscillation observations. The dominant contribution was an outcome of the Type II seesaw mechanism whereas the sub-dominant one was obtained by employing Type I seesaw [33–36].

In order to establish that the mass matrices used in Chapter 3 are not entirely arbitrary but a result of some underlying symmetry of the Lagrangian, in Chapter 4 we imposed the discrete group symmetry $A4$ on it [37]. No soft symmetry breaking was allowed. Symmetry was broken only spontaneously when the scalars acquired their *vev* to give the masses to the charged leptons and the neutrinos. The model could predict octant of θ_{23}, effective mass for $0\nu2\beta$ i.e., $|m_{\nu_e\nu_e}|$ as functions of the lightest neutrino mass (Fig. 4.2) as well as the CP phase δ (Fig. 4.3). The predictions of CP phase δ of our model is in agreement with NOνA observation of δ preference towards $-\frac{\pi}{2}$.

In Chapter 5, the discrete flavour symmetry S_3 was appointed to obtain the mass matrices[44]. The dominant Type II seesaw contribution with vanishing solar splitting was studied for all the four mixing patterns [38]. A Type I seesaw subdominant contribution was capable of providing the necessary corrections to obtain the oscillation parameters in the desired data allowed range. Our model has several testable predictions including the CP phase δ for all the four mixing patterns (Fig. 5.2).

Departure of experimental observations in future from the predictions obtained from our models can rule them out. Thus our models are testable in the light of recent oscillation data. Both the models had rich scalar sectors that were scrutinised to the extent of local minimization in the appendices of Chapters 4, 5.

[44]Here also soft symmetry breaking was prohibited.

Chapter 2

Model independent formalism I

2.1 Introduction

This chapter is based on our works presented in the references [24, 32]. The measurement [15, 39] of a non-zero θ_{13} which is small compared to the other neutrino mixing angles created a stir in the world of particle physics.

The Daya Bay collaboration after 127 days exposure had obtained for θ_{13} [39]

$$\sin^2 2\theta_{13} = 0.089 \pm 0.010\ (\text{stat}) \pm 0.005\ (\text{syst}) \quad (\text{Daya Bay}) \tag{2.1}$$

and from the RENO experiment with 229 days data [40] it had been reported

$$\sin^2 2\theta_{13} = 0.113 \pm 0.013\ (\text{stat}) \pm 0.019\ (\text{syst}) \quad (\text{RENO}) \tag{2.2}$$

The Double Chooz [41], MINOS [42], and T2K [10] experiments also determined $\sin^2 2\theta_{13}$, all consistent with the above but with larger uncertainties[45].

Earlier there already was in place a strong upper bound on this angle [43]. The measured value is close to this limit, leading to θ_{13} getting referred to occasionally as 'large'. Now that in the lepton sector, as for the quarks, all three mixing angles are non-zero the door has been opened for CP violation[46]. Many alternative strategies are being considered to explore leptonic CP violation as well as mixing and the future prospects are rich.

The other face of the neutrino sector is the mass spectrum. Indeed, from the several oscillation studies at accelerators and reactors complementing the solar and atmospheric neutrino measurements the mass splittings are now very well established though the absolute mass remains an unknown. From 1σ global fits the currently favoured values of the neutrino mixing parameters are [44, 45]:

$$\Delta m^2_{21} \;=\; (7.50^{+0.18}_{-0.19}) \times 10^{-5}\,\text{eV}^2, \;\; \theta_{12} = (33.36^{+0.81}_{-0.78})^\circ,$$

[45] For current 3σ global fit value of θ_{13} see Eq. (1.24)

[46] CP violation in the heavy neutrino sector could be the origin of matter-antimatter asymmetry through leptogenesis.

$$
\begin{aligned}
|\Delta m^2_{31}| &= (2.473^{+0.070}_{-0.067}) \times 10^{-3}\,\mathrm{eV}^2,\ \ \theta_{23} = (40.0^{+2.1}_{-1.5} \oplus 50.4 \pm 0.13)^\circ \\
\theta_{13} &= (8.66^{+0.44}_{-0.46})^\circ,\ \ \delta = (300^{+66}_{-138})^\circ\ . \qquad (2.3)
\end{aligned}
$$

Recall that the atmospheric mixing angle, θ_{23}, is no longer consistent with maximal mixing ($\theta_{23} = \pi/4$) at 1σ. There are best fit values in both the first and second octants; determining the θ_{23} octant is one of the priorities of future experiments. In this chapter to simplify the discussion and minimize parameters we will nonetheless take $\theta_{23} = \pi/4$. We comment on the effect of the small departure from maximality on the results. In the global fit θ_{12} is also large but not maximal while θ_{13} is the smallest of the three. Another noteworthy feature here is that the solar splitting is about two orders of magnitude smaller than the atmospheric splitting[47]. Thus it is useful to define $R_{\rm mass} \equiv |\Delta m^2_{21}/\Delta m^2_{31}| = (3.03 \pm 0.16) \times 10^{-2}$.

The non-zero value of θ_{13} close to its upper bound ('large') and yet small compared to the other mixing angles has attracted a great deal of attention from diverse angles. We list a sampling of this body of literature. For example, the role of $\mu - \tau$ symmetry [46], see-saw models [47], charged lepton contributions [48], and renormalization group effects [49] are among the avenues explored. A perturbative approach has been espoused in [50]. Other attempts have been based on diverse discrete symmetries [51, 52].

In this work we seek to address the following question: Is it possible that at some level the small quantities, the ratio $R_{\rm mass}$ and θ_{13}, are vanishing[48] and that a single perturbation induces the observed non-zero values for both? The answer is in the affirmative. To our knowledge, this result was pointed out for the first time through a specific example in [54]. Here, we make an exhaustive analysis and show that the existence (or not) of a viable solution depends on two factors: the ordering of the neutrino masses and the mass of the lightest neutrino, m_0. For normal ordering, for a large choice of parameters the requirements can be met[49]. The perturbation can be real or complex. In the latter case, CP violation is present. The inverted ordering is less favoured if the perturbation is real. In this case one would have to admit significant differences in the sizes of the matrix elements of the perturbation to get satisfactory solutions.

This chapter is structured as follows. In the next section we set up the framework for our discussion. In the following section we elaborate on the degenerate perturbative mechanism which we will adopt. Next we discuss to what extent the global fits of the mixing parameters constrain the choice of the perturbation. Our main results are presented in the following section where we show the allowed ranges of the perturbation matrix for the two mass orderings and the predictions for CP violation. We then briefly indicate how the perturbation can arise from a mass model. We end this chapter with some discussions.

[47] In [44] for inverted ordering a best-fit value of Δm^2_{32} has been given. It is consistent to within 1σ with the best-fit value of $|\Delta m^2_{31}|$ we have cited from their normal ordering fits.

[48] This may arise from a symmetry such as $O(2)$ [53].

[49] An earlier work relating θ_{13} to the solar oscillation parameters which favoured normal mass ordering can be found in [55].

2.2 Neutrino mass and mixing scenarios

We restrict ourselves to the case of three flavours of neutrinos. We also work in a basis where the charged lepton mass matrix is diagonal. In this basis the entire lepton mixing resides in the neutrino mass matrix, see Eq. (1.3).

Our starting point will be the unperturbed Majorana neutrino mass matrix, M^0, which is always symmetric. We choose a form such that the solar splitting is absent; i.e., in the mass basis one has

$$(M^0)^{mass} = diag(m_1^{(0)}, m_1^{(0)}, m_3^{(0)}). \tag{2.4}$$

For a specific mass ordering, the lightest neutrino mass, m_0, determines $m_1^{(0)}$ and $m_3^{(0)}$. As already noted it is useful to define[50] $m^{\pm} = (m_3^{(0)} \pm m_1^{(0)})$. m^- is positive (negative) for normal (inverted) mass ordering.

In the flavour basis the mass matrix becomes:

$$(M^0)^{flavour} = U^0 \begin{pmatrix} m_1^{(0)} & & \\ & m_1^{(0)} & \\ & & m_3^{(0)} \end{pmatrix} U^{0T} , \tag{2.5}$$

where U^0 is the lowest order leptonic mixing matrix. The columns of U^0 are the unperturbed flavour eigenstates. Neutrino mass models lead to predictions for U^0 of which three often-discussed variants are the Tribimaximal, Bimaximal, and the Golden Ratio forms. Each of these imply $\theta_{13} = 0$ and $\theta_{23} = \pi/4$. They differ only in θ_{12}. We will consider them in turn along with a further option where there is no solar mixing to start with.

Our goal is to check whether in each case a perturbation mass matrix, M' (also symmetric), can be identified which will add corrections to M^0 and U^0 leading to mass splittings and mixing angles in agreement with observations, in particular that the correct Δm^2_{21} and θ_{13} are realized.

2.2.1 General parametrization for popular lepton mixings

A vivid analysis about the popular lepton mixings can be found in Sec. 1.1.3. In general as long as $\theta_{13} = 0$ and the atmospheric mixing is maximal ($\theta_{23} = \pi/4$) the leptonic mixing matrix can be parametrized as[51]:

$$U^0 = \begin{pmatrix} b & a & 0 \\ -a/\sqrt{2} & b/\sqrt{2} & \sqrt{\frac{1}{2}} \\ a/\sqrt{2} & -b/\sqrt{2} & \sqrt{\frac{1}{2}} \end{pmatrix}, \tag{2.6}$$

[50] We take $m_i^{(0)}$ $(i = 1, 3)$ to be real and positive. This can be accomplished by a suitable choice of the Majorana phases.

[51] This form has appeared earlier in the literature, e.g. [56].

Mixing parameter	Global fit 1σ		Global fit 3σ		TBM	BM	GR
	a_{min}	a_{max}	a_{min}	a_{max}			
a	0.539	0.561	0.515	0.585	0.577	0.707	0.526

Table 2.1: The limits on the mixing parameter $a \equiv \sin\theta_{12}^0$ as obtained from the global fit. The values of a for the TBM, BM, and GR forms are also shown. For NSM case $a = 0$.

with

$$a^2 + b^2 = 1. \tag{2.7}$$

For the above U^0 the solar mixing angle[52] is given by $\tan\theta_{12}^0 = a/b$. The experimentally determined range of θ_{12} in Eq. (2.3) corresponds to $0.539 \leq a \leq 0.561$ at 1σ. In Table 2.1 we list the allowed range of a from the global fit and its values in the TBM, BM, and the GR models. Finally, we also examine the possibility that the unperturbed mixing matrix has $a = 0$. This would imply one degenerate state decoupled and the other maximally mixed to the third (nondegenerate) state. For this choice $\theta_{12}^0 = 0$. Another case with one decoupled degenerate state is $b = 0$ for which $\theta_{12}^0 = \pi/2$. These cases give identical physics results.

As noted, the unperturbed matrix, M^0, is such that the solar splitting is absent and two eigenvalues are degenerate. Due to this degeneracy the two corresponding eigenstates are non-unique. The perturbation, M', which splits the degeneracy determines the actual eigenstates which will be rotated with respect to the first two columns of U^0 – Eq. (2.6) – by an angle ζ also determined by M'. Therefore, on inclusion of the perturbation we have a resultant solar mixing angle given by $\theta_{12} = \theta_{12}^0 + \zeta$.

2.3 Perturbation Strategy

In this chapter we work in the mass basis unless explicitly mentioned otherwise. Our discussion will involve only first order perturbative corrections. The perturbation M' is a (3×3) symmetric matrix which could be real or complex. These two cases will be treated sequentially. The former provides a good starting point for the latter.

After removing an irrelevant constant part the perturbation, M', can be written as:

$$M' = m^+ \begin{pmatrix} 0 & \gamma & \xi \\ \gamma & \alpha & \eta \\ \xi & \eta & \beta \end{pmatrix} \quad . \tag{2.8}$$

[52]Note that in this chapter we are renaming $\cos\theta_{12}^0$ and $\sin\theta_{12}^0$ as b and a respectively so that the equations look less cumbersome as can be easily read off by comparing Eq. (2.6) with Eq. (1.25).

2.3.1 Real Perturbation

In this case all entries in the matrix M' are real. For perturbation theory to be acceptable the dimensionless entities $\alpha, \beta, \gamma, \xi, \eta$ should be small compared to unity. Taken together with the unperturbed M^0 – Eq. (2.4) – at lowest order the perturbation will induce the solar oscillation parameters through α and γ; θ_{13} will be determined by ξ and η; while β will result in a small correction to $m_3^{(0)}$.

2.3.2 Complex Perturbation

If M' is complex symmetric then it is not hermitian[53]. In such an event one takes the hermitian combination $(M^0 + M')^\dagger(M^0 + M')$ and considers $M^{0\dagger}M^0$ as the unperturbed term and $H' \equiv (M^{0\dagger}M' + M'^\dagger M^0)$ as the lowest order perturbation. The unperturbed eigenvalues will now be $(m_i^{(0)})^2$ and the perturbation matrix with

$$f(\varphi) = m^+ \mathrm{Re}(\varphi) + i\ m^- \mathrm{Im}(\varphi) \ \text{ is given by}$$

$$H' = m^+ \begin{pmatrix} 0 & 2m_1^{(0)}\mathrm{Re}(\gamma) & f^*(\xi) \\ 2m_1^{(0)}\mathrm{Re}(\gamma) & 2m_1^{(0)}\mathrm{Re}(\alpha) & f^*(\eta) \\ f(\xi) & f(\eta) & 2m_3^{(0)}\mathrm{Re}(\beta) \end{pmatrix}. \tag{2.9}$$

The imaginary parts of α, β, and γ do not appear in Eq. (2.9). However, they do contribute at higher order *via* the $M'^\dagger M'$ term.

2.4 Relating elements of M' to the data

We look for solutions which are consistent with the global neutrino parameter fits up to 1σ. In particular, the solar mass splitting and θ_{13} must both emerge from the perturbation. We discuss these aspects now.

2.4.1 The solar mixing angle

Due to the degeneracy, to lowest order, the solar mass splitting is obtained *via* the (2×2) submatrix of the perturbation, M', in the space of the first two generations. For real M' in terms of $r = \gamma/\alpha$ from Eq. (2.8) this submatrix is:

$$M'_{(2\times2)} = m^+\alpha \begin{pmatrix} 0 & r \\ r & 1 \end{pmatrix} \text{ for Real } M' \,. \tag{2.10}$$

If M' is complex then $r = \mathrm{Re}(\gamma)/\mathrm{Re}(\alpha)$ and

$$(M^{0\dagger}M' + M'^\dagger M^0)_{(2\times2)} = 2m^+ m_1^{(0)}\mathrm{Re}(\alpha) \begin{pmatrix} 0 & r \\ r & 1 \end{pmatrix} \text{ for Complex } M' \ . \tag{2.11}$$

[53] M^0 is hermitian by construction.

Parameter	TBM		BM		GR		NSM	
	r_{min}	r_{max}	r_{min}	r_{max}	r_{min}	r_{max}	r_{min}	r_{max}
r $(\times 10^2)$	-4.59	-1.95	-23.1	-19.9	1.54	4.18	108	125

Table 2.2: The range of the off-diagonal entry, $r = \gamma/\alpha$, in the 2×2 submatrix of the perturbation (see Eqs. (2.10, 2.11)) for the TBM, BM, and GR alternatives that produces a θ_{12} consistent with the global fits at 1σ. The NSM alternative is also noted.

If $r = 0$ then M' will produce a mass splitting but will not change the solar mixing. For r non-zero the eigenstates are rotated from those in U^0 through an angle ζ given by

$$\zeta = \frac{1}{2}\tan^{-1}(2r)\ , \tag{2.12}$$

independent of the prefactor of the matrix. As noted, the Tribimaximal, Bimaximal and Golden Ratio mixing models do not satisfy the currently measured value of θ_{12} within 1σ. Therefore for these cases we choose $r \neq 0$ in such a manner that when the mass degeneracy is removed the mixing angle is tweaked to within the allowed range. In Table 2.2 we show the ranges of r for each of the three models that result in θ_{12} values consistent with observations. It is noteworthy that r is small in every case (but for the NSM alternative when it is $\mathcal{O}(1)$). Since it is a ratio of two elements of the perturbation matrix it could, in principle, be $\mathcal{O}(1)$. The smallness can be traced to the fact that as $r \to 0$ the mass matrix in the flavour basis exhibits a $Z_2 \times Z_2$ symmetry[54] of the unperturbed model generated by:

$$U_1 = 1 - 2\begin{pmatrix} a^2 & ab/\sqrt{2} & -ab/\sqrt{2} \\ ab/\sqrt{2} & b^2/2 & -b^2/2 \\ -ab/\sqrt{2} & -b^2/2 & b^2/2 \end{pmatrix} \quad \text{and}$$

$$U_2 = 1 - 2\begin{pmatrix} b^2 & -ab/\sqrt{2} & ab/\sqrt{2} \\ -ab/\sqrt{2} & a^2/2 & -a^2/2 \\ ab/\sqrt{2} & -a^2/2 & a^2/2 \end{pmatrix}\ . \tag{2.13}$$

Before closing this subsection it is worth noting that to lowest order in degenerate perturbation theory the first two eigenstates are:

$$|\psi_1\rangle = \cos\zeta\left[\begin{pmatrix} b \\ -a/\sqrt{2} \\ a/\sqrt{2} \end{pmatrix} - \bar{\xi}\begin{pmatrix} 0 \\ 1/\sqrt{2} \\ 1/\sqrt{2} \end{pmatrix}\right] - \sin\zeta\left[\begin{pmatrix} a \\ b/\sqrt{2} \\ -b/\sqrt{2} \end{pmatrix} - \bar{\eta}\begin{pmatrix} 0 \\ 1/\sqrt{2} \\ 1/\sqrt{2} \end{pmatrix}\right]\ , \tag{2.14}$$

$$|\psi_2\rangle = \sin\zeta\left[\begin{pmatrix} b \\ -a/\sqrt{2} \\ a/\sqrt{2} \end{pmatrix} - \bar{\xi}\begin{pmatrix} 0 \\ 1/\sqrt{2} \\ 1/\sqrt{2} \end{pmatrix}\right] + \cos\zeta\left[\begin{pmatrix} a \\ b/\sqrt{2} \\ -b/\sqrt{2} \end{pmatrix} - \bar{\eta}\begin{pmatrix} 0 \\ 1/\sqrt{2} \\ 1/\sqrt{2} \end{pmatrix}\right]\ , \tag{2.15}$$

[54]This is often a subgroup of a larger symmetry such as $A4$.

with ζ defined in Eq. (2.12) and

$$\bar{\xi} = \left(\frac{m^+}{m^-}\right)\xi, \;\; \bar{\eta} = \left(\frac{m^+}{m^-}\right)\eta \text{ for Real } M', \tag{2.16}$$

and

$$\bar{\xi} = \left(\frac{m^+}{m^-}\right)\text{Re}(\xi)+i\,\text{Im}(\xi), \;\; \bar{\eta} = \left(\frac{m^+}{m^-}\right)\text{Re}(\eta)+i\,\text{Im}(\eta) \text{ for Complex } M' \,. \tag{2.17}$$

2.4.2 The solar mass splitting

The solar mass splitting is determined by the eigenvalues of the submatrix in Eqs. (2.10) and (2.11).

For real M' the first order corrections to the degenerate eigenvalues are:

$$m^{(1)}_{2,1} = m^+ \, \frac{\alpha}{2}\left[1 \pm \sqrt{1+4r^2}\right] \,. \tag{2.18}$$

Identifying the heavier eigenvalue with m_2, as required by the solar data, one has:

$$m_2^2 - m_1^2 = 2m^+ m_1^{(0)} \alpha\sqrt{1+4r^2} \,. \tag{2.19}$$

Up to small perturbative corrections m^+m^- gives the atmospheric mass splitting. Hence:

$$R_{\text{mass}} = |(m_2^2 - m_1^2)/(m_3^2 - m_1^2)| = 2\frac{m_1^{(0)}}{|m^-|}\,\alpha\sqrt{1+4r^2} \,. \tag{2.20}$$

For complex M' the corrections are to the squared masses and one directly obtains Eqs. (2.19) and (2.20) but for the replacement $\alpha \to \text{Re}(\alpha)$.

We will return to this equation when we discuss numerical estimates of the element α.

2.4.3 Generating $\theta_{13} \neq 0$

Using first order degenerate perturbation theory the corrected wave-function $|\psi_3\rangle$ is given by:

$$|\psi_3\rangle = \begin{pmatrix} 0 \\ 1/\sqrt{2} \\ 1/\sqrt{2} \end{pmatrix} + \bar{\xi}^* \begin{pmatrix} b \\ -a/\sqrt{2} \\ a/\sqrt{2} \end{pmatrix} + \bar{\eta}^* \begin{pmatrix} a \\ b/\sqrt{2} \\ -b/\sqrt{2} \end{pmatrix} \,. \tag{2.21}$$

To minimize the number of free parameters we will restrict ourselves to only those perturbations which leave the atmospheric mixing angle θ_{23} fixed at the maximal value[55] of $\pi/4$. This gives the relationship:

$$\left(\frac{\bar{\xi}}{\bar{\eta}}\right)^* = \frac{b}{a} \tag{2.22}$$

[55]We remark about deviations from maximal mixing at the end.

Since a and b are real Eq. (2.22) implies that $\bar{\xi}$ and $\bar{\eta}$ and hence ξ and η have the same phase. Comparing with Eq. (1.15) one then has:

$$\sin\theta_{13}\; e^{-i\delta} = \left[b\;\bar{\xi}^* + a\;\bar{\eta}^*\right] = \frac{\bar{\xi}^*}{b}\;, \tag{2.23}$$

where we have used $(a^2 + b^2) = 1$.

For real M' one has $\delta = 0$. Hence, from Eq. (2.16)

$$\xi = \left(\frac{m^-}{m^+}\right) b \sin\theta_{13}\;. \tag{2.24}$$

In the next section, these formulae will be used to relate M' to the neutrino masses and mixings.

2.5 Results

We now have all the ingredients in place to determine the full perturbation matrix and extract the consequences. Once the neutrino mass ordering is chosen and the lightest neutrino mass, m_0, specified, the unperturbed mass spectrum is fixed. The matrix element α is determined from the solar splitting through Eq. (2.20). The element β makes a small contribution (a few per cent) to the atmospheric neutrino splitting and does not affect the physics at hand and so will not be pursued any further in this section. γ is fixed by the ratio r (see Table 2.2). Finally, ξ and η are determined through Eqs. (2.22) - (2.24). The question to be examined, for each of the popular mixing patterns for both mass ordering options, is for what range of m_0 are these matrix elements of acceptable magnitude as a perturbation?

2.5.1 Real perturbation

First we consider M' real which amounts to $\delta = 0$ and CP conservation. In this case one can determine the dependence of α on m_0 using Eq. (2.20). Since ξ and η are proportional to each other – see Eq. (2.22) – presenting any one of them is adequate. Here we present ξ (which is larger than (equal to) η for the TBM and GR (BM) mixing models) as a function of m_0 as obtained from Eq. (2.24).

Normal mass ordering

The results for normal ordering are in the left panel of Fig. 2.1. α is presented as a function of the lightest neutrino mass m_0. We have shown the case for $r = 0$. We have verified that using the small values of r required to fit the solar mixing angle θ_{12} for the popular models – see Table 2.2 – in Eq. (2.20) causes no perceptible

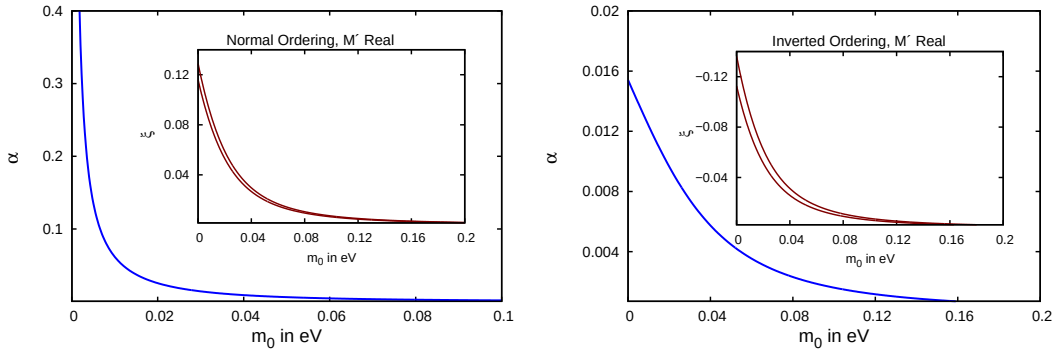

Figure 2.1: α and ξ (inset) as a function of the lightest neutrino mass m_0 for real M'. The left (right) panel is for normal (inverted) mass ordering. In the insets the region between the two curves is allowed when θ_{13} is varied over its 1σ range. The results for ξ ($\propto b$) are for Tribimaximal mixing ($b_{TBM} = \sqrt{\frac{2}{3}} \sim 0.816$). The corresponding plots for Bimaximal ($b_{BM} = \frac{1}{\sqrt{2}} = 0.707$), Golden Ratio mixing ($b_{GR} = \sqrt{\frac{\phi}{\sqrt{5}}} \sim 0.851$), and the NSM case ($b = 1$) can be obtained by scaling.

change[56] in α. r is larger for the NSM case and this effectively reduces α by a factor of around 2. As expected, α diverges as m_0 tends to zero.

In the inset we show ξ as a function of m_0 for the 1σ limits of θ_{13}. In these plots $b = \sqrt{\frac{2}{3}}$ corresponding to Tribimaximal mixing. For the other commonly considered alternatives – Bimaximal ($b = \frac{1}{\sqrt{2}}$) and Golden Ratio ($b = \sqrt{\frac{\phi}{\sqrt{5}}}$) mixing – the ordinate should be scaled appropriately, see Eq. (2.24). For the NSM case one must use $b = 1$.

At this stage one can identify a favoured region of m_0 by requiring that the elements of M' – such as ξ and α – should be of similar order. For this purpose, we plot in Fig. 2.2 the ratio $|\xi/\alpha|$ as a function of m_0 (green solid curves). For easy identification we have shown where this ratio corresponds to the values 3 and $\frac{1}{3}$ (dot-dashed black lines), two limits separated by an order of magnitude. Notice that for normal ordering the ratio is within the above limits only if 2.3×10^{-3} eV $\leq m_0 \leq 3.7 \times 10^{-2}$ eV. If from other experiments a larger value of m_0 is determined then that could be an indication that M' must be complex, as we discuss in the following section. Recall that these curves are for Tribimaximal mixing. For the Bimaximal (Golden Ratio) case the ξ/α curves will be lowered (raised) by about 13.35 % (4.28 %). For the NSM case α is reduced by a factor of about 2 while ξ is enhanced by 25%. As an upshot ξ/α is 2.5 times larger, squeezing allowed m_0 to smaller values.

[56]The corrections are $\mathcal{O}(r^2)$.

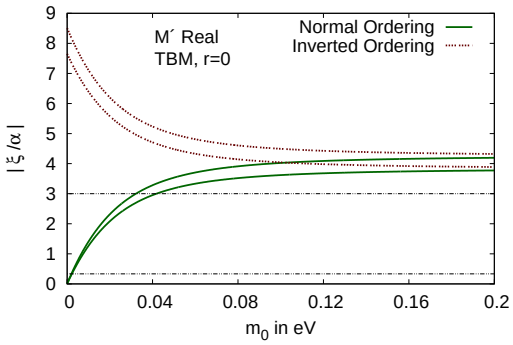

Figure 2.2: The ratio $|\xi/\alpha|$ is plotted as function of the lightest neutrino mass m_0 for both mass orderings when the perturbation M' is real. The area between the two curves of the same type is allowed when θ_{13} is varied over its 1σ range. Also indicated are the values $\frac{1}{3}$ and 3 for $|\xi/\alpha|$ – black dot-dashed lines.

Inverted mass ordering

The results for inverted ordering appear in the right panel of Fig. 2.1. As before, α as a function of m_0 is shown for $r = 0$ while ξ for the 1σ range of θ_{13} is given in the inset. As for normal ordering, inclusion in Eq. (2.20) of the small values of r required to achieve the best-fit θ_{12} in the TBM, BM, and GR models causes essentially no change in α. For the NSM case α is roughly halved. Once again, we have used the TBM value $b = \sqrt{\frac{2}{3}}$ for the calculation of ξ. In this case ξ turns out to be negative. The two curves in the ξ panel correspond to the 1σ limits of θ_{13}.

The noteworthy difference from normal ordering is that α is about an order of magnitude smaller than $|\xi|$ for most of the range of m_0. The brown dotted curves in Fig. 2.2 depict the ratio $|\xi/\alpha|$ for inverted ordering. It is seen that they lie outside the range of 1/3 to 3 for all m_0 considered. Thus the inverted ordering case would be a less favoured alternative for this picture if the perturbation is real.

2.5.2 Complex perturbation

We now turn to the case of complex M'. If perturbation theory is to be meaningful then we should expect the magnitudes of the different dimensionless complex elements of M' to be small compared to unity. Barring fine tuning, they should also be of roughly similar order. Below, we take a conservative stand and set:

$$\alpha = \epsilon \exp(i\phi_\alpha),\ \gamma = \epsilon \exp(i\phi_\gamma),\ \xi = \epsilon \exp(i\phi_\xi). \tag{2.25}$$

The dimensionless quantity ϵ sets the scale of the perturbation. The phases ϕ_α, ϕ_γ and ϕ_ξ are left arbitrary[57].

[57]The magnitude of η is determined through Eq. (2.22). ξ and η have the same phase.

It is seen from Eq. (2.17) that

$$\tan\delta = \tan\phi_{\bar{\xi}} = \left(\frac{m^-}{m^+}\right)\tan\phi_\xi \tag{2.26}$$

where $\phi_{\bar{\xi}}$ is the phase of $\bar{\xi}$.

As we elaborate in the following, the phase freedom still leaves room for some flexibility. In particular, we will mostly focus on those ranges of m_0 which are disfavoured for real M' as they do not satisfy the chosen criterion $3 \geq |\xi/\alpha| \geq 1/3$. We show that such m_0 are accommodated for complex M'.

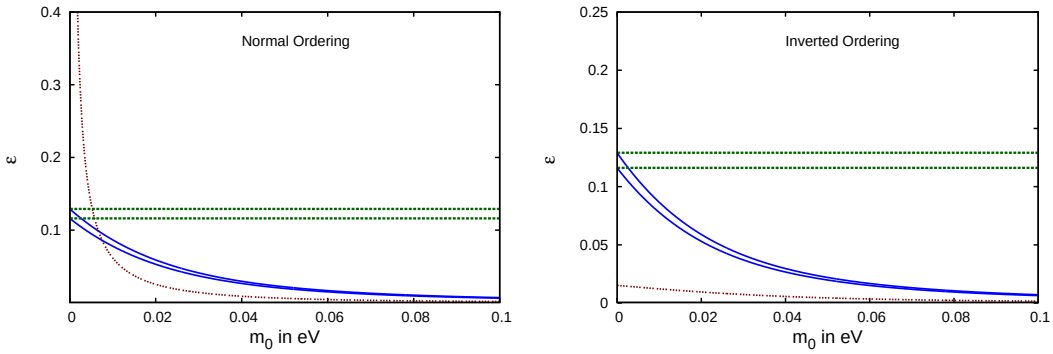

Figure 2.3: The limits on the scale of the perturbation, ϵ, for normal (left panel) and inverted (right panel) mass orderings as a function of the lightest neutrino mass m_0. The upper (lower) limits from Eq. (2.27) for Tribimaximal mixing are the green dashed (blue solid) curves. The region between the curves of the same type correspond to θ_{13} values in the 1σ range. The dotted maroon curves are the lower limits from Eq. (2.28). Here $r = 0$ has been taken.

The choice of ϵ is not entirely arbitrary. In particular, Eq. (2.17) implies:

$$\left|\frac{m^+}{m^-}\right| \epsilon \;\geq\; |\bar{\xi}| \;\geq\; \epsilon \;. \tag{2.27}$$

These limits are presented in the left (right) panel of Fig. 2.3 for the normal (inverted) mass ordering. The upper and lower limits on ϵ are shown as the green dashed and blue solid curves. The two curves of each type show how the limit changes as θ_{13} is allowed to vary over its 1σ range. Tribimaximal mixing has been assumed for these plots.

In addition, from Eq. (2.20) one has

$$\epsilon \geq \left|\frac{m^-}{2m_1^{(0)}\sqrt{1+4r^2}}\right| R_{\rm mass} \;. \tag{2.28}$$

The lower limit from this equation is indicated by the dotted maroon curves in the two panels of Fig. 2.3. This limit is independent of both (a) the choice of θ_{13}

and (b) whether the mixing is of the Tribimaximal, Bimaximal, or Golden Ratio nature. We have checked that the dependence on r is insignificant for the physics calculations. It can be seen from the left (right) panel of Fig. 2.3 that for the normal ordering (inverted ordering) for most values of m_0 (for all values m_0) the lower limit on ϵ from $\bar{\xi}$ is more restrictive. Guided by these results, in the following we choose $\epsilon = 0.1$, 0.05, and 0.025.

Normal mass ordering

From Fig. 2.2 it is seen that for real M' and normal mass ordering $|\xi/\alpha|$ is outside the chosen range for $m_0 \geq 0.04$ eV. If M' is complex, α in Eq. (2.20) is replaced by $\mathrm{Re}(\alpha)$. Demanding that the solar splitting is correctly obtained fixes ϕ_α when ϵ is chosen. The results are shown in the left panel of Fig. 2.4 for $\epsilon = 0.1$, 0.05, and 0.025.

One can conclude from Fig. 2.1 that as m_0 increases $\mathrm{Re}(\alpha)$ approaches zero. This is reflected in Fig. 2.4 (left panel) where ϕ_α tends to $\pi/2$ asymptotically for all choices of ϵ. For a particular ϵ the lightest neutrino mass m_0 has a lower limit set by Eq. (2.27) where the curves have been terminated. The corresponding ϕ_α can be read off from Fig. 2.3 – $\cos\phi_\alpha$ is the ratio of the value of the dot-dashed maroon curve to that of the blue solid curve at this m_0. For these plots we have taken $r = 0$; the small corrections $\mathcal{O}(r^2)$ for the TBM, BM, and GR models are insignificant. In the NSM case $\mathrm{Re}(\alpha)$ is reduced to about half and so ϕ_α tends closer to $\pi/2$. One should bear in mind that we have used the central value of R_{mass} which has a $\pm 5\%$ uncertainty.

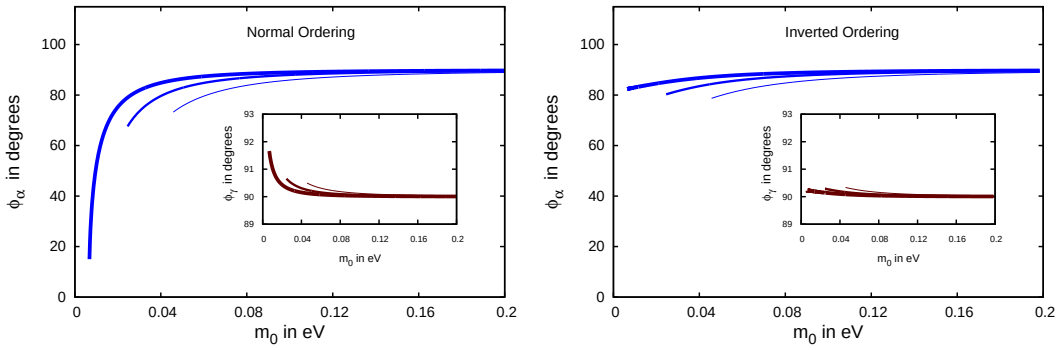

Figure 2.4: ϕ_α (ϕ_γ) for a complex M' is shown as a function of m_0 for normal mass ordering in the left panel (left panel inset) for three values of ϵ: in decreasing order of line-thickness 0.1, 0.05 and 0.025. In the right panel the same plots are displayed for inverted mass ordering.

As presented in Table 2.2, in the TBM, BM, and GR models the ratio $r = \mathrm{Re}(\gamma)/\mathrm{Re}(\alpha) = \cos\phi_\gamma/\cos\phi_\alpha$ is tightly constrained from the solar mixing angle θ_{12}. Thus ϕ_γ also tends to $\pi/2$ as m_0 increases and since r is small it does so faster than ϕ_α. This can be seen from the inset in Fig. 2.4.

δ is not a free parameter in this model. Rather, picking a value for θ_{13} amounts to fixing $|\bar{\xi}|$ from Eq. (2.23). Now, by choice $|\xi| = \epsilon$, hence from Eq. (2.17) one can get ϕ_ξ. This in turn determines the phase of $\bar{\xi}$ which equals δ. The results so obtained are presented in the left panel of Fig. 2.5 for the TBM (red solid), BM (violet dashed), and GR (green dot-dashed) models for $\epsilon = 0.1$. The brown dotted curves are for $a = 0, b = 1$ i.e., NSM case. For each model the two curves correspond to the 1σ upper and lower limits of θ_{13}. It is worthwhile to point out that the procedure for extracting δ using $|\bar{\xi}|$ leaves a two-fold uncertainty $\delta \leftrightarrow \pi+\delta$. Keeping this in mind we have shown δ in the first quadrant in Fig. 2.5 even though the 1σ range of the global fit – Eq. (2.3) – would prefer the partner $\pi + \delta$ solution.

In the right panel of Fig. 2.5 we restrict to the case of Tribimaximal mixing and show the dependence of δ on the scale of perturbation ϵ. The conclusion that can be drawn from these panels is that δ is largely independent of the lightest neutrino mass and varies over a limited region as θ_{13} covers its 1σ range or ϵ is varied.

A reparametrization invariant measure of CP violation is the Jarlskog parameter, J [57]. For arbitrary mixing it turns out to be

$$J = \mathrm{Im}[U_{e1}U_{\mu 2}U^*_{e2}U^*_{\mu 1}] = \frac{1}{4b}\left[(b^2 - a^2)\sin 2\zeta + 2ab\cos 2\zeta\right] Im(\bar{\xi}) \ , \qquad (2.29)$$

where in the last step only the lowest order perturbation effect is retained. In the inset of the right panel of Fig. 2.5 we show this CP violation measure as a function of m_0. Note that J changes sign under $\delta \to \pi + \delta$. We remark at this stage that for the $b = 0$ case $J = 0$.

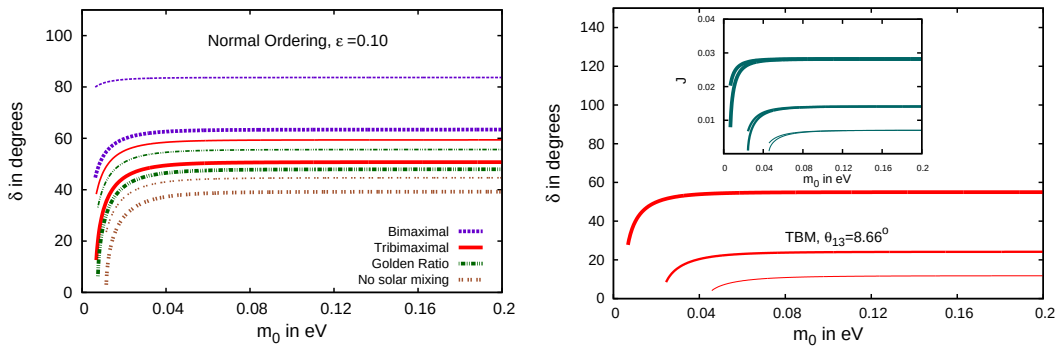

Figure 2.5: In the left panel δ for different models is plotted for the 1σ limiting values of θ_{13}, namely, 9.1° (thick curves) and 8.2° (thin curves). ϵ has been taken to be 0.1. The right panel is for the TBM model. Three values of ϵ are chosen – in decreasing order of thickness ϵ = 0.1, 0.05, 0.025 – and θ_{13} is taken at the best-fit value. In the inset is shown the Jarlskog parameter J for the chosen ϵ and the 1σ limits of θ_{13}. Both panels are for normal mass ordering. For inverted ordering $\delta \to (\pi - \delta)$ and J is unchanged.

Inverted mass ordering

The analysis procedure for inverted mass ordering is essentially the same. In the right-panel of Fig. 2.4 we show ϕ_α (with ϕ_γ in the inset) as a function of m_0. The difference from normal ordering arises due to the appearance of $m_1^{(0)}$ in Eq. (2.20) which is larger in this case. Hence, ϕ_α and ϕ_γ remain closer to $\pi/2$ for all m_0. The determination of δ using Eqs. (2.23) and (2.26) on the other hand involves only $m^\pm$ and not $m_i^{(0)}$. Consequently, it can be seen from Eq. (2.26) that for any m_0 the CP phase in the inverted and normal mass orderings are simply related by $\delta \leftrightarrow (\pi - \delta)$. J remains unchanged. So, δ and J for the inverted mass ordering can be read off from Fig. 2.5.

2.6 Mass models

The discussion thus far has not been tied to any specific model for neutrino masses. We restrict ourselves to just a few remarks here. The perturbation matrix in the flavour basis[58] corresponding to the general form of the mixing matrix in Eq. (2.6) is:

$$(M')^{flavour} = m^+ \begin{pmatrix} a^2\alpha & \chi & -\sqrt{2}ab\alpha + \chi \\ \chi & (b^2\alpha + \beta)/2 & (-b^2\alpha + \beta)/2 \\ -\sqrt{2}ab\alpha + \chi & (-b^2\alpha + \beta)/2 & (b^2\alpha + \beta)/2 \end{pmatrix} \tag{2.30}$$

where use has been made of Eq. (2.22) and we have set $\chi = (ab\alpha + b\xi + a\eta)/\sqrt{2}$.

Attempting to relate the above matrix in its general form to the popular mass models will take us beyond the scope of this chapter. Rather, we indicate here a limit when it can arise from a Zee-type model [58]. The required condition is:

$$\beta = \alpha(2 - 3b^2) \tag{2.31}$$

It is seen using Eq. (2.7) that for this choice the diagonal elements of $(M')^{flavour}$ become equal and can be subsumed in the unperturbed matrix. The remaining terms can be obtained from a Zee-type model[59]. In these models $(M')_{ij}^{flavour}$ is proportional to $(M_i^2 - M_j^2)$, M_i $(i = 1, 2, 3)$ being the charged lepton masses. Since $m_\tau \gg m_\mu \gg m_e$, without unnatural fine-tunings one would prefer χ to be much smaller than the other elements of the matrix. This was already noted earlier [54]; further details and references can be found therein. An explicit $A4$ based model which exhibits most of these features is given in [52].

For Tribimaximal mixing, i.e., $a = \frac{1}{\sqrt{3}}$ and $b = \sqrt{\frac{2}{3}}$, Eq. (2.31) amounts to taking $\beta = 0$. For Bimaximal mixing ($a = b = \frac{1}{\sqrt{2}}$) it is accomplished with the

[58] As noted, γ is small compared to the scale of the perturbation fixed by α, ξ, and η. In this section, we neglect γ.

[59] An alternate derivation of $\theta_{13} \neq 0$ using the Zee model can be found in [59].

choice $\beta = \alpha/2$. For the Golden Ratio mixing ($a = \sqrt{\frac{1}{\sqrt{5}\phi}}, b = \sqrt{\frac{\phi}{\sqrt{5}}}$) the choice $\beta = \alpha(\phi - 2)/(2\phi - 1)$ brings $(M')^{flavour}$ to the Zee form.

2.7 Conclusion

The neutrino mass spectrum and the mixing angles exhibit two noteworthy features: the mixing angle θ_{13} is small compared to the the other two angles, namely, θ_{12} and θ_{23}, and the solar mass splitting is two orders of magnitude smaller than the atmospheric splitting, $R_{\rm mass} = |\Delta m^2_{21}/\Delta m^2_{31}| \simeq 10^{-2}$. We show that both of these small quantities could be the result[60] of a perturbation of a simpler partially degenerate neutrino mass matrix ($m_1^{(0)} = m_2^{(0)}$) along with a mixing matrix, U^0, which has $\theta_{13} = 0$.

The perturbation matrix can be chosen to be real only if the neutrino mass ordering is normal and the lightest neutrino mass, m_0, less than about 0.04 eV. In this case there will be no CP violation in the lepton sector.

For larger values of m_0 the pertubation M' has to be complex. We show that depending on the overall scale of the perturbation, which we have indicated by ϵ, the CP phase, δ, is calculable and could be near maximal ($\delta = \pi/2, 3\pi/2$) in some cases. CP violation varies for the different popular models – e.g., Tribimaximal, Bimaximal, Golden Ratio, etc. It depends significantly on ϵ – a smaller perturbation resulting in a smaller δ – but is essentially independent of m_0. It also varies with θ_{13} – in the Tribimaximal model the current 1σ (3σ) range of θ_{13} translates to about 10° (35°) variation in δ.

In this chapter we have taken the atmospheric mixing to be maximal ($\theta_{23} = \pi/4$). The current best-fit values are in the two adjoining octants, both more than 1σ away from maximality. We have repeated the analysis using these two best-fit values of θ_{23}. We find that the CP violation effects are changed by less than 10% in both cases[61].

As they stand, none of the popular mixing models are consistent with the current value of θ_{12} at 1σ. We ensure that for every model the perturbation takes care of this shortcoming. In passing, we also consider the possibility that in the unperturbed case $\theta_{12} = 0$ in addition to the vanishing θ_{13}. In such a scenario, both these angles arise from the perturbation. In this case δ is the smallest among all models.

Neutrino mass matrices which exhibit the features of the unperturbed mass matrix are common in the literature. The perturbative contribution can arise from a subdominant loop contribution from a Zee-type model.

[60] An attempt to generate the solar splitting and θ_{13} at low energies starting from a partially degenerate mass spectrum and $\theta_{13} = 0$ at a high scale through renormalization group effects in a supersymmetric model has been made in [60].

[61] Models have been proposed where the deviation of θ_{23} from maximality is correlated with the value of θ_{13} [61].

Chapter 3

Seesaw based model independent analysis

3.1 Introduction

This chapter is based on our publications [33, 34] and the conference proceedings [35,36]. In the previous chapter we have presented a perturbative scheme by which, through a two-component formalism, one can reproduce the known neutrino masses and mixing angles. In this chapter we show that seesaw mechanism provides a framework in which these ideas can be implemented in a natural way. Here we restrict ourselves to the NSM scenario. It is unique in the sense that the mixing angles are initially either maximal, namely $\pi/4$ (θ_{23}), or zero (θ_{13}, θ_{12}) and the solar splitting absent. In this spirit, here a proposal is put forward under which the atmospheric mass splitting and maximal mixing in this sector arise from a zero-order mass matrix while the smaller solar mass splitting and realistic θ_{13} and θ_{23} are generated by a Type I seesaw [62] which acts as a perturbation. θ_{12} also arises out of the same perturbation and as a consequence of degeneracy is not constrained to be small.

The three non-zero mixing angles open the possibility of CP violation in the lepton sector[62]. This model accommodates a CP phase δ which must be close to maximal ($\delta \sim \pi/2,\ 3\pi/2$) if the neutrinos have an inverted mass ordering or if they are quasidegenerate [33]. Earlier work which partially address similar issues can be traced to [63, 64], but to our knowledge this is the first time that *all* the small parameters have been shown to have the same perturbative origin and are consistent with the latest data.

[62]For the lepton mixing matrix the standard PMNS form is used, see Eq. (1.15)

3.2 The model

The unperturbed neutrino mass matrix in the mass basis is $M^0 = \text{diag}\{m_1^{(0)}, m_1^{(0)}, m_3^{(0)}\}$ with the mixing matrix of the form

$$U^0 = \begin{pmatrix} 1 & 0 & 0 \\ 0 & \sqrt{\frac{1}{2}} & \sqrt{\frac{1}{2}} \\ 0 & -\sqrt{\frac{1}{2}} & \sqrt{\frac{1}{2}} \end{pmatrix} \quad . \tag{3.1}$$

Here $\Delta m^2_{atm} = (m_3^{(0)})^2 - (m_1^{(0)})^2$. By suitably choosing the Majorana phases the masses $m_1^{(0)}, m_3^{(0)}$ are taken to be real and positive. The columns of U^0 are the unperturbed flavour eigenstates[63]. As stated, $\Delta m^2_{solar} = 0$ and $\theta_{13} = 0$. Since the first two states are degenerate in mass, one can also take $\theta_{12} = 0$. It is possible to generate this mass matrix from a Type II seesaw as we will see from the next chapter onwards.

In the flavour basis the neutrino mass matrix is $(M^0)^{flavour} = U^0 M^0 U^{0T}$ which in terms of $m^{\pm} = m_3^{(0)} \pm m_1^{(0)}$ is

$$(M^0)^{flavour} = \frac{1}{2} \begin{pmatrix} 2m_1^{(0)} & 0 & 0 \\ 0 & m^+ & m^- \\ 0 & m^- & m^+ \end{pmatrix} \quad . \tag{3.2}$$

A smaller additional contribution, which we include perturbatively, is obtained by a Type I seesaw. To reduce the number of independent parameters, in the flavour basis the Dirac mass term is taken to be proportional to the identity, i.e.,

$$M_D = m_D \, \mathbb{I} \, . \tag{3.3}$$

This choice completely determines the right-handed flavour basis although the form of $M_R^{flavour}$ can be chosen at will to suit our purpose. In the interest of minimality we seek symmetric matrices with the fewest non-zero entries. Five texture zero matrices fail the invertibility criterion[64] and therefore are not pursued. Next we try four texture zero options. By examining the different alternatives it can be seen that all the perturbation goals that we have set for ourselves could be achieved by only two such candidates out of which one is scripted below[65]:

$$M_R^{flavour} = m_R \begin{pmatrix} 0 & xe^{-i\phi_1} & 0 \\ xe^{-i\phi_1} & 0 & 0 \\ 0 & 0 & ye^{-i\phi_2} \end{pmatrix} \quad , \tag{3.4}$$

where x, y are dimensionless constants of $\mathcal{O}(1)$. The Dirac mass is kept real without any loss of generality.

[63] In the flavour basis the charged lepton mass matrix is diagonal.

[64] Existence of the inverse of M_R is an essential condition for the see-saw mechanism.

[65] The other alternative is a mere $2 \leftrightarrow 3$ exchange of this configuration and the corresponding results vary only up to a relative sign.

3.3 Real M_R ($\phi_1 = 0$ or $\pi, \phi_2 = 0$ or π)

As a warm-up consider first the real case, i.e., $\phi_1 = 0$ or $\pi, \phi_2 = 0$ or π. For notational convenience in the following the phase factors are not displayed; instead x (y) is taken as positive or negative depending on whether ϕ_1 (ϕ_2) is 0 or π.

The Type I seesaw contribution in the mass basis is:

$$M'^{mass} = U^{0T}\left[M_D^T (M_R^{flavour})^{-1} M_D\right] U^0 = \frac{m_D^2}{\sqrt{2}\, xym_R} \begin{pmatrix} 0 & y & y \\ y & \frac{x}{\sqrt{2}} & -\frac{x}{\sqrt{2}} \\ y & -\frac{x}{\sqrt{2}} & \frac{x}{\sqrt{2}} \end{pmatrix} \ . \tag{3.5}$$

The effect on the solar sector is governed by the submatrix of M'^{mass} in the subspace of the two degenerate states,

$$M'^{mass}_{2\times 2} = \frac{m_D^2}{\sqrt{2}\, xym_R} \begin{pmatrix} 0 & y \\ y & x/\sqrt{2} \end{pmatrix} \ . \tag{3.6}$$

To first order in the perturbation:

$$\tan 2\theta_{12} = 2\sqrt{2}\left(\frac{y}{x}\right) \ . \tag{3.7}$$

For $y/x = 1$ one obtains the Tribimaximal mixing value of θ_{12} which, though allowed by the data[66] at 3σ, is beyond the 1σ region. Since for the entire range of θ_{12} one has $\tan 2\theta_{12} > 0$, x and y must be chosen of the same sign. Therefore, either $\phi_1 = 0 = \phi_2$ or $\phi_1 = \pi = \phi_2$. Furthermore, the allowed values of θ_{12} are such that one has $\sin 2\theta_{12} > 0$ and $\cos 2\theta_{12} > 0$. This rules out the second option, i.e., only $x, y > 0$ is allowed. From the global fits to the experimental results one finds:

$$0.695 < \frac{y}{x} < 1.112 \text{ at } 3\sigma \ . \tag{3.8}$$

Further, from eq. (3.6),

$$\Delta m^2_{solar} = \frac{m_D^2}{xym_R}\ m_1^{(0)} \sqrt{x^2 + 8y^2} \ . \tag{3.9}$$

To first order in the perturbation the corrected wave function $|\psi_3\rangle$ is:

$$|\psi_3\rangle = \begin{pmatrix} \kappa \\ \frac{1}{\sqrt{2}}(1 - \frac{\kappa}{\sqrt{2}}\frac{x}{y}) \\ \frac{1}{\sqrt{2}}(1 + \frac{\kappa}{\sqrt{2}}\frac{x}{y}) \end{pmatrix} \quad , \tag{3.10}$$

where

$$\kappa \equiv \frac{m_D^2}{\sqrt{2}\, xm_R m^-} \ . \tag{3.11}$$

[66] We use the 3σ ranges $7.02 \leq \Delta m^2_{21}/10^{-5}\,\mathrm{eV}^2 \leq 8.08$ and $31.52^\circ \leq \theta_{12} \leq 36.18^\circ$ as in Eq. (1.24).

As x is positive the sign of κ is fixed by that of m^-. Since by convention all the mixing angles θ_{ij} are in the first quadrant, from Eq. (3.10) one must identify:

$$\sin\theta_{13}\cos\delta = \kappa = \frac{m_D^2}{\sqrt{2}\; x m_R m^-} \quad , \tag{3.12}$$

where the PMNS phase $\delta = 0$ for normal mass ordering and $\delta = \pi$ for inverted mass ordering. Needless to say, both these cases are CP conserving. We show later that the IO case cannot satisfactorily fit the observations.

An immediate consequence of Eqs. (3.12), (3.7), and (3.9) is

$$\Delta m^2_{solar} = m^- m_1^{(0)} \; \frac{4\sin\theta_{13}\cos\delta}{\sin 2\theta_{12}} \; , \tag{3.13}$$

which exhibits how the solar sector and θ_{13} are intertwined. The positive sign of Δm^2_{solar}, preferred by the data, is trivially verified since $m^-\sin\theta_{13}\cos\delta > 0$ from Eq. (3.12). However, Eq. (3.13) excludes inverted ordering. Once the neutrino mass square splittings, θ_{12}, and θ_{13} are chosen, Eq. (3.13) determines the lightest neutrino mass, m_0. Defining $z = m^- m_1^{(0)}/\Delta m^2_{atm}$ and $m_0/\sqrt{|\Delta m^2_{atm}|} = \tan\xi$, one has

$$\begin{aligned} z &= \sin\xi/(1+\sin\xi) \;\; \text{(normal ordering)}, \\ z &= 1/(1+\sin\xi) \;\; \text{(inverted ordering)} \; . \end{aligned} \tag{3.14}$$

It is seen that $0 \le z \le 1/2$ for NO and $1/2 \le z \le 1$ for IO, with $z \to 1/2$ corresponding to quasidegeneracy, i.e., $m_0 \to$ large, in both cases. From Eq. (3.13)

$$z = \left(\frac{\Delta m^2_{solar}}{|\Delta m^2_{atm}|}\right)\left(\frac{\sin 2\theta_{12}}{4\sin\theta_{13}|\cos\delta|}\right) \quad , \tag{3.15}$$

with $|\cos\delta| = 1$ for real M_R. As shown below, the allowed ranges of the oscillation parameters imply $z \sim 10^{-2}$ and so inverted mass ordering is disallowed. The remaining discussion in this section is confined to normal ordering only.

From Eq. (3.10) one further finds:

$$\tan\theta_{23} \equiv \tan(\pi/4 - \omega) = \frac{1 - \frac{\kappa}{\sqrt{2}}\frac{x}{y}}{1 + \frac{\kappa}{\sqrt{2}}\frac{x}{y}} \quad , \tag{3.16}$$

where, using Eqs. (3.7) and (3.12),

$$\tan\omega = \frac{2\sin\theta_{13}\cos\delta}{\tan 2\theta_{12}} \; . \tag{3.17}$$

θ_{23} is in the first octant, i.e., the sign of ω is positive as $\delta = 0$.

In Fig. 3.1 the global-fit 3σ range of $\sin\theta_{13}$ and $\tan 2\theta_{12}$ is shown as the brown dashed box with the best-fit value indicated by a red dot. Once the atmospheric and solar mass splittings are fixed, for any point within this region Eq. (3.15) determines a z, or equivalently an m_0, which leads to the correct solar splitting.

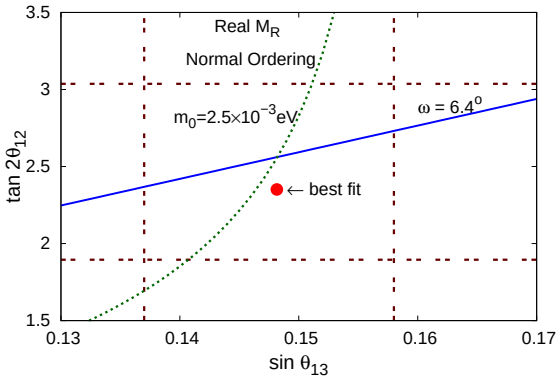

Figure 3.1: The brown dashed box is the global-fit 3σ allowed range of $\sin\theta_{13}$ and $\tan 2\theta_{12}$. The best-fit point is shown as a red dot. The green dotted curve is from Eq. (3.13) with $m_0 = 2.5$ meV when the best-fit values of the two mass-splittings are used. The portion below the blue solid straight line is excluded by θ_{23} at 3σ – Eq. (3.17) – for the first octant. In case of inverted ordering no solution of Eq. (3.13) is allowed for real M_R.

From the 3σ data in Eq. (1.24) $\omega_{min} = 0$ and $\omega_{max} = 6.4^\circ$ for the first octant. As $\cos\delta = 1$ for the real M_R case, in this model one has from Eq. (3.17) $\omega \geq 5.14^\circ$ at 3σ. Thus the range of θ_{23} that can be obtained is rather limited[67]. The blue solid straight line is from Eq. (3.17) for ω_{max}. The region *below* this line is excluded in this model.

Using the 3σ global-fit limits of θ_{13} and θ_{12}, from Eq. (3.15) one gets $z_{max} = 6.03 \times 10^{-2}$ implying that $(m_0)_{max} = 3.10$ meV. Also, consistency with both Eqs. (3.17) at ω_{max} and (3.15) sets $z_{min} = 4.01 \times 10^{-2}$ corresponding to $(m_0)_{min} = 2.13$ meV. If, as a typical example, $m_0 = 2.5$ meV is taken and the best-fit values of the solar and atmospheric mass splittings are used then Eq. (3.13) gives the green dotted curve in Fig. 3.1.

In summary, for real M_R the free parameters are m_0, m_D^2/xm_R and y with which the solar mass splitting, $\theta_{12}, \theta_{13}, \theta_{23}$ in first octant are reproduced for normal mass ordering. Inverted ordering cannot be accommodated.

3.4 Complex M_R

Reverting now to complex M_R in Eq. (3.4) one has in the mass basis in place of Eq. (3.5):

$$M'^{mass} = \frac{m_D^2}{\sqrt{2}xym_R}\begin{pmatrix} 0 & ye^{i\phi_1} & ye^{i\phi_1} \\ ye^{i\phi_1} & \frac{xe^{i\phi_2}}{\sqrt{2}} & \frac{-xe^{i\phi_2}}{\sqrt{2}} \\ ye^{i\phi_1} & \frac{-xe^{i\phi_2}}{\sqrt{2}} & \frac{xe^{i\phi_2}}{\sqrt{2}} \end{pmatrix}. \tag{3.18}$$

[67] This range is excluded at 1σ for the first octant.

x and y are now positive. M' is no longer hermitian. This is addressed, as usual, by defining the hermitian combination $(M^0+M')^\dagger(M^0+M')$ and treating $M^{0\dagger}M^0$ as the unperturbed term and $H'^{mass} \equiv (M^{0\dagger}M' + M'^\dagger M^0)$ as the perturbation to lowest order. The zero order eigenvalues are now $(m_i^{(0)})^2$ and the complex yet hermitian perturbation matrix is

$$H'^{mass} = \frac{m_D^2}{\sqrt{2}xym_R} \begin{pmatrix} 0 & 2m_1^{(0)} y\cos\phi_1 & yf(\phi_1) \\ 2m_1^{(0)} y\cos\phi_1 & \frac{2}{\sqrt{2}} m_1^{(0)} x\cos\phi_2 & -\frac{1}{\sqrt{2}} xf(\phi_2) \\ yf^*(\phi_1) & -\frac{1}{\sqrt{2}} xf^*(\phi_2) & \frac{2}{\sqrt{2}} m_3^{(0)} x\cos\phi_2 \end{pmatrix}, \quad (3.19)$$

where

$$f(\xi) = m^+\cos\xi - im^-\sin\xi \ . \quad (3.20)$$

The subsequent analysis is similar to the one for real M_R.

The perturbation which splits the degenerate solar sector is the 2×2 block of Eq. (3.19). The solar mixing angle now is

$$\tan 2\theta_{12} = 2\sqrt{2}\ \frac{y}{x}\ \frac{\cos\phi_1}{\cos\phi_2}\ . \quad (3.21)$$

The limits of Eq. (3.8) apply on the ratio $(y\cos\phi_1/x\cos\phi_2)$. Also, $(\cos\phi_1/\cos\phi_2)$ must be positive. Furthermore, $\cos\phi_1, \cos\phi_2 > 0$, i.e., ϕ_1, ϕ_2 can be in the first or the fourth quadrants.

Including first order corrections the wave function $|\psi_3\rangle$ is

$$|\psi_3\rangle = \begin{pmatrix} \kappa f(\phi_1)/m^+ \\ \frac{1}{\sqrt{2}}(1 - \frac{\kappa}{\sqrt{2}}\frac{x}{y}\ f(\phi_2)/m^+) \\ \frac{1}{\sqrt{2}}(1 + \frac{\kappa}{\sqrt{2}}\frac{x}{y}\ f(\phi_2)/m^+) \end{pmatrix}. \quad (3.22)$$

κ is positive (negative) for NO (IO). One immediately has

$$\begin{aligned} \sin\theta_{13}\cos\delta &= \kappa\cos\phi_1\ , \\ \sin\theta_{13}\sin\delta &= \kappa\ \frac{m^-}{m^+}\sin\phi_1\ . \end{aligned} \quad (3.23)$$

The sign of $\cos\delta$ is positive (negative) for normal (inverted) mass ordering. Further, $\sin\phi_1$ determines the combination $\sin\theta_{13}\sin\delta$ that appears in the Jarlskog parameter, J. Note, ϕ_2 plays no role in fixing the CP phase δ.

It is seen that for normal ordering ($\kappa > 0$) the quadrant of δ is the same as that of ϕ_1 i.e., the first or the fourth quadrant. For inverted ordering ($\kappa < 0$) δ is in the second (third) quadrant if ϕ_1 is in the first (fourth) quadrant.

θ_{23} obtained from Eq. (3.22) is

$$\tan\theta_{23} = \frac{1 - \frac{\kappa}{\sqrt{2}}\frac{x}{y}\cos\phi_2}{1 + \frac{\kappa}{\sqrt{2}}\frac{x}{y}\cos\phi_2} \quad , \quad (3.24)$$

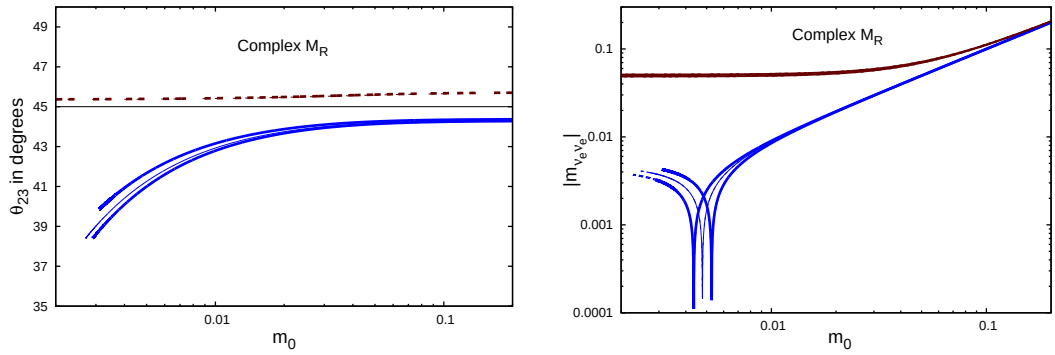

Figure 3.2: θ_{23} ($|m_{\nu_e\nu_e}|$ in eV) as a function of the lightest neutrino mass m_0 (in eV) is shown in the left (right) panel. The blue (brown) curves are for the normal (inverted) mass ordering. For every plot the region allowed at 3σ is between the thick curves while the thin curves are for the best-fit values of the inputs. The solid (dashed) curves correspond to the first (second) octant of θ_{23}.

where, using Eqs. (3.21) and (3.23),

$$\tan\omega = \frac{2\sin\theta_{13}\cos\delta}{\tan 2\theta_{12}} \ . \tag{3.25}$$

Eq. (3.17) is recovered when $\cos\delta = +1$. As $\cos\delta$ is positive (negative) for normal (inverted) mass ordering, from Eq. (3.25) θ_{23} is in the first (second) octant.

A straight-forward calculation after expressing m_D and m_R in terms of $\sin\theta_{13}\cos\delta$, yields

$$\Delta m^2_{solar} = m^- m_1^{(0)} \ \frac{4\sin\theta_{13}\cos\delta}{\sin 2\theta_{12}} \ , \tag{3.26}$$

which bears a strong similarity with Eq. (3.13) for real M_R. Eqs. (3.14) and (3.15) continue to hold. Noting the factors determining the sign of $\cos\delta$, one concludes that Δm^2_{solar} is positive for both mass orderings. Thus, satisfying the solar mass splitting leaves room for either octant of θ_{23}. The allowed range of δ can be easily read off if we re-express Eq. (3.15) as:

$$|\cos\delta| = \left(\frac{\Delta m^2_{solar}}{|\Delta m^2_{atm}|}\right)\left(\frac{\sin 2\theta_{12}}{4\sin\theta_{13}\ z}\right) \ . \tag{3.27}$$

In the following enterprise m_0, θ_{13}, and θ_{12} are taken as inputs and δ and θ_{23} are obtained using Eqs. (3.27) and (3.25). From these the CP violation measure, J, and the combination $|m_{\nu_e\nu_e}|$ which determines the rate of neutrinoless double beta decay are calculated.

In the left panel of Fig. 3.2 marked by the thick curves is shown the dependence of θ_{23} on the lightest neutrino mass m_0 when the neutrino mass square splittings and the angles θ_{13} and θ_{12} are varied over their allowed ranges at 3σ. The thin curves correspond to taking the best-fit values. The blue (brown) curves are for normal

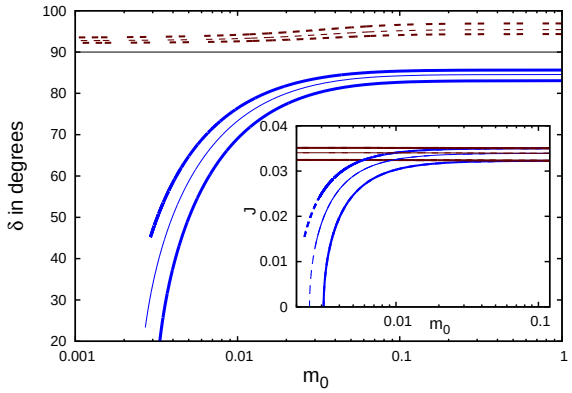

Figure 3.3: The CP phase δ is plotted as a function of m_0 (in eV). Inset: The leptonic CP violation measure J is shown. The conventions are the same as that of Fig. 3.2.

(inverted) mass ordering. For inverted ordering the thick and thin curves are very close and cannot be distinguished in this figure. Notice that the 3σ predictions from this model are not consistent with $\theta_{23} = \pi/4$. Its range for inverted ordering falls outside the 1σ global fits but are consistent at 3σ. An improvement in the determination of θ_{23} will be the easiest way to exclude one of the orderings unless one is in the quasidegenerate regime. For normal ordering the smallest value of m_0 is determined by the 3σ limit of θ_{23} in the first octant. Eq. (3.26) permits arbitrarily small m_0 for inverted mass ordering (see later).

In the right panel of Fig. 3.2 $|m_{\nu_e\nu_e}|$ has been plotted. The sensitivity of direct neutrino mass measurements is expected to reach around 200 meV [19] in the near future. Planned neutrinoless double beta decay experiments will also probe the quasidegenerate range of m_0 [65]. As can be seen from this figure, to distinguish the two mass orderings at least a further one order improvement in sensitivity will be needed. Long-baseline experiments or large atmospheric neutrino detectors such as INO will settle the mass ordering more readily.

In Fig. 3.3 is displayed the variation of δ with m_0 for both mass orderings while J is shown in the inset. The conventions are the same as in Fig. 3.2. For NO (IO) δ can be in first (second) or the fourth (third) quadrants and accordingly J has positive or negative values. With this proviso in mind, Fig. 3.3 has been plotted keeping δ in the first or second quadrant and J has been taken as positive. For inverted mass ordering both δ and J remain nearly independent of m_0.

For m_0 smaller than 10 meV, the CP phase δ is significantly larger for inverted ordering[68]. This could provide a clear test of this model when the mass ordering is known and CP violation in the neutrino sector is measured. The real limit ($\delta = 0$) is seen to be admissible, as expected from Fig. 3.1, only for normal ordering and that too not for the entire 3σ range.

[68]In fact for inverted ordering δ remains close to $\pi/2$ or $3\pi/2$ for all m_0.

Since $0 \leq z \leq 1/2$ for NO and $1/2 \leq z \leq 1$ for IO, the allowed values of δ in the two orderings as seen from Eq. (3.27) are complementary tending towards a common value as $z \to 1/2$, the quasidegenerate limit, which begins to set in from around $m_0 = 100$ meV. The main novelty from the real M_R case is that in Eq. (3.15) by choosing $\cos\delta$ sufficiently small (in magnitude) one can make $z \equiv m^- m_1^{(0)}/\Delta m^2_{atm} \sim 1$ so that solutions exist for m_0 for inverted mass ordering corresponding to even vanishing m_0 unlike the case of normal ordering where the lower limit of m_0 is set by $\cos\delta = 1$, i.e., real M_R.

We have checked that the size of the perturbation is at most around 20% of the unperturbed contribution for all cases.

3.5 Conclusions

In conclusion, a model for neutrino masses has been proposed in which the atmospheric mass splitting together with $\theta_{23} = \pi/4$ has an origin different from that of the solar mass splitting, θ_{12}, θ_{13}, and $\omega = \pi/4 - \theta_{23}$, all of which arise from a single perturbation resulting from a Type I seesaw. The global fits to the mass splittings, θ_{12} and θ_{13} completely pin-down the model and the CP phase δ and the octant of θ_{23} are predicted in terms of the lightest neutrino mass m_0. Both mass orderings are allowed, the inverted ordering being associated with near-maximal CP violation. Both octants of θ_{23} can be accommodated; the first (second) octant being associated with normal (inverted) ordering. Further improvements in the determination of θ_{23}, a measurement of the CP phase δ, along with a knowledge of the neutrino mass ordering will put this model to test from several directions.

Chapter 4

Seesaw model based on $A4$ symmetry

4.1 Introduction

This chapter is based on our paper [37]. As already noted in Chapter 1, many neutrino oscillation experiments have established that neutrinos are massive and non-degenerate and that the flavour eigenstates are not identical with the mass eigenstates. For the three neutrino paradigm the two independent mass square splittings are the solar (Δm^2_{solar}) and the atmospheric (Δm^2_{atmos}). The mass and flavour bases are related through the PMNS matrix usually parametrized as:

$$U = \begin{pmatrix} c_{12}c_{13} & s_{12}c_{13} & s_{13}e^{-i\delta} \\ -c_{23}s_{12} + s_{23}s_{13}c_{12}e^{i\delta} & c_{23}c_{12} + s_{23}s_{13}s_{12}e^{i\delta} & -s_{23}c_{13} \\ -s_{23}s_{12} - c_{23}s_{13}c_{12}e^{i\delta} & s_{23}c_{12} - c_{23}s_{13}s_{12}e^{i\delta} & c_{23}c_{13} \end{pmatrix} , \qquad (4.1)$$

where $c_{ij} = \cos\theta_{ij}$ and $s_{ij} = \sin\theta_{ij}$.

The recent measurement of a non-zero value for θ_{13} [66], which is small compared to the other mixing angles, has led to a flurry of activity in developing neutrino mass models which incorporate this feature. Earlier in Chapter 2 we had demonstrated that a direction which bears exploration is whether two small quantities in the neutrino sector, namely, θ_{13} and the ratio, $R \equiv \Delta m^2_{solar}/\Delta m^2_{atmos}$, could in fact be related to each other, both resulting from a small perturbation. Subsequently in Chapter 3, we had shown that it is possible to envisage scenarios where only the larger Δm^2_{atmos} and $\theta_{23} = \pi/4$ are present in a basic structure of neutrino mass and mixing and the rest of the quantities, namely, θ_{13}, θ_{12}, the deviation of θ_{23} from $\pi/4$, and Δm^2_{solar} all have their origin in a smaller seesaw induced perturbation[69]. Obviously, this gets reflected in constraints on the measured quantities. A vanishing θ_{13} follows rather easily from certain symmetries and indeed many of the newer models are based on perturbations of such structures [67, 68].

[69] Early work on neutrino mass models where some variables are much smaller than others can be found in [63].

Encouraged by the success of this program we present a model based on the group $A4$ which relies on the seesaw mechanism [62] in which the lightest neutrino mass, m_0, the seesaw scale and one other parameter determine θ_{13}, R, θ_{12}, and the deviation of θ_{23} from $\pi/4$. If this last parameter is complex then the CP phase δ is also a prediction. Here, the atmospheric mass splitting is taken as an input which together with the lightest neutrino mass completely defines the unperturbed mass matrix generated by the Type II seesaw. The size of the perturbation is determined by the Type I seesaw and is of the form m_D^2/m_R where m_D and m_R respectively are the scale of the Dirac and right-handed Majorana mass terms.

After a brief summary of the $A4$ group properties and the structure of the model in the following section we describe the implications of the model in the next section. The comparison of this model with the experimental data appears next. We end with our conclusions. The model has a rich scalar field content. In an Appendix we discuss the $A4$ invariant scalar potential and the conditions under which the desired potential minimum can be realized.

It should be noted that neutrino mass models based on $A4$ have also been investigated earlier [69–71]. In a majority of them the neutrino mass matrix is obtained from a Type II seesaw and the earlier emphasis was on obtaining Tribimaximal mixing. Recent work has focussed on obtaining more realistic mixing patterns [72] sometimes taking recourse to breaking of $A4$ symmetry [73]. Our work is unique in the following aspect. It uses a combination of Type II and Type I seesaw mechanisms where the former yields mixing angles which are either vanishing (θ_{12} and θ_{13}) or maximal – i.e., $\pi/4$ – (θ_{23}) while keeping the solar splitting absent. This kind of a scenario has not been considered before. The Type I seesaw acting as a perturbation results in a non-zero CP phase and realistic mixing angles while at the same time creating the correct solar splitting.

4.2 The Model

$A4$ is the group of even permutations of four objects comprising of 12 elements which can be generated using the two basic permutations S and T satisfying $S^2 = T^3 = (ST)^3 = \mathbb{I}$. The group has four inequivalent irreducible representations one of 3 dimension and three of 1 dimension denoted by $1, 1'$ and $1''$. The one-dimensional representations are all singlets under S and transform as 1, ω, and ω^2 under T respectively, where ω is the cube root of unity. Thus $1' \times 1'' = 1$.

For the three-dimensional representation

$$S = \begin{pmatrix} 1 & 0 & 0 \\ 0 & -1 & 0 \\ 0 & 0 & -1 \end{pmatrix} \quad \text{and} \quad T = \begin{pmatrix} 0 & 1 & 0 \\ 0 & 0 & 1 \\ 1 & 0 & 0 \end{pmatrix} \ . \tag{4.2}$$

This representation satisfies the product rule

$$3 \otimes 3 = 1 \oplus 1' \oplus 1'' \oplus 3 \oplus 3 \ . \tag{4.3}$$

The two triplets arising from the product of $3_a \equiv a_i$ and $3_b \equiv b_i$, where $i = 1, 2, 3$, can be identified as $3_c \equiv c_i$ and $3_d \equiv d_i$ with

$$\begin{aligned} c_i &= \left(\frac{a_2b_3 + a_3b_2}{2}, \frac{a_3b_1 + a_1b_3}{2}, \frac{a_1b_2 + a_2b_1}{2}\right) \text{ or } c_i \equiv \alpha_{ijk} a_j b_k \ , \\ d_i &= \left(\frac{a_2b_3 - a_3b_2}{2}, \frac{a_3b_1 - a_1b_3}{2}, \frac{a_1b_2 - a_2b_1}{2}\right) \text{ or } d_i \equiv \beta_{ijk} a_j b_k \ , (i, j, k, \text{are cyclic}). \end{aligned} \tag{4.4}$$

In this notation the one-dimensional representations in the $3 \otimes 3$ product can be written as:

$$\begin{aligned} 1 &= a_1b_1 + a_2b_2 + a_3b_3 \equiv \rho_{1ij} a_i b_j \ , \\ 1' &= a_1b_1 + \omega^2 a_2b_2 + \omega a_3b_3 \equiv \rho_{3ij} a_i b_j \ , \\ 1'' &= a_1b_1 + \omega a_2b_2 + \omega^2 a_3b_3 \equiv \rho_{2ij} a_i b_j \ . \end{aligned} \tag{4.5}$$

Further details of the group $A4$ are available in the literature [69, 70].

Fields	Notations	$A4$	$SU(2)_L$ (Y)	L
Left-handed leptons	$(\nu_i, l_i)_L$	3	2 (-1)	1
Right-handed charged leptons	l_{1R}	1	1 (-2)	1
	l_{2R}	$1'$		
	l_{3R}	$1''$		
Right-handed neutrinos	N_{iR}	3	1 (0)	-1

Table 4.1: The fermion content of the model. The transformation properties under $A4$ and $SU(2)_L$ are shown. The hypercharge of the fields, Y, and their lepton number, L, are also indicated.

In the proposed model the left-handed lepton doublets of the three flavours are assumed to form an $A4$ triplet while the right-handed charged leptons are taken as $1(e_R)$, $1'(\mu_R)$, and $1''(\tau_R)$ under $A4$. The remaining leptons, the right-handed neutrinos, form an $A4$ triplet[70]. The lepton content of the model with the $A4$ and $SU(2)_L$ properties as well as the lepton number assignments is shown in Table 4.1. Note that the right-handed neutrinos are assigned lepton number -1. This choice is made to ensure that the neutrino Dirac mass matrix takes a form proportional to the identity matrix, as we remark in the following. The assignment of $A4$ quantum

[70]We closely follow the notation of [69].

numbers of the leptons is by no means unique. The entire list of options for this have been catalogued in [74]. Our choice corresponds to class B of [74]. We do not discuss the extension of this model to the quark sector[71].

Mass of	Notations	$A4$	$SU(2)_L$ (Y)	L
Charged fermion	$\Phi = \begin{pmatrix} \phi_1^+ & \phi_1^0 \\ \phi_2^+ & \phi_2^0 \\ \phi_3^+ & \phi_3^0 \end{pmatrix}$	3	2 (1)	0
Neutrino Dirac	$\eta = (\eta^0, \eta^-)$	1	2 (-1)	2
Type I seesaw	$\hat{\Delta}^L = \begin{pmatrix} \hat{\Delta}_1^{++} & \hat{\Delta}_1^+ & \hat{\Delta}_1^0 \\ \hat{\Delta}_2^{++} & \hat{\Delta}_2^+ & \hat{\Delta}_2^0 \\ \hat{\Delta}_3^{++} & \hat{\Delta}_3^+ & \hat{\Delta}_3^0 \end{pmatrix}^L$	3	3 (2)	-2
Type I seesaw	$\Delta_\zeta^L = (\Delta_\zeta^{++}, \Delta_\zeta^+, \Delta_\zeta^0)^L$	1	3 (2)	-2
		$1'$	3 (2)	-2
		$1''$	3 (2)	-2
Right-handed neutrino	$\hat{\Delta}^R = \begin{pmatrix} \hat{\Delta}_1^0 \\ \hat{\Delta}_2^0 \\ \hat{\Delta}_3^0 \end{pmatrix}^R$	3	1 (0)	2
Right-handed neutrino	$\Delta_3^R = (\Delta_3^0)^R$	$1''$	1 (0)	2

Table 4.2: The scalar content of the model. The transformation properties under $A4$ and $SU(2)_L$ are shown. The hypercharge of the fields, Y, and their lepton number, L are also indicated.

All lepton masses arise from $A4$-invariant Yukawa-type couplings. This requires several scalar fields[72] which develop appropriate vacuum expectation values. To generate the charged lepton masses one uses an $SU(2)_L$ doublet $A4$ triplet of scalar fields Φ_i $(i = 1, 2, 3)$. The Type II seesaw for left-handed neutrino masses requires

[71] For $A4$-based models dealing with the quark sector see, for example, [75] and [76].

[72] Alternate $A4$ models address this issue by separating the $SU(2)_L$ and $A4$ breakings [70]. The former proceeds through the conventional doublet and triplet scalars which do not transform under $A4$. The $A4$ breaking is triggered through the *vev* of $SU(2)_L$ singlet 'flavon' scalars which transform non-trivially under $A4$. While economy is indeed a virtue here, one pays a price in the form of the effective dimension-5 interactions which have to be introduced to couple the fermion fields simultaneously to the two types of scalars.

$SU(2)_L$ triplet scalars. The product rule in Eq. (4.3) indicates that these could be in the triplet ($\hat{\Delta}_i^L$), or the singlet 1, 1′, 1″ ($\Delta_\zeta^L,\ \zeta = 1,2,3$) representations of $A4$. As discussed in the following, *all* of these are required to obtain the dominant Type II seesaw neutrino mass matrix of the form of our choice. The Type I seesaw results in a smaller contribution whose effect is included perturbatively. For the Dirac mass matrix of the neutrinos an $A4$ singlet $SU(2)_L$ doublet η, with lepton number -1, is introduced[73]. The right-handed neutrino mass matrix also arises from Yukawa couplings which respect $A4$ symmetry[74]. The scalar fields required for this are all $SU(2)_L$ singlets and under $A4$ they transform as triplet ($\hat{\Delta}_i^R$) or the singlet 1″ (Δ_3^R). The scalar fields of the model, their transformation properties under the $A4$ and $SU(2)_L$ groups, and their lepton numbers are summarized in Table 4.2.

The Type I and Type II mass terms for the neutrinos as well as the charged lepton mass matrix arise from the $A4$ and $SU(2)_L$ conserving Lagrangian[75]:

$$\begin{aligned}
\mathscr{L}_{mass} &= y_j \rho_{jik} \bar{l}_{Li} l_{Rj} \Phi_k^0 \quad \text{(charged lepton mass)} \\
&+ f \rho_{1ik} \bar{\nu}_{Li} N_{Rk} \eta^0 \quad \text{(neutrino Dirac mass)} \\
&+ \Big[\frac{1}{2}(\hat{Y}^L\ \alpha_{ijk} \nu_{Li}^T C^{-1} \nu_{Lj} \hat{\Delta}_k^{L0} \\
&+ Y_\zeta^L\ \rho_{\zeta ij} \nu_{Li}^T C^{-1} \nu_{Lj} \Delta_\zeta^{L0})\Big] \quad \text{(neutrino Type II seesaw mass)} \\
&+ \Big[\frac{1}{2}(\hat{Y}^R\ \alpha_{ijk} N_{Ri}^T C^{-1} N_{Rj} \hat{\Delta}_k^{R0} \\
&+ Y_3^R\ \rho_{3ij} N_{Ri}^T C^{-1} N_{Rj} \Delta_3^{R0})\Big] \quad \text{(rh neutrino mass)} + h.c.
\end{aligned} \tag{4.6}$$

The scalar fields in the above Lagrangian get the following *vev*s (suppressing the $SU(2)_L$ part):

$$\langle \Phi^0 \rangle = \frac{v}{\sqrt{3}} \begin{pmatrix} 1 \\ 1 \\ 1 \end{pmatrix}\ ,\ \langle \hat{\Delta}^{L0} \rangle = v_L \begin{pmatrix} 1 \\ 0 \\ 0 \end{pmatrix}\ ,\ \langle \Delta_1^{L0} \rangle = \langle \Delta_2^{L0} \rangle = \langle \Delta_3^{L0} \rangle = u_L\ , \tag{4.7}$$

$$\langle \eta^0 \rangle = u\ ,\ \langle \hat{\Delta}^{R0} \rangle = v_R \begin{pmatrix} 1 \\ \omega^2 \\ \omega \end{pmatrix}\ ,\ \langle \Delta_3^{R0} \rangle = u_R\ . \tag{4.8}$$

The scalar potential involving the fields listed in Table 4.2 has many terms and is given in an Appendix. There we indicate the conditions under which the scalars achieve the *vev* listed in Eqs. (4.7) and (4.8).

[73]The assignment of opposite lepton numbers to ν_L and N_R forbids their Yukawa coupling with Φ and the Dirac mass matrix can be kept proportional to the identity.

[74]Since the right-handed neutrinos are $SU(2)_L$ singlets, in principle, one can include direct Majorana mass terms for them. These dimension three terms would break $A4$ softly.

[75]Note that the Dirac mass terms are also L conserving.

This results in the charged lepton mass matrix and the left-handed neutrino Majorana mass matrix of the following forms:

$$M_{e\mu\tau} = \frac{v}{\sqrt{3}} \begin{pmatrix} y_1 & y_2 & y_3 \\ y_1 & \omega y_2 & \omega^2 y_3 \\ y_1 & \omega^2 y_2 & \omega y_3 \end{pmatrix} \ ,$$

$$M_{\nu L} = \begin{pmatrix} (Y_1^L + 2Y_2^L)u_L & 0 & 0 \\ 0 & (Y_1^L - Y_2^L)u_L & \hat{Y}^L v_L/2 \\ 0 & \hat{Y}^L v_L/2 & (Y_1^L - Y_2^L)u_L \end{pmatrix} \ . \tag{4.9}$$

where we have chosen $Y_2^L = Y_3^L$. In the above the Yukawa couplings satisfy $y_1 v = m_e$, $y_2 v = m_\mu$, $y_3 v = m_\tau$. The Type II seesaw generates, $M_{\nu L}$, the dominant contribution to the neutrino mass matrix. In the absence of the solar splitting this involves just two masses $m_1^{(0)}$ and $m_3^{(0)}$. To obtain the requisite structure one must identify $3Y_1^L u_L = 2[2m_1^{(0)} - m_3^{(0)}]$, $3Y_2^L u_L = m_1^{(0)} + m_3^{(0)}$, and $\hat{Y}^L v_L = 2[m_1^{(0)} + m_3^{(0)}]$. The neutrino Dirac mass matrix and the mass matrix of the right-handed neutrinos are:

$$M_D = fu\, \mathbb{I} \ , \ \ M_{\nu R} = \begin{pmatrix} Y_3^R u_R & \hat{Y}^R v_R \omega/2 & \hat{Y}^R v_R \omega^2/2 \\ \hat{Y}^R v_R \omega/2 & Y_3^R u_R \omega^2 & \hat{Y}^R v_R/2 \\ \hat{Y}^R v_R \omega^2/2 & \hat{Y}^R v_R/2 & Y_3^R u_R \omega \end{pmatrix} \ . \tag{4.10}$$

The two unknown combinations appearing in M_R above are expressed as $Y_3^R u_R \equiv (2a + b)$ and $\hat{Y}^R v_R \equiv 2(b - a)$.

The mass matrices in Eq. (4.9) can be put in a more tractable form by using two transformations, the first being U_L on the left-handed fermion doublets and the other V_R on the right-handed neutrino singlets. U_L and V_R are given by

$$U_L = \frac{1}{\sqrt{3}} \begin{pmatrix} 1 & 1 & 1 \\ 1 & \omega^2 & \omega \\ 1 & \omega & \omega^2 \end{pmatrix} = V_R \ . \tag{4.11}$$

No transformation is applied on the right-handed charged leptons. In the new basis, which we call the *flavour* basis, the charged lepton mass matrix is diagonal and the entire lepton mixing resides in the neutrino sector. The mass matrices now are:

$$M_{e\mu\tau}^{flavour} = \begin{pmatrix} m_e & 0 & 0 \\ 0 & m_\mu & 0 \\ 0 & 0 & m_\tau \end{pmatrix} \ , \ \ M_{\nu L}^{flavour} = \frac{1}{2} \begin{pmatrix} 2m_1^{(0)} & 0 & 0 \\ 0 & m^+ & -m^- \\ 0 & -m^- & m^+ \end{pmatrix} \ , \tag{4.12}$$

and

$$M_D = fu\, \mathbb{I} \ , \ \ M_{\nu R}^{flavour} = \frac{1}{2} \begin{pmatrix} 0 & a & 0 \\ a & 0 & 0 \\ 0 & 0 & b \end{pmatrix} \ . \tag{4.13}$$

Here $m^\pm = m_3^{(0)} \pm m_1^{(0)}$. m^- is positive for normal ordering of masses while it is negative for inverted ordering. We use the notation $m_D = fu$.

4.3 Model implications

The $A4$ model we have presented results in the four mass matrices in Eqs. (4.12) and (4.13). The lepton mixing and CP violation will be determined, in this basis, entirely by the neutrino sector on which we focus from here on.

The left-handed neutrino mass matrix $M_{\nu L}^{flavour}$, obtained via a Type II seesaw, dominates over the Type I seesaw contribution from the mass matrices in Eq. (4.13). The contribution from the latter is included using perturbation theory.

In the 'mass basis' the left-handed neutrino mass matrix is diagonal. The columns of the diagonalising matrix are the unperturbed flavour eigenstates in this basis. We find from $M_{\nu L}^{flavour}$:

$$M^0 = M_{\nu L}^{mass} = U^{0T} M_{\nu L}^{flavour} U^0 = \begin{pmatrix} m_1^{(0)} & 0 & 0 \\ 0 & m_1^{(0)} & 0 \\ 0 & 0 & m_3^{(0)} \end{pmatrix} \quad , \tag{4.14}$$

the orthogonal matrix, U^0, being

$$U^0 = \begin{pmatrix} 1 & 0 & 0 \\ 0 & \frac{1}{\sqrt{2}} & -\frac{1}{\sqrt{2}} \\ 0 & \frac{1}{\sqrt{2}} & \frac{1}{\sqrt{2}} \end{pmatrix} . \tag{4.15}$$

From Eqs. (4.14), (4.1) and (4.15) it is seen that the solar splitting is absent, $\theta_{12} = 0,\ \theta_{13} = 0$, $\delta = 0$, and $\theta_{23} = \pi/4$.

Before proceeding with the analysis we would like to remark on the right-handed neutrino Majorana mass matrix in Eq. (4.13), $M_{\nu R}^{flavour}$, which follows from the $A4$ symmetric Lagrangian. It has a four-zero texture. This has the virtue of being of a form of $M_{\nu R}^{flavour}$ with the most number of texture zeros. For the seesaw to be operative, the matrix has to be invertible. This eliminates matrices with five texture zeros in the flavour basis. Of the 15 possibilities with four texture zeros there are only two which are invertible and also meet the requirements of the model (i.e., result in a non-zero θ_{12}, θ_{13}, and shift θ_{23} from $\pi/4$). These are:

$$M_1 = \frac{1}{2} \begin{pmatrix} 0 & a & 0 \\ a & 0 & 0 \\ 0 & 0 & b \end{pmatrix} \quad , \quad M_2 = \frac{1}{2} \begin{pmatrix} 0 & 0 & a \\ 0 & b & 0 \\ a & 0 & 0 \end{pmatrix} \quad . \tag{4.16}$$

Note, $M_1 \leftrightarrow M_2$ under $2 \leftrightarrow 3$ exchange[76]. The results from these two alternatives are very similar except for a few relative signs in the interrelationships among θ_{13}, θ_{12}, and θ_{23}. The $M_{\nu R}^{flavour}$ in Eq. (4.13) is of the form of M_1. We remark in the end about the changes which entail if the M_2 alternative is used.

[76] In the Lagrangian in Eq. (4.6) the replacement $\Delta_3^R \to \Delta_2^R$, where Δ_2^R transforms like a $1'$ under $A4$, yields an $M_{\nu R}^{flavour}$ of the form of M_2.

Taking a and b as complex we express $M_{\nu R}^{flavour}$ as:

$$M_{\nu R}^{flavour} = m_R \begin{pmatrix} 0 & xe^{-i\phi_1} & 0 \\ xe^{-i\phi_1} & 0 & 0 \\ 0 & 0 & ye^{-i\phi_2} \end{pmatrix} \quad , \tag{4.17}$$

where x, y are dimensionless real constants of $\mathcal{O}(1)$ and m_R sets the mass-scale. No generality is lost by keeping the Dirac mass real.

In the flavour basis, the Type I seesaw contribution, which we treat as a perturbation, is:

$$M'^{flavour} = \left[M_D^T (M_{\nu R}^{flavour})^{-1} M_D\right] = \frac{m_D^2}{xym_R} \begin{pmatrix} 0 & y\ e^{i\phi_1} & 0 \\ y\ e^{i\phi_1} & 0 & 0 \\ 0 & 0 & x\ e^{i\phi_2} \end{pmatrix} \quad . \tag{4.18}$$

In the mass basis it is:

$$M'^{mass} = U^{0T} M'^{flavour} U^0 = \frac{m_D^2}{\sqrt{2}\ xym_R} \begin{pmatrix} 0 & y\ e^{i\phi_1} & -y\ e^{i\phi_1} \\ y\ e^{i\phi_1} & \frac{x\ e^{i\phi_2}}{\sqrt{2}} & \frac{x\ e^{i\phi_2}}{\sqrt{2}} \\ -y\ e^{i\phi_1} & \frac{x\ e^{i\phi_2}}{\sqrt{2}} & \frac{x\ e^{i\phi_2}}{\sqrt{2}} \end{pmatrix} \quad . \tag{4.19}$$

4.4 Results

After having presented the group-theoretic underpinnings of the model we now indicate its predictions which could be tested in the near future. As noted, from Eq. (4.15) one has $\theta_{23} = \pi/4$ and the other mixing angles are vanishing. Further, once a choice of m_0, the lightest neutrino mass, is made, depending on the mass ordering either $m_1^{(0)}$ or $m_3^{(0)}$ is determined. The remaining one of these two is fixed so that the atmospheric mass splitting is correctly reproduced. The solar mass splitting, θ_{12}, θ_{13} and the deviation of θ_{23} from maximality are all realized through the first order perturbation, which results in inter-relationships between them. These offer a scope of subjecting the model to experimental probing. From Eq. (4.14) it is seen that to obtain the solar mixing parameters one must take recourse to degenerate perturbation theory.

4.4.1 Real M_R ($\phi_1 = 0$ or $\pi, \phi_2 = 0$ or π)

M_R is real if the phases $\phi_{1,2}$ in Eq. (4.17) are 0 or π. For notational simplicity, instead of retaining these phases we allow x (y) to be of either sign, thus capturing the possibilities of ϕ_1 (ϕ_2) being 0 or π.

In the real limit Eq. (4.19) becomes

$$M'^{mass} = \frac{m_D^2}{\sqrt{2}\ xym_R} \begin{pmatrix} 0 & y & -y \\ y & \frac{x}{\sqrt{2}} & \frac{x}{\sqrt{2}} \\ -y & \frac{x}{\sqrt{2}} & \frac{x}{\sqrt{2}} \end{pmatrix} \quad . \tag{4.20}$$

The effect of this perturbation on the degenerate solar sector is obtained from the following 2×2 submatrix of the above,

$$M'^{mass}_{2\times 2} = \frac{m_D^2}{\sqrt{2}\ xym_R} \begin{pmatrix} 0 & y \\ y & x/\sqrt{2} \end{pmatrix} \ . \tag{4.21}$$

This yields

$$\tan 2\theta_{12} = 2\sqrt{2} \left(\frac{y}{x}\right) \ . \tag{4.22}$$

From the data, $\tan 2\theta_{12} > 0$ always, implying x and y have to be either both positive or both negative. In other words, $\phi_1 = \phi_2$ and can be either 0 or π. Moreover, from the data $2\theta_{12} < \frac{\pi}{2}$ at 3σ. This implies that only $x, y > 0$ is allowed or equivalently $\phi_1 = \phi_2 = 0$. The fitted range of θ_{12} translates to

$$0.695 < \frac{y}{x} < 1.112 \text{ at } 3\sigma \ . \tag{4.23}$$

Eq. (4.21) also implies

$$\Delta m^2_{solar} = \frac{m_D^2}{xym_R}\ m_1^{(0)} \sqrt{x^2 + 8y^2} \ . \tag{4.24}$$

Including the first-order corrections from Eq. (4.20) the wave function for the non-degenerate state, $|\psi_3\rangle$, becomes:

$$|\psi_3\rangle = \begin{pmatrix} -\kappa \\ -\frac{1}{\sqrt{2}}(1 - \frac{\kappa}{\sqrt{2}}\frac{x}{y}) \\ \frac{1}{\sqrt{2}}(1 + \frac{\kappa}{\sqrt{2}}\frac{x}{y}) \end{pmatrix} \quad , \tag{4.25}$$

with

$$\kappa \equiv \frac{m_D^2}{\sqrt{2}\ xm_R m^-} \quad . \tag{4.26}$$

The sign of κ is the same as that of m^-. Comparing with the third column of Eq. (4.1) one then has

$$\sin\theta_{13}\cos\delta = -\kappa = -\frac{m_D^2}{\sqrt{2}\ xm_R m^-} \quad . \tag{4.27}$$

In the case of normal ordering $\delta = \pi$ while for inverted ordering $\delta = 0$, CP remaining conserved in both cases[77]. Notice the difference from the result in Chapter 3 where NO (IO) corresponds to $\delta = 0 \ \ (\pi)$ for real M_R. From Eqs. (4.27), (4.22), and (4.24) one can write,

$$\Delta m^2_{solar} = m^- m_1^{(0)}\ \frac{4\sin\theta_{13}\cos\delta}{\sin 2\theta_{12}} \ , \tag{4.28}$$

which relates[78] the solar sector with θ_{13}. Once the neutrino mass splittings, and the angles θ_{12}, and θ_{13} are given, Eq. (4.28) fixes the lightest neutrino mass, m_0.

[77]Recall, the mixing angles θ_{ij} are kept in the first quadrant and δ ranges from $-\pi$ to π, as is the convention.

[78]It is readily seen from Eq. (4.27) that $m^-\cos\delta$ is always positive, ensuring $\Delta m^2_{solar} > 0$.

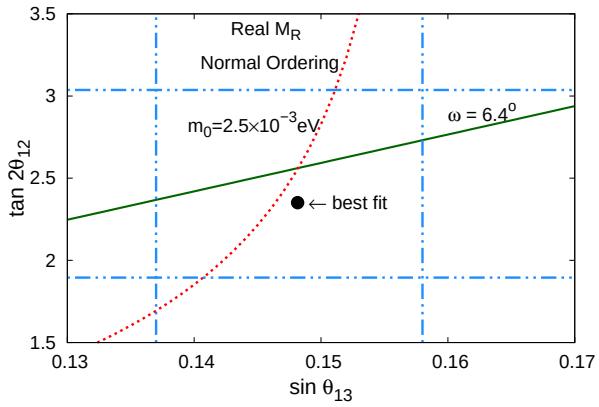

Figure 4.1: The area inside blue dot-dashed box in the $\sin\theta_{13}$ - $\tan 2\theta_{12}$ plane is allowed by the experimental data at 3σ. The best-fit point is shown as a black dot. The red dotted curve gives the best-fit solar splitting – from Eq. (4.28) – for $m_0 = 2.5$ meV. Using Eq. (4.32) for θ_{23} the area excluded at 3σ is below the green solid straight line for the first octant. Only normal ordering is allowed for real M_R.

It can be checked that Eq. (4.28) does not permit inverted ordering. To this end, one defines $z \equiv m^- m_1^{(0)}/\Delta m^2_{atmos}$ and $\tan\xi \equiv m_0/\sqrt{|\Delta m^2_{atmos}|}$. Note that z is positive for both mass orderings and one has:

$$\begin{aligned} z &= \sin\xi/(1+\sin\xi) \ \text{(normal ordering)}, \\ z &= 1/(1+\sin\xi) \ \text{(inverted ordering)} \ . \end{aligned} \tag{4.29}$$

This implies $0 \leq z \leq 1/2$ for NO while $1/2 \leq z \leq 1$ for IO. In both cases z approaches $1/2$ as $m_0 \to$ large, i.e., one tends towards quasidegeneracy. From Eq. (4.28)

$$z = \left(\frac{\Delta m^2_{solar}}{|\Delta m^2_{atmos}|}\right)\left(\frac{\sin 2\theta_{12}}{4\sin\theta_{13}|\cos\delta|}\right) \ . \tag{4.30}$$

Bearing in mind that for real M_R one has $|\cos\delta| = 1$ and using the measured values of the other oscillation parameters one finds $z \sim 10^{-2}$. This excludes the inverted mass ordering option.

Further, Eq. (4.25) implies:

$$\tan\theta_{23} \equiv \tan(\pi/4-\omega) = \frac{1-\frac{\kappa}{\sqrt{2}}\frac{x}{y}}{1+\frac{\kappa}{\sqrt{2}}\frac{x}{y}} \ . \tag{4.31}$$

Taken together with Eqs. (4.22) and (4.27) one has

$$\tan\omega = \frac{\kappa}{\sqrt{2}}\frac{x}{y} = -\frac{2\sin\theta_{13}\cos\delta}{\tan 2\theta_{12}} \ . \tag{4.32}$$

As noted, for NO, which is the only allowed ordering, one has $\delta = \pi$. Thus ω is positive and θ_{23} is in the first octant.

We are now in a position to state the consequences of this model for real M_R. There are three independent input parameters, namely, m_0, κ, and y/x which determine $\theta_{12}, \theta_{13}, \theta_{23}$, and Δm^2_{solar} for NO. For real M_R inverted ordering is not permitted.

In Fig. 4.1 the main consequences of this model for real M_R are displayed. It is similar to what has already been noted in Chapter 3. The region inside the blue dot-dashed box is the 3σ range of $\sin\theta_{13}$ and $\tan 2\theta_{12}$ from the global fits, the best-fit point being the black dot. From the data in Sec. 1.1.2 $\omega_{min} = 0$ at 3σ and $\omega_{max} = 6.4^\circ$ for the first octant. For ω_{max} Eq. (4.32) of this model corresponds to the green solid straight line, the area below being excluded. Further, for real M_R, as $\cos\delta = 1$, from Eq. (4.32) we get $\omega \geq 5.14^\circ$. So far, we have not considered the solar mass splitting. Once Δm^2_{solar} and $|\Delta m^2_{atmos}|$ are specified, the z (or equivalently m_0) that produces the correct solar splitting for any chosen point in the plane is determined by Eq. (4.30). In this way, using the 3σ ranges of θ_{13} and θ_{12} one finds $z_{max} = 6.03 \times 10^{-2}$, corresponding to $(m_0)_{max} = 3.10$ meV. The consistency of Eq. (4.30) with Eq. (4.32) at ω_{max} sets $z_{min} = 4.01 \times 10^{-2}$ for the first octant which translates to $(m_0)_{min} = 2.13$ meV. As an example, choosing $m_0 = 2.5$ meV and taking the best-fit points of the solar and atmospheric mass splittings Eq. (4.28) gives the red dotted curve in Fig. 4.1.

4.4.2 Complex M_R

The shortcomings of the real M_R case – no CP violation, inverted ordering disallowed – can be overcome when M_R is complex. One then has, as in Eq. (4.19),

$$M'^{mass} = \frac{m_D^2}{\sqrt{2}xym_R} \begin{pmatrix} 0 & ye^{i\phi_1} & -ye^{i\phi_1} \\ ye^{i\phi_1} & \frac{xe^{i\phi_2}}{\sqrt{2}} & \frac{xe^{i\phi_2}}{\sqrt{2}} \\ -ye^{i\phi_1} & \frac{xe^{i\phi_2}}{\sqrt{2}} & \frac{xe^{i\phi_2}}{\sqrt{2}} \end{pmatrix} . \tag{4.33}$$

x and y are now both positive. Since M' is not hermitian any more the hermitian combination $(M^0 + M')^\dagger (M^0 + M')$ is considered, treating $M^{0\dagger}M^0$ as the unperturbed piece and $H'^{mass} \equiv (M^{0\dagger}M' + M'^\dagger M^0)$ as the perturbation at lowest order. The zero-order eigenvalues are $(m_i^{(0)})^2$. Written as a 3×3 hermitian matrix the perturbation is

$$H'^{mass} = \frac{m_D^2}{\sqrt{2}xym_R} \begin{pmatrix} 0 & 2m_1^{(0)} y\cos\phi_1 & -yf(\phi_1) \\ 2m_1^{(0)} y\cos\phi_1 & \frac{2}{\sqrt{2}} m_1^{(0)} x\cos\phi_2 & \frac{1}{\sqrt{2}} xf(\phi_2) \\ -yf^*(\phi_1) & \frac{1}{\sqrt{2}} xf^*(\phi_2) & \frac{2}{\sqrt{2}} m_3^{(0)} x\cos\phi_2 \end{pmatrix} . \tag{4.34}$$

Above

$$f(\varphi) = m^+ \cos\varphi - im^- \sin\varphi \ . \tag{4.35}$$

Eq. (4.34) provides the basis for the remaining calculation.

In a manner similar to the real M_R case, from Eq. (4.34) we get

$$\tan 2\theta_{12} = 2\sqrt{2}\ \frac{y}{x}\ \frac{\cos\phi_1}{\cos\phi_2} \ . \tag{4.36}$$

Since $\tan 2\theta_{12}$ remains positive at 3σ, $\cos\phi_1$ and $\cos\phi_2$ must be of the same sign. Further, $\cos 2\theta_{12}$ and $\sin 2\theta_{12}$ are both positive from allowed range of θ_{12} in Eq. (1.24). This implies $\cos\phi_1 > 0$, $\cos\phi_2 > 0$. The allowed possibilities for these phases are shown in Table 4.3. We can take over the limits in Eq. (4.23) which now apply on $(y/x)(\cos\phi_1/\cos\phi_2)$.

In place of Eq. (4.25) we now have at first order:

$$|\psi_3\rangle = \begin{pmatrix} -\kappa f(\phi_1)/m^+ \\ -\frac{1}{\sqrt{2}}[1 - \frac{\kappa}{\sqrt{2}}\frac{x}{y}\, f(\phi_2)/m^+] \\ \frac{1}{\sqrt{2}}[1 + \frac{\kappa}{\sqrt{2}}\frac{x}{y}\, f(\phi_2)/m^+] \end{pmatrix} . \tag{4.37}$$

Since x, y are now positive quantities, the sign of κ is determined by that of m^-, i.e., κ is positive (negative) for normal (inverted) ordering. From Eqs. (4.1) and (4.37)

$$\begin{aligned} \sin\theta_{13}\cos\delta &= -\kappa\cos\phi_1 \ , \\ \sin\theta_{13}\sin\delta &= -\kappa\,\frac{m^-}{m^+}\sin\phi_1 \ . \end{aligned} \tag{4.38}$$

Using Eq. (4.38) one can immediately relate the quadrant of δ with that of ϕ_1 for both orderings. These are also presented in Table 4.3. Notice[79] that near maximal values of δ can be obtained in all cases for a suitable choice of ϕ_1. As an example for NO (IO) if $\phi_1 = \frac{\pi}{2} - \epsilon$ then $\delta \simeq -\frac{\pi}{2} + \epsilon$ ($\simeq -\frac{\pi}{2} - \epsilon$) while $\phi_1 = -\frac{\pi}{2} + \epsilon$ implies $\delta \simeq \frac{\pi}{2} + \epsilon$ ($\simeq \frac{\pi}{2} - \epsilon$).

ϕ_1 quadrant	ϕ_2 quadrant	Normal Ordering		Inverted Ordering	
		δ quadrant	θ_{23} octant	δ quadrant	θ_{23} octant
$0-\pi/2$	$0-\pi/2$ or -$\pi/2-0$	-π − -$\pi/2$	$0-\pi/4$	-$\pi/2-0$	$\pi/4-\pi/2$
-$\pi/2-0$	$0-\pi/2$ or -$\pi/2-0$	$\pi/2-\pi$	$0-\pi/4$	$0-\pi/2$	$\pi/4-\pi/2$

Table 4.3: The options for the phase ϕ_1 in M_R and the consequent ranges of the other phase ϕ_2 in M_R, the leptonic CP phase δ, and the octant of θ_{23} for both mass orderings. All angles are in radians. For inverted ordering or quasidegeneracy $\delta \sim \pi/2$ or $-\pi/2$.

In addition, for θ_{23} Eq. (4.37) implies

$$\tan\theta_{23} = \frac{1 - \frac{\kappa}{\sqrt{2}}\frac{x}{y}\cos\phi_2}{1 + \frac{\kappa}{\sqrt{2}}\frac{x}{y}\cos\phi_2} \quad . \tag{4.39}$$

The deviation from maximality, ω, can be obtained from the above and using Eqs. (4.36) and (4.38) expressed as

$$\tan\omega = -\frac{2\sin\theta_{13}\cos\delta}{\tan 2\theta_{12}} \ , \tag{4.40}$$

[79]We point again about the prominent difference from the Chapter 3 result in the correlation of mass ordering and the allowed quadrants of δ.

which has the same form as Eq. (4.32) for the real M_R case except that now $\cos\delta$ can deviate from ± 1. The octant of θ_{23} for different choices of ϕ_1 quadrants is given in Table 4.3 for both mass orderings. Note that NO (IO) always goes with first (second) octant as in Chapter 3 model.

Substituting for m_D^2/m_R in terms of $\sin\theta_{13}\cos\delta$, using Eq. (4.38) one has from Eq. (4.34)

$$\Delta m^2_{solar} = -\, m^- m_1^{(0)}\, \frac{4\sin\theta_{13}\cos\delta}{\sin 2\theta_{12}}\ , \tag{4.41}$$

which is reminiscent of Eq. (4.28) for real M_R. Keeping in mind that $\cos\phi_1/\cos\phi_2$ must be positive and using Eq. (4.38) it is easy to see that $\Delta m^2_{solar} > 0$ always.

As in Eq. (4.30) one again has

$$|\cos\delta| = \left(\frac{\Delta m^2_{solar}}{|\Delta m^2_{atmos}|}\right)\left(\frac{\sin 2\theta_{12}}{4\sin\theta_{13}\ z}\right)\ , \tag{4.42}$$

with the further proviso that $|\cos\delta|$ can now be anywhere between zero and unity. This freedom removes the bar which applied on inverted ordering for real M_R.

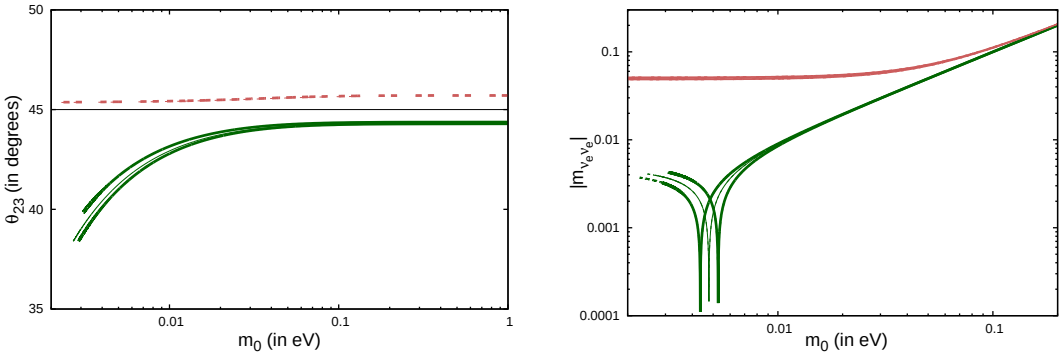

Figure 4.2: θ_{23} (left panel) and $|m_{\nu_e\nu_e}|$, the quantity controlling neutrinoless double beta decay, in eV (right panel) as a function of the lightest neutrino mass m_0 (in eV). The green (pink) curves are for NO (IO). The 3σ allowed region is between the thick curves while the thin curves are for the best-fit input values. The solid (dashed) curves are for the first (second) octant of θ_{23}.

Here we use m_0, θ_{13}, and θ_{12} as inputs to fix the model parameters. Eqs. (4.40) and (4.42) then determine θ_{23} and δ respectively, as shown in Figs. 4.2 and 4.3. One can also obtain $|m_{\nu_e\nu_e}|$, which determines the neutrinoless double beta decay rate, in terms of the mass eigenvalues and the mixing angles. In these figures the green (pink) curves are for NO (IO).

In the left panel of Fig. 4.2 the dependence of θ_{23} on m_0 is presented while the right panel shows $|m_{\nu_e\nu_e}|$ again as a function of m_0. The thick lines delimit the 3σ allowed regions while the thin lines correspond to the best-fit values of input parameters. The solid (dashed) curves are for the first (second) octant of θ_{23} i.e., NO (IO). The thick and thin curves for IO overlap and cannot be distinguished.

The experimental 3σ bound on θ_{23} determines a minimum permitted m_0 for NO. For IO there is no such lower bound. Planned experiments to measure the neutrino mass [19] are sensitive to m_0 not less than 200 meV. From Fig. 4.2 it is seen that at such a scale the two mass orderings have close predictions though in different octants, which is a reflection of quasidegeneracy.

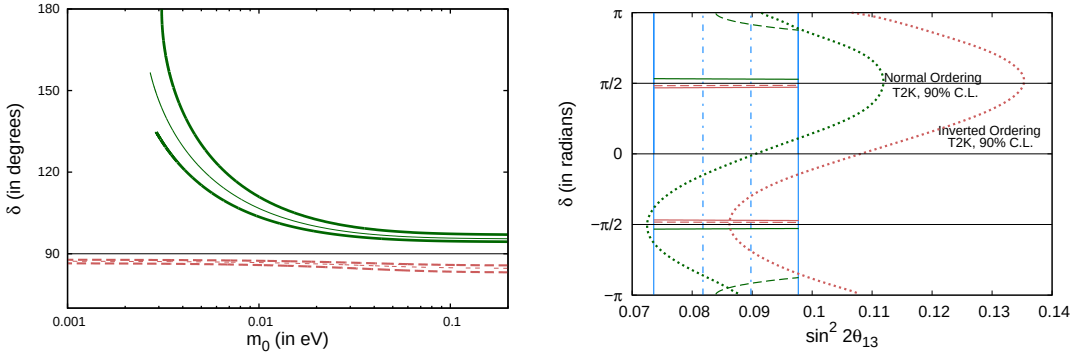

Figure 4.3: The CP phase δ from this model. The green (pink) curves are for NO (IO). Left: δ as a function of m_0 in eV. The line-type conventions are as in Fig. 4.2. Results are shown only for the first and second quadrants. Right: The blue vertical solid (dot-dashed) lines are the 3σ (1σ) allowed ranges of $\sin^2 2\theta_{13}$ from global fits. Dependence of δ for $m_0 = 0.5$ eV ($m_0 = 2.5$ meV) on $\sin^2 2\theta_{13}$ within the allowed range are the solid (dashed) lines. Also shown are the 90% C.L. curves (dotted) obtained by T2K [9] which disallow the region to their left.

In the left panel of Fig. 4.3 we show the dependence of δ on m_0 for both NO and IO. The line-type conventions are the same as in Fig. 4.2. As noted in Table 4.3 and Eq. (4.38), δ can be in any of the second and third (first and fourth) quadrants for NO (IO) depending on the choice of ϕ_1. Eq. (4.42) indicates that for all these four cases, namely, $\pm\delta$ and $\pm(\pi - \delta)$, the dependence of $|\cos\delta|$ on m_0 is identical for a chosen mass ordering. Keeping this in mind, Fig. 4.3 (left panel) has been plotted with δ in the second quadrant for NO and first quadrant for IO. For m_0 smaller than ~ 10 meV, δ changes sharply for normal ordering. As expected from Fig. 4.1, the real M_R limit, i.e., $\delta = \pi$, is obtained only for NO.

The variation of δ with $\sin^2 2\theta_{13}$ obtained from Eq. (4.41) for both mass orderings for two representative values of $m_0 = 0.5$ eV (solid curves) and 2.5 meV (dashed curves) is shown in the right panel of Fig. 4.3. Here the best-fit values of the two mass splittings and θ_{12} have been used. The allowed range of $\sin^2 2\theta_{13}$ from the global fits at 3σ (1σ) is bounded by the blue solid (dot-dashed) vertical lines. For IO δ remains close to but less (more) than $+\pi/2$ ($-\pi/2$) for all m_0. For NO, with $m_0 = 0.5$ eV, δ is slightly above (below) but close to $+\pi/2$ ($-\pi/2$) while for m_0 = 2.5 meV one finds δ around $\pm\pi$ and that too for a limited range of $\sin^2 2\theta_{13}$. In this panel we have also shown 90% C.L. exclusion limits in the $\sin^2 2\theta_{13} - \delta$ plane – dotted curves – identified by the T2K collaboration. The regions to the left of the curves are disfavoured. Notice that $\delta = -\pi/2$ is preferred, which in our model is consistent with IO for all masses but a limited range of $\sin^2 2\theta_{13}$ while for NO

though the full range of the latter is consistent one must have $m_0 \geq 100$ meV. More precise measurements of neutrino parameters will test this model closely.

Finally, it is noteworthy that the phase ϕ_2 enters only in two places: in the combination $x \cos\phi_2/y$ in the expressions for $\tan 2\theta_{12}$ and $\tan\theta_{23}$ - Eqs. (4.36) and (4.39). So, its effect can be entirely subsumed by redefining $\cos\phi_2/y \to 1/y$. Therefore for complex M_R the free input parameters are really m_0, κ, y/x and ϕ_1 which determine the three mixing angles, the solar mass splitting, and the CP phase δ.

Before concluding, we would like to make a comment on our choice of M_R. In Eq. (4.16) two four-zero textures, M_1 and M_2, were identified both of which could be admissible for M_R. We had chosen M_1 for this work. If instead, we had chosen M_2 then the discussion would go through essentially unchanged except for the replacement $\kappa \to -\kappa$. This would bring the model to a close match of the results in Chapter 3.

4.5 Conclusions

In this chapter we have proposed a model for neutrino masses and lepton mixing which relies on an underlying $A4$ symmetry. All masses are generated from $A4$ invariant Yukawa couplings. There are contributions to the neutrino masses from both Type I and Type II seesaw terms of which the latter is dominant. It generates the atmospheric mass splitting and keeps the mixing angles either maximal, e.g., $\pi/4$ for θ_{23}, or vanishing, for θ_{13} and θ_{12}. The solar splitting is absent. The Type I seesaw contribution, which is treated perturbatively, results in θ_{13}, θ_{12}, and θ_{23} consistent with the global fits and generates the solar splitting. Testable relationships between these quantities, characteristic of this model, are derived. In particular, normal ordering is associated with first octant of θ_{23} while for inverted ordering only the second octant is allowed. As another example, inverted ordering of neutrino masses is correlated with a near-maximal CP phase δ and allows arbitrarily small neutrino masses. For normal ordering δ can vary over the entire range and approaches maximality in the quasidegenerate limit. The lightest neutrino mass cannot be lower than a few meV in this case.

4.A Appendix: The scalar potential minimization

In this Appendix we discuss the nature of the scalar potential of the model in some detail. We also identify the conditions which must be satisfied by the parameters of the potential so that the *vev*s take the values considered in the model. Needless

to say, the conditions ensure that the potential is locally minimized by this choice. To check whether it is also a *global* minimum is beyond the scope of this thesis[80].

The scalars listed in Table 4.2 have fields transforming under $A4$, $SU(2)_L$, and $U(1)_Y$ which also carry a lepton number. The scalar potential has to be of the most general quartic form which is a singlet under all these symmetries. Below we include all terms that are permitted by the symmetries. Invariance under $SU(2)_L$, $U(1)_Y$ and lepton number are easy to verify.

4.A.1 $A4$ invariants: Notation and generalities

Here we give a brief account of our notation and the $A4$-invariant terms. First recall that there are scalars which transform as $1, 1', 1''$, and 3 under $A4$. One must include in the potential up to quartics in these fields which give rise to $A4$ singlets. The product rules of the one-dimensional representations $1, 1'$ and $1''$ are simple, it is the $A4$ triplet which requires some discussion. To this end consider two $A4$ triplet fields $A \equiv (a_1, a_2, a_3)^T$ and $B \equiv (b_1, b_2, b_3)^T$ where a_i, b_i may have $SU(2)_L \times U(1)_Y$ transformation properties which we suppress here. As noted in Eq. (4.3), combining A and B one can obtain

$$3_A \otimes 3_B = 1 \oplus 1' \oplus 1'' \oplus 3 \oplus 3 \ . \tag{4.A.1}$$

We denote the irreducible representations on the right-hand-side by $O_1(A,B)$, $O_2(A,B)$, $O_3(A,B)$, $T_s(A,B)$ and $T_a(A,B)$, respectively, where, as noted in Eqs. (4.4, 4.5)

$$\begin{aligned} O_1(A,B) &\equiv 1 = a_1b_1 + a_2b_2 + a_3b_3 \equiv \rho_{1ij} a_i b_j \ , \\ O_2(A,B) &\equiv 1' = a_1b_1 + \omega^2 a_2b_2 + \omega a_3b_3 \equiv \rho_{3ij} a_i b_j \ , \\ O_3(A,B) &\equiv 1'' = a_1b_1 + \omega a_2b_2 + \omega^2 a_3b_3 \equiv \rho_{2ij} a_i b_j \ , \end{aligned} \tag{4.A.2}$$

and

$$\begin{aligned} T_s(A,B) &\equiv 3 = \left(\frac{a_2b_3 + a_3b_2}{2}, \ \frac{a_3b_1 + a_1b_3}{2}, \ \frac{a_1b_2 + a_2b_1}{2} \right)^T \ , \\ T_a(A,B) &\equiv 3 = \left(\frac{a_2b_3 - a_3b_2}{2}, \ \frac{a_3b_1 - a_1b_3}{2}, \ \frac{a_1b_2 - a_2b_1}{2} \right)^T \ . \end{aligned} \tag{4.A.3}$$

Note that $O_3(A^\dagger, A) = [O_2(A^\dagger, A)]^\dagger$ and $T_a(A,A) = 0$.

The scalar potential can be written in this notation keeping in mind the following:

- No two scalar multiplets have all quantum numbers the same. So terms in the potential cannot be related by replacing any one field by some other.

[80] For example, the global minima of the relatively simple case of one $A4$ triplet $SU(2)_L$ doublet scalar multiplet have been identified in [77] and used in the context of a model for leptons in [78].

- Neither is there a scalar which is a singlet under all the symmetries.

Thus the scalar potential can consist of terms of the following forms (displaying only $A4$ behaviour):

1. Quadratic: $W^\dagger W$,
2. Cubic: $X_i X'_j X''_k, X_i X_j X_k,\ X'_i X'_j X'_k,\ X''_i X''_j X''_k,\ O_1(Y_i,Y_j)X_k,\ O_2(Y_i,Y_j)X''_k,$ $O_3(Y_i,Y_j)X'_k,$
3. Quartic: $(W_i^\dagger W_i)(W_j^\dagger W_j),\ (X_i X_j)(X_k X_l),\ (X_i X_j)(X'_k X''_l),\ (X'_i X''_j)(X'_k X''_l),$ $(X'_i X'_j)(X'_k X_l), (X''_i X''_j)(X''_k X_l), O_1(Y_i,Y_j)X_k X_l,\ O_1(Y_i,Y_j)X'_k X''_l,$ $O_2(Y_i,Y_j)X'_k X'_l,\ O_2(Y_i,Y_j)X_k X''_l, O_3(Y_i,Y_j)X''_k X''_l,\ O_3(Y_i,Y_j)X_k X'_l,$ $O_1(Y_i,Y_j)O_1(Y_k,Y_l), O_2(Y_i,Y_j)^\dagger O_2(Y_k,Y_l), O_3(Y_i,Y_j)^\dagger O_3(Y_k,Y_l),$ $O_2(Y_i,Y_j)O_3(Y_k,Y_l), O_1(T_s(Y_i,Y_j),T_s(Y_k,Y_l)),$ $O_1(T_s(Y_i,Y_j),T_a(Y_k,Y_l)), O_1(T_a(Y_i,Y_j),T_a(Y_k,Y_l)), O_1(T_s(Y_i,Y_j),Y_k)X_l,$ $O_2(T_s(Y_i,Y_j),Y_k)X''_l,\ O_3(T_s(Y_i,Y_j),Y_k)X'_l,$ $O_1(T_a(Y_i,Y_j),Y_k)X_l,\ O_2(T_a(Y_i,Y_j),Y_k)X''_l,\ O_3(T_a(Y_i,Y_j),Y_k)X'_l\ .$

In the above W is any field, X, X', and X'' stand for generic fields transforming as 1, 1′, and 1″ under $A4$ while Y is a generic $A4$ triplet field. We have not separately listed the invariants formed using $X^\dagger$, $X'^\dagger$, $X''^\dagger$, and $Y^\dagger$.

Because of the large number of scalar fields in our model – e.g., $SU(2)_L$ singlets, doublets, and triplets – the scalar potential has many terms. To simplify this discussion, we exclude cubic terms in the fields and take all couplings in the potential to be real. For ease of presentation, we list the potential in separate pieces: (a) those restricted to any one $SU(2)_L$ sector, and (b) those coupling scalars of different $SU(2)_L$ sectors. Since the *vev* of the $SU(2)_L$ singlets, which are responsible for the right-handed neutrino mass, are much larger than that of the other scalars, in the latter category we keep only the terms which couple the singlet fields to either the doublet or the triplet sectors.

4.A.2 $SU(2)_L$ Singlet Sector:

In the $SU(2)_L$ singlet scalar sector there is an $A4$ triplet $\hat{\Delta}^R$ and another scalar Δ_3^R that transforms as a 1″. Eq. (4.A.1) shows that two $\hat{\Delta}^R$ triplets can combine to give different $A4$ irreducible representations. For this purpose we introduce the notations:

$$O_1^{ss} \equiv O_1(\hat{\Delta}^{R\dagger}, \hat{\Delta}^R);\ O_2^{ss} \equiv O_2(\hat{\Delta}^{R\dagger}, \hat{\Delta}^R);\ T_s^{ss} \equiv T_s(\hat{\Delta}^R, \hat{\Delta}^R). \tag{4.A.4}$$

Generically, we will use the notation $\widetilde{O}_i$ or $\widetilde{T}_{s,a}$ if the second $A4$ triplet field in the argument is replaced by its hermitian conjugate. For example, here

$$\widetilde{O}_3^{ss} \equiv O_3(\hat{\Delta}^{R\dagger}, \hat{\Delta}^{R\dagger}) \text{ and } \widetilde{T}_s^{ss} \equiv T_s(\hat{\Delta}^R, \hat{\Delta}^{R\dagger}). \tag{4.A.5}$$

We will also require the combinations:

$$\mathscr{O}_2^{ss} \equiv O_2(\hat{\Delta}^R, T_s^{ss\dagger}). \tag{4.A.6}$$

From the $A4$ singlet Δ_3^R one can make the combination

$$Q_3^{ss} \equiv \Delta_3^{R\dagger}\Delta_3^R \ , \tag{4.A.7}$$

which is obviously a singlet under all the symmetries.

Using this notation the most general scalar potential of this sector is given by:

$$\begin{aligned} V_{singlet} &= m^2_{\Delta_3^R} Q_3^{ss} + m^2_{\hat{\Delta}^R} O_1^{ss} \\ &+ \frac{1}{2}\lambda_1^s \left[Q_3^{ss}\right]^2 + \frac{1}{2}\lambda_2^s \left\{[O_1^{ss}]^2 + (O_2^{ss})^\dagger O_2^{ss} + O_1(T_s^{ss}, T_s^{ss\dagger})\right\} \\ &+ \frac{1}{2}\lambda_3^s \left[Q_3^{ss} O_1^{ss}\right] + \lambda_4^s \left[\mathscr{O}_2^{ss}\Delta_3^R + \text{ h.c.}\right] + \lambda_5^s \left[\widetilde{O}_3^{ss}\Delta_3^R\Delta_3^R + \text{ h.c.}\right] \ . \end{aligned} \tag{4.A.8}$$

In the above, we have taken λ_2^s as the common coefficient of the different $A4$ singlets that can be obtained from the combination of two $\hat{\Delta}^R$ and two $(\hat{\Delta}^R)^\dagger$ fields. We also follow a similar principle for the fields with other $SU(2)_L$ behaviour.

4.A.3 $SU(2)_L$ Doublet Sector:

The $SU(2)_L$ doublet scalar sector comprises of the two fields Φ and η transforming as 3 and 1 under $A4$ respectively. Recall that Φ and η have opposite hypercharge. In analogy to the singlet sector we denote the required $A4$ triplet Φ combinations as:

$$O_1^{dd} \equiv O_1(\Phi^\dagger, \Phi);\ O_2^{dd} \equiv O_2(\Phi^\dagger, \Phi);\ T_s^{dd} \equiv T_s(\Phi, \Phi), \tag{4.A.9}$$

and from the $A4$ singlet η

$$Q_\eta^{dd} \equiv \eta^\dagger \eta \ . \tag{4.A.10}$$

The potential for this sector is:

$$\begin{aligned} V_{doublet} &= m_\eta^2 Q_\eta^{dd} + m_\Phi^2 O_1^{dd} + \frac{1}{2}\lambda_1^d \left[Q_\eta^{dd}\right]^2 + \frac{1}{2}\lambda_2^d \left\{[O_1^{dd}]^2 + \{O_2^{dd}\}^\dagger O_2^{dd}\right. \\ &+ \left. O_1(T_s^{dd}, T_s^{dd\dagger})\right\} + \frac{1}{2}\lambda_3^d \left[Q_\eta^{dd} O_1^{dd}\right]. \end{aligned} \tag{4.A.11}$$

4.A.4 $SU(2)_L$ Triplet Sector:

The $SU(2)_L$ triplet sector consists of four fields, viz, $\hat{\Delta}^L$, Δ_1^L, Δ_2^L and Δ_3^L transforming as 3, 1, $1'$, $1''$ under $A4$.

We define

$$O_1^{tt} \equiv O_1(\hat{\Delta}^{L\dagger}, \hat{\Delta}^L);\ O_2^{tt} \equiv O_2(\hat{\Delta}^{L\dagger}, \hat{\Delta}^L);\ T_s^{tt} \equiv T_s(\hat{\Delta}^L, \hat{\Delta}^L), \tag{4.A.12}$$

$$Q_i^{tt} \equiv \Delta_i^{L\dagger}\Delta_i^L\ \ ,\ \ (i=1,2,3), \tag{4.A.13}$$

and

$$\mathscr{O}_i^{tt} \equiv O_i(\hat{\Delta}^L, T_s^{tt\dagger})\ \ (i=1,2,3). \tag{4.A.14}$$

The scalar potential for this sector:

$$\begin{aligned} V_{triplet} &= \sum_{i=1}^{3} m^2_{\Delta_i^L}\ Q_i^{tt} + m^2_{\hat{\Delta}^L}\ O_1^{tt} + \frac{1}{2}\sum_{i=1}^{3}\lambda_{1_i}^t\left[Q_i^{tt}\right]^2 + \frac{1}{2}\sum_{k<j,\,k=1}^{2}\sum_{j=2}^{3}\lambda_{2jk}^t Q_j^{tt}Q_k^{tt} \\ &+ \frac{1}{2}\lambda_3^t\left\{[O_1^{tt}]^2 + \{O_2^{tt}\}^\dagger O_2^{tt} + O_1(T_s^{tt}, T_s^{tt\dagger})\right\} + \frac{1}{2}\sum_{i=1}^{3}\lambda_{4_i}^t\left[Q_i^{tt}O_1^{tt}\right] \\ &+ \lambda_5^t\left[\mathscr{O}_1^{tt}\Delta_1^L + \text{ h.c.}\right] + \lambda_6^t\left[\mathscr{O}_3^{tt}\Delta_2^L + \text{ h.c.}\right] + \lambda_7^t\left[\mathscr{O}_2^{tt}\Delta_3^L + \text{ h.c.}\right] \\ &+ \sum_{i=1}^{3}\lambda_{8_i}^t\left[\widetilde{O}_i^{tt}\Delta_i^L\Delta_i^L + \text{ h.c.}\right] + \left[\lambda_{9_1}^t\widetilde{O}_1^{tt}\Delta_2^L\Delta_3^L + \text{ h.c.} + \text{ cyclic}\right] \end{aligned} \tag{4.A.15}$$

4.A.5 Inter-sector terms:

So far, we have listed the terms in the potential that involve scalar fields which belong to any one of three sectors: singlets, doublets, or triplets of $SU(2)_L$. Besides these, there will also be terms in the scalar potential which involve fields from multiple sectors. Below we list the terms which arise from couplings of the singlet sector with either the doublet or the triplet sector. The other inter-sector terms – doublet-triplet type – are dropped. Since the vacuum expectation values of the singlet fields are by far the largest this is not an unreasonable approximation.

Inter-sector Singlet-Doublet terms:

It is useful to define,

$$\widetilde{T}_s^{ss} \equiv T_s(\hat{\Delta}^R, \hat{\Delta}^{R\dagger}),\ \text{ and }\ \widetilde{T}_s^{dd} \equiv T_s(\Phi, \Phi^\dagger), \tag{4.A.16}$$

and

$$O_{1S}^{sd} \equiv O_1(\widetilde{T}_s^{dd}, \widetilde{T}_s^{ss});\ \mathscr{O}_3^{sd} \equiv O_3(\hat{\Delta}^R, \widetilde{T}_s^{dd})\ \ . \tag{4.A.17}$$

For simplicity, we do not keep the combinations $\widetilde{T}_a^{ss} \equiv T_a(\hat{\Delta}^R, \hat{\Delta}^{R\dagger})$ and $\widetilde{T}_a^{dd} \equiv T_a(\Phi, \Phi^\dagger)$.

In terms of the above:

$$\begin{aligned} V_{sd} &= \frac{1}{2}\lambda_1^{sd}\left[Q_3^{ss}Q_\eta^{dd}\right] + \frac{1}{2}\lambda_2^{sd}\left[Q_3^{ss}O_1^{dd}\right] + \frac{1}{2}\lambda_3^{sd}\left[Q_\eta^{dd}O_1^{ss}\right] + \lambda_4^{sd}\left[\{\mathscr{O}_3^{sd}\}^\dagger\Delta_3^R + h.c.\right] \\ &+ \frac{1}{2}\lambda_5^{sd}\left[O_1^{dd}O_1^{ss} + \{O_2^{ss}\}^\dagger O_2^{dd} + \{O_2^{dd}\}^\dagger O_2^{ss} + O_{1S}^{sd}\right]. \end{aligned} \tag{4.A.18}$$

Here, in the last term, we have made the simplifying assumption that there is a common coupling λ_5^{sd} for the terms in the potential which arise from various combinations of $(\Phi^\dagger\Phi)(\hat{\Delta}^{R\dagger}\hat{\Delta}^R)$, each of the four fields being $A4$ triplets.

Inter-sector Singlet-Triplet terms:

For this case the following combinations arise:

$$\begin{aligned} O_i^{ts} &\equiv O_i(\hat{\Delta}^{R\dagger}, \hat{\Delta}^L) \ \ (i=1,2,3); O_{1S}^{ts} \equiv O_1(\widetilde{T}_s^{tt}, \widetilde{T}_s^{ss}); \\ \mathscr{O}_i^{ts} &\equiv O_i(\widetilde{T}_s^{ss}, \hat{\Delta}^L) \ \ (i=1,2,3); \widetilde{\mathscr{O}}_3^{ts} \equiv O_3(\widetilde{T}_s^{tt}, \hat{\Delta}^R) \ . \end{aligned} \tag{4.A.19}$$

In line with the convention introduced earlier: $\widetilde{O}_i^{ts} \equiv O_i(\hat{\Delta}^{R\dagger}, \hat{\Delta}^{L\dagger}) \ \ (i=1,2,3)$.

The intersector potential for this case is given by:

$$\begin{aligned} V_{ts} &= \frac{1}{2}\sum_{i=1}^{3}\lambda_{1_i}^{ts}\left[Q_3^{ss}Q_i^{tt}\right] + \frac{1}{2}\lambda_2^{ts}\left[Q_3^{ss}O_1^{tt}\right] + \frac{1}{2}\sum_{i=1}^{3}\lambda_{3_i}^{ts}\left[Q_i^{tt}O_1^{ss}\right] \\ &+ \frac{1}{2}\lambda_4^{ts}\left[O_1^{tt}O_1^{ss} + \{O_2^{ss}\}^\dagger O_2^{tt} + \{O_2^{tt}\}^\dagger O_2^{ss} + O_{1S}^{ts}\right] \\ &+ \sum_{i=1}^{3}\lambda_{5_i}^{ts}\left[\mathscr{O}_i^{ts}\Delta_i^{L\dagger} + h.c.\right] + \lambda_6^{ts}\left[\widetilde{\mathscr{O}}_3^{ts}\Delta_3^{R\dagger} + h.c.\right] \\ &+ \lambda_7^{ts}\left[O_1^{ts}\Delta_3^{L\dagger}\Delta_3^R + h.c.\right] + \lambda_8^{ts}\left[O_2^{ts}\Delta_1^{L\dagger}\Delta_3^R + h.c.\right] + \lambda_9^{ts}\left[O_3^{ts}\Delta_2^{L\dagger}\Delta_3^R + h.c.\right] \\ &+ \lambda_{10}^{ts}\left[\widetilde{O}_3^{ts}\Delta_3^R\Delta_1^L + h.c.\right] + \lambda_{11}^{ts}\left[\widetilde{O}_2^{ts}\Delta_3^R\Delta_3^L + h.c.\right] + \lambda_{12}^{ts}\left[\widetilde{O}_1^{ts}\Delta_3^R\Delta_2^L + h.c.\right] \ . \end{aligned} \tag{4.A.20}$$

4.A.6 The minimization conditions:

After having presented the scalar potential we now seek to find the conditions under which the *vev* we have used in the model – see Eqs. (4.7) and (4.8) constitute a local minimum. For ready reference the *vev* are:

$$\langle\Phi^0\rangle = \frac{v}{\sqrt{3}}\begin{pmatrix}1\\1\\1\end{pmatrix} \ , \ \langle\hat{\Delta}^{L0}\rangle = v_L\begin{pmatrix}1\\0\\0\end{pmatrix} \ , \ \langle\hat{\Delta}^{R0}\rangle = v_R\begin{pmatrix}1\\\omega^2\\\omega\end{pmatrix} \ , \tag{4.A.21}$$

$$\langle\eta^0\rangle = u \ , \ \langle\Delta_1^{L0}\rangle = \langle\Delta_2^{L0}\rangle = \langle\Delta_3^{L0}\rangle = u_L \ , \langle\Delta_3^{R0}\rangle = u_R \ . \tag{4.A.22}$$

where the $SU(2)_L$ nature of the fields is suppressed.

It can be seen from Eq. (4.A.21) that the $A4$ triplet fields – $\hat{\Delta}^{L,R}$ and Φ – acquire *vev* which have been shown to be global minima in [77]. While this is certainly encouraging, that result is for one $A4$ triplet in isolation. Here there are many other fields and so it is not straight-forward to directly extend the results of [77].

In the following we list, sector by sector, the conditions under which the *vev* in Eqs. (4.A.21) and (4.A.22) correspond to a minimum.

$SU(2)_L$ **singlet sector:**

The *vev* of the singlet fields $\hat{\Delta}_i^R$ and Δ_3^R are much larger than those of the $SU(2)_L$ doublet and triplet scalars. So, the contributions to the minimization equations from the inter-sector terms can be neglected.

Using the singlet sector potential in Eq. (4.A.8) and the *vev* in Eqs. (4.A.21) and (4.A.22) we get (bearing in mind v_R is real):

$$\frac{\partial V_{singlet}|_{min}}{\partial u_R^*} = 0 \Rightarrow u_R \left[m^2_{\Delta_3^R} + \lambda_1^s u_R^* u_R + \frac{3}{2}\lambda_3^s v_R^2 \right] + 3v_R^2 \left[\lambda_4^s v_R + 2\lambda_5^s u_R^* \right] = 0 \ , \tag{4.A.23}$$

and

$$\begin{aligned} \frac{\partial V_{singlet}|_{min}}{\partial v_{Ri}^*} &= 0 \\ &\Rightarrow \ v_R \left[m^2_{\hat{\Delta}^R} + 4\lambda_2^s v_R^2 + \frac{\lambda_3^s}{2} u_R^* u_R + \lambda_4^s v_R (2u_R + u_R^*) + 2\lambda_5^s u_R^2 \right] = 0 \ . \end{aligned} \tag{4.A.24}$$

$SU(2)_L$ **doublet sector:**

In this sector we have to include the contributions from both the doublet sector itself – Eq. (4.A.11) – as well as the inter-sector terms in Eq. (4.A.18). We define $V_{\mathscr{D}} = V_{doublet} + V_{sd}$.

In order that the potential minimum corresponds to the *vev* in Eqs. (4.A.21) and (4.A.22) we must have:

$$\frac{\partial V_{\mathscr{D}}|_{min}}{\partial u^*} = 0 \Rightarrow u \left[2m_\eta^2 + 2\lambda_1^d u^* u + \lambda_3^d v^* v + \lambda_1^{sd} u_R^* u_R + 3\lambda_3^{sd} v_R^2 \right] = 0. \tag{4.A.25}$$

and

$$\begin{aligned} \frac{\partial V_{\mathscr{D}}|_{min}}{\partial v_i^*} &= 0 \\ &\Rightarrow \ \frac{v}{\sqrt{3}} \left[m_\Phi^2 + 4\lambda_2^d \left(\frac{v^* v}{3} \right) + \lambda_3^d u^* u + \frac{1}{2}\lambda_2^{sd} u_R^* u_R \right. \\ &+ \ \left. \lambda_4^{sd} (u_R^* + u_R) v_R + \frac{5}{4}\lambda_5^{sd} v_R^2 \right] = 0. \end{aligned} \tag{4.A.26}$$

Notice that one has to resort to some degree of fine-tuning to satisfy Eqs. (4.A.25) and (4.A.26) which involve both $SU(2)_L$ doublet and singlet *vev* of quite different magnitudes.

$SU(2)_L$ **triplet sector:**

Using Eqs. (4.A.8) and (4.A.20) we define $V_{\mathscr{T}} = V_{triplet} + V_{ts}$.

In this sector there are a plethora of couplings. To ease the presentation we choose

$$\begin{aligned}
m_{\Delta_1^L} &= m_{\Delta_2^L} = m_{\Delta_3^L} = m_{\Delta^L} \;\; ; \;\; \lambda^t_{1_1} = \lambda^t_{1_2} = \lambda^t_{1_3} = \lambda^t_a \;\; ; \;\; \lambda^t_{4_1} = \lambda^t_{4_2} = \lambda^t_{4_3} = \lambda^t_b \\
\lambda^t_{221} &= \lambda^t_{232} = \lambda^t_{231} = \lambda^t_c \;\; ; \;\; \lambda^t_{8_1} = \lambda^t_{8_2} = \lambda^t_{8_3} = \lambda^t_d \;\; ; \;\; \lambda^t_{9_1} = \lambda^t_{9_2} = \lambda^t_{9_3} = \lambda^t_e \\
\lambda^{ts}_{1_1} &= \lambda^{ts}_{1_2} = \lambda^{ts}_{1_3} = \lambda^{ts}_a \;\; ; \;\; \lambda^{ts}_{3_1} = \lambda^{ts}_{3_2} = \lambda^{ts}_{3_3} = \lambda^{ts}_b \;\; ; \;\; \lambda^{ts}_{5_1} = \lambda^{ts}_{5_2} = \lambda^{ts}_{5_3} = \lambda^{ts}_c \\
\lambda^{ts}_{10} &= \lambda^{ts}_{11} = \lambda^{ts}_{12} = \lambda^{ts}_d \;\; ; \;\; \lambda^{ts}_7 = \lambda^{ts}_8 = \lambda^{ts}_9 = \lambda^{ts}_f .
\end{aligned} \tag{4.A.27}$$

For the minimization of $V_{\mathscr{T}}$ so as to arrive at the *vev* in Eqs. (4.A.21) and (4.A.22) one must satisfy:

$$\begin{aligned}
\frac{\partial V_{\mathscr{T}}|_{min}}{\partial u_L^*} &= 0 \\
&\Rightarrow \;\; u_L \left[m^2_{\Delta^L} + (\lambda^t_a + \lambda^t_c) u_L^* u_L + \frac{1}{2}\lambda^t_b v_L^* v_L + \frac{1}{2}\lambda^{ts}_a u_R^* u_R + \frac{3}{2}\lambda^{ts}_b v_R^2 \right] \\
&+ \;\; 2 v_L^2 u_L^* (\lambda^t_d + \lambda^t_e) + v_L v_R \left[-\frac{1}{2}\lambda^{ts}_c v_R + \lambda^{ts}_d u_R^* + \lambda^{ts}_f u_R \right] = 0.
\end{aligned} \tag{4.A.28}$$

Again:

$$\begin{aligned}
\frac{\partial V_{\mathscr{T}}|_{min}}{\partial v_{L1}^*} &= 0 \\
&\Rightarrow \;\; v_L \left[m^2_{\hat{\Delta}^L} + \frac{3}{2}\lambda^t_b u_L^* u_L + 2\lambda^t_3 v_L^* v_L + \frac{1}{2}\lambda^{ts}_2 u_R^* u_R + \frac{3}{2}\lambda^{ts}_4 v_R^2 \right] \\
&+ \;\; u_L \left[6 u_L v_L^* (\lambda^t_d + \lambda^t_e) - \frac{3}{2}\lambda^{ts}_c v_R^2 + 3\lambda^{ts}_f u_R^* v_R + 3\lambda^{ts}_d u_R v_R \right] = 0.
\end{aligned} \tag{4.A.29}$$

Also we have

$$\begin{aligned}
\frac{\partial V_{\mathscr{T}}|_{min}}{\partial v_{L2}^*} &= \frac{\partial V_{\mathscr{T}}|_{min}}{\partial v_{L3}^*} = 0 \\
&\Rightarrow \;\; v_L v_R \left[-\frac{1}{4}\lambda^{ts}_4 v_R + \lambda^{ts}_6 (u_R^* + u_R) \right] = 0.
\end{aligned} \tag{4.A.30}$$

Here again fine-tuning is required to ensure that Eqs. (4.A.28) - (4.A.30) are satisfied.

Chapter 5

Seesaw model based on discrete group $S3$

5.1 Introduction

This chapter is based on our paper [38]. In this chapter we propose a neutrino mass model based on the direct product group $S3\times Z3$. The elements of $S3$ correspond to the permutations of three objects[81]. Needless to say, $S3$-based models of neutrino mass have been considered earlier [79,80]. A popular point of view [81] has been to note that a permutation symmetry between the three neutrino states is consistent with[82] (a) a democratic mass matrix, M_{dem}, all whose elements are equal, and (b) a mass matrix proportional to the identity matrix, I. A general combination of these two forms, e.g., $c_1 I + c_2 M_{dem}$, where c_1, c_2 are complex numbers, provides a natural starting point. One of the eigenstates, namely, an equal weighted combination of the three states, is one column of the popular Tribimaximal mixing matrix. Many models have been presented [81] which add perturbations to this structure to accomplish realistic neutrino masses and mixing. Variations on this theme [82] explore mass matrices with such a form in the context of Grand Unified Theories, in models of extra dimensions, and examine renormalization group effects on such a pattern realised at a high energy. Other variants of the $S3$-based models, for example [83], rely on a 3-3-1 local gauge symmetry, tie it to a $(B-L)$-extended model, or realise specific forms of mass matrices through soft symmetry breaking, etc. As discussed later, the irreducible representations of $S3$ are one and two-dimensional. The latter provides a natural mechanism to get maximal mixing in the $\nu_\mu - \nu_\tau$ sector [84].

The present model, also based on $S3$ symmetry, breaks new ground in the following directions. Firstly, it involves an interplay of Type I and Type II seesaw contributions. Secondly, it presents a general framework encompassing many popular

[81] More details of $S3$ can be found in Appendix 5.A.

[82] Note, however, there is no 3-dimensional irreducible representation of $S3$ (see Appendix 5.A). So these models entail fine tuning.

Model	TBM	BM	GR	NSM
θ_{12}^0	35.3°	45.0°	31.7°	0.0°

Table 5.1: The solar mixing angle, θ_{12}^0 for the TBM, BM, and GR mixing patterns. NSM stands for the case where the solar mixing angle is initially vanishing.

mixing patterns such as Tribimaximal mixing. Further, the model does not invoke any soft symmetry breaking terms. All the symmetries are broken spontaneously.

We briefly outline here the strategy of this work. We use the standard notation for the leptonic mixing matrix – the Pontecorvo Maki Nakagawa Sakata (PMNS) matrix – U defined in Eq. (1.15). The neutrino masses and mixings arise through a two-stage mechanism as in Chapter 4. In the first step, from the Type II seesaw the larger atmospheric mass splitting, Δm^2_{atmos}, is generated while the solar splitting, Δm^2_{solar}, is absent. Also, $\theta_{13} = 0$, $\theta_{23} = \pi/4$ and the model parameters can be varied in a continuous manner to obtain any desired θ_{12}^0. Of course, in reality $\theta_{13} \neq 0$ [12], the solar splitting is non-zero, and there are indications that θ_{23} is large but non-maximal. Experiments have also set limits on θ_{12}. The Type I seesaw addresses all the above issues and relates the masses and mixings to each other.

The starting form incorporates several well-studied mixing patterns such as TBM, BM, and GR mixings within its fold. These alternatives all have $\theta_{13} = 0$ and $\theta_{23} = \pi/4$. They differ only in the value of the third mixing angle θ_{12}^0 as displayed in Table 5.1. The fourth option in this Table, NSM, exhibits the attractive feature that the mixing angles are either maximal, i.e., $\pi/4$ (θ_{23}) or vanishing (θ_{13} and θ_{12}^0).

In the following section we furnish a description of the model including the assignment of $S3 \times Z3$ quantum numbers to the leptons and symmetry-breaking scalar fields. The consequences of the model are described next where we also compare with the experimental data. A summary and conclusions follow. The scalar potential of this model has a rich structure. In two Appendices we present the essence of $S3$ symmetry and discuss the $S3$ invariant scalar potential, deriving the conditions which must be satisfied by the scalar coefficients to obtain the desired minimum.

5.2 The Model

In the model under discussion fermion and scalar multiplets are assigned $S3 \times Z3$ quantum numbers in a manner such that spontaneous symmetry breaking naturally yields mass matrices which lead to the seesaw features espoused earlier. All terms allowed by the symmetries of the model are included in the Lagrangian. No soft symmetry-breaking terms are required.

To begin it will be useful to formulate the conceptual structure behind the model. Neutrino masses arise from a combination of Type I and Type II seesaw contri-

butions of which the latter dominates. In the neutrino mass basis, which is also the basis in which the Lagrangian will be presented, the Type II seesaw yields a diagonal matrix in which two states are degenerate:

$$M_{\nu L} = \begin{pmatrix} m_1^{(0)} & 0 & 0 \\ 0 & m_1^{(0)} & 0 \\ 0 & 0 & m_3^{(0)} \end{pmatrix} \ . \tag{5.1}$$

This mass matrix results in $\Delta m^2_{atmos} = (m_3^{(0)})^2 - (m_1^{(0)})^2$ while $\Delta m^2_{solar} = 0$. Later, we find the combinations $m^{\pm} = m_3^{(0)} \pm m_1^{(0)}$ useful. m^- signals the mass ordering; it is positive for normal ordering and negative for inverted ordering.

Fields	Notations	$S3$ ($Z3$)	$SU(2)_L(Y)$	L
Left-handed leptons	L_e L_μ L_τ	$1'$ (1) $1'$ (ω) 1 (ω)	2 (-1)	+1
Right-handed charged leptons	e_R $\begin{pmatrix}\mu_R \\ \tau_R\end{pmatrix}$	$1'$ (1) 2 (1)	1 (-2)	+1
Right-handed neutrinos	N_{1R} N_{2R} N_{3R}	$1'$ (1) $1'$ (ω) 1 (ω)	1 (0)	0

Table 5.2: The fermion content of the model. The transformation properties under $S3$, $Z3$, and $SU(2)_L$ are shown. The hypercharge of the fields, Y, and their lepton number, L, are also indicated. Here $L_\alpha^T = (\nu_\alpha \ \ l_\alpha^-)$.

At this stage the mixing resides entirely in the charged lepton sector. We follow the convention

$$\Psi_{flavour} = U_\Psi \Psi_{mass} \ , \tag{5.2}$$

for the fermions Ψ, so that the PMNS matrix, U, is given by

$$U = U_l^\dagger U_\nu \ . \tag{5.3}$$

As noted, at this level $\theta_{12} = \theta_{12}^0$, where alternate choices of θ_{12}^0 result in popular mixing patterns such as Tribimaximal, Bimaximal, and Golden Ratio with the common feature that $\theta_{13} = 0$ and $\theta_{23} = \pi/4$. $\theta_{12}^0 = 0$ is another interesting alternative [37] where initially the lepton mixing angles are either vanishing $\theta_{13} = 0 = \theta_{12}$ or maximal, i.e., $\pi/4$ (θ_{23}). Thus, till Type I seesaw effects are included,

the leptonic mixing matrix takes the form:

$$U^0 = \begin{pmatrix} \cos\theta_{12}^0 & \sin\theta_{12}^0 & 0 \\ -\frac{\sin\theta_{12}^0}{\sqrt{2}} & \frac{\cos\theta_{12}^0}{\sqrt{2}} & \frac{1}{\sqrt{2}} \\ \frac{\sin\theta_{12}^0}{\sqrt{2}} & -\frac{\cos\theta_{12}^0}{\sqrt{2}} & \frac{1}{\sqrt{2}} \end{pmatrix} = U_l^\dagger U_\nu^0 \,, \tag{5.4}$$

where $U_\nu^0 = I$ and the charged lepton mass matrix is:

$$M_{e\mu\tau} = U_l \begin{pmatrix} m_e & 0 & 0 \\ 0 & m_\mu & 0 \\ 0 & 0 & m_\tau \end{pmatrix} I = \begin{pmatrix} m_e\cos\theta_{12}^0 & -\frac{m_\mu}{\sqrt{2}}\sin\theta_{12}^0 & \frac{m_\tau}{\sqrt{2}}\sin\theta_{12}^0 \\ m_e\sin\theta_{12}^0 & \frac{m_\mu}{\sqrt{2}}\cos\theta_{12}^0 & -\frac{m_\tau}{\sqrt{2}}\cos\theta_{12}^0 \\ 0 & \frac{m_\mu}{\sqrt{2}} & \frac{m_\tau}{\sqrt{2}} \end{pmatrix} \,. \tag{5.5}$$

The identity matrix, I, at the right in the first step above indicates that no transformation needs to be applied on the right-handed charged leptons which are $SU(2)_L$ singlets.

In this basis, the matrices responsible for the Type I seesaw have the forms:

$$M_D = m_D\,\mathbb{I} \;\text{ and }\; M_R = \frac{m_R}{2xy}\begin{pmatrix} 0 & xe^{-i\phi_1} & xe^{-i\phi_1} \\ xe^{-i\phi_1} & ye^{-i\phi_2}/\sqrt{2} & -ye^{-i\phi_2}/\sqrt{2} \\ xe^{-i\phi_1} & -ye^{-i\phi_2}/\sqrt{2} & ye^{-i\phi_2}/\sqrt{2} \end{pmatrix} \,, \tag{5.6}$$

where m_D and m_R set the scale for the Dirac and right-handed Majorana masses while x and y are dimensionless real quantities of $\mathcal{O}(1)$. We take the Dirac mass matrix M_D proportional to the identity for ease of presentation. We have checked that the same results can be reproduced so long as M_D is simply diagonal. The right-handed neutrino Majorana mass matrix, M_R, has a $N_{2R} \leftrightarrow N_{3R}$ discrete symmetry. This choice too can be relaxed without jeopardising the final outcome.

We will show later how the mass matrices in Eqs. (5.1) - (5.6) lead to a good fit to the neutrino data and yield testable predictions. But before this we must ensure that the above matrices can arise from the $S3 \times Z3$ symmetric Lagrangian.

The behaviour of the fermions, i.e., the three lepton generations[83] including three right-handed neutrinos, is summarised in Table 5.2. The gauge interactions of the leptons are universal and diagonal in this basis. A feature worth noting is that the right-handed neutrinos have lepton number $L = 0$. We discuss later how this leads to a diagonal neutrino Dirac mass matrix. The lepton mass matrices arise from the Yukawa couplings allowed by the $S3 \times Z3$ symmetry.

The $S3 \times Z3$ structure of the lepton sector is matched by a rich scalar sector which we have presented in Table 5.3. The requirement of charged lepton masses and Type I and Type II seesaw neutrino masses dictates the inclusion of $SU(2)_L$ singlet, doublet, and triplet scalar fields. The $S3 \times Z3$ properties of the scalars are chosen bearing in mind the $S3$ and $Z3$ combination rules. In particular, for the former the representations are 1, 1′, and 2 which satisfy the multiplication rules (see Appendix 5.A):

$$1 \times 1' = 1' \,,\;\; 1' \times 1' = 1 \;\;, \text{ and } \; 2 \times 2 = 2 + 1 + 1' \,. \tag{5.7}$$

[83]The scope of this model is restricted to the lepton sector.

Purpose	Notations	$S3$ ($Z3$)	$SU(2)_L$ (Y)	L	vev
$M_{e\mu\tau}$	$\eta \equiv (\eta^+ \ \eta^0)$	1 (1)	2 (1)	0	$\langle\eta\rangle = v_\eta(0\ 1)$
	$\Phi_a \equiv \begin{pmatrix} \phi_1^+ & \phi_1^0 \\ \phi_2^+ & \phi_2^0 \end{pmatrix}$	2 (1)	2 (1)	0	$\langle\Phi_a\rangle = \frac{v_a}{\sqrt{2}} \begin{pmatrix} 0 & w_1 \\ 0 & w_2 \end{pmatrix}$
	$\Phi_b \equiv \begin{pmatrix} \phi_3^+ & \phi_3^0 \\ \phi_4^+ & \phi_4^0 \end{pmatrix}$	2 (ω)	2 (1)	0	$\langle\Phi_b\rangle = \frac{v_b}{\sqrt{2}} \begin{pmatrix} 0 & w_3 \\ 0 & w_4 \end{pmatrix}$
	$\alpha \equiv (\alpha^+ \ \alpha^0)$	1 (ω)	2 (1)	0	$\langle\alpha\rangle = v_\alpha(0\ 1)$
M_D	$\beta \equiv (\beta^0 \ \beta^-)$	1 (1)	2 (-1)	1	$\langle\beta\rangle = v_\beta\,(1\ 0)$
M_L^ν	$\Delta_L \equiv (\Delta_L^{++},\ \Delta_L^+,\ \Delta_L^0)$	1 (1)	3 (2)	-2	$\langle\Delta_L\rangle = v_\Delta\,(0\ 0\ 1)$
	$\rho_L \equiv (\rho_L^{++},\ \rho_L^+,\ \rho_L^0)$	1 (ω)	3 (2)	-2	$\langle\rho_L\rangle = v_\rho\,(0\ 0\ 1)$
M_R	$\chi \equiv \chi^0$	1 (ω)	1 (0)	0	$\langle\chi\rangle = u_\chi$
	$\gamma \equiv \gamma^0$	1′ (ω)	1 (0)	0	$\langle\gamma\rangle = u_\gamma$

Table 5.3: The scalar content of the model. The transformation properties under $S3$, $Z3$, and $SU(2)_L$ are shown. The hypercharge of the fields, Y, their lepton number, L, and the vacuum expectation values are also indicated. w_i $(i = 1 \ldots 4)$ are dimensionless.

The scalar multiplets are chosen such that the mass matrices appear with specific structures as discussed below[84]. It can be seen from Table 5.3 that all neutral scalars pick up a *vev*. The *vev* of the $SU(2)_L$ singlets, namely, u_χ and u_γ, can be much higher than the electroweak scale, v, and determine the masses of the right-handed neutrinos. The other *vev* break $SU(2)_L$. We take $v_\Delta \sim v_\rho \ll v_\eta \sim v_a \sim v_b \sim v_\alpha \sim v_\beta \sim v$ to maintain consistency with the "ρ" parameter.

Charged lepton and neutrino masses are obtained from the Yukawa terms in a Lagrangian constructed out of the fields in Tables 5.2 and 5.3. Including all terms which respect the $SU(2)_L \times U(1)_Y$ gauge symmetry and the $S3 \times Z3$ flavour symmetry so long as lepton number, L, is also conserved one is led to the Lagrangian

[84]In general the multiple scalar fields in models based on discrete symmetries also result in flavour changing neutral currents induced by the neutral scalars. Discussions of this aspect in the context of $S3$ can be found, for example, in [85].

mass terms

$$
\begin{aligned}
\mathscr{L}_{mass} &= f_1\ \bar{e}_L(\mu_R\phi_2^0 - \tau_R\phi_1^0) + f_2\ \bar{\mu}_L(\mu_R\phi_4^0 - \tau_R\phi_3^0) + f_3\ \bar{\tau}_L(\mu_R\phi_4^0 + \tau_R\phi_3^0) \\
&+ f_4\ \bar{\mu}_L e_R\alpha^0 + f_5\ \bar{e}_L e_R\eta^0 \quad \text{(charged lepton mass)} \\
&+ (h_1\bar{\nu}_{eL}N_{1R} + h_2\bar{\nu}_{\mu L}N_{2R} + h_3\bar{\nu}_{\tau L}N_{3R})\beta^0 \quad \text{(neutrino Dirac mass)} \\
&+ \Bigg[\frac{1}{2}g_1\ \nu_{eL}^T C^{-1}\nu_{eL}\Delta_L^0 \\
&+ \frac{1}{2}\left(g_2\ \nu_{\mu L}^T C^{-1}\nu_{\mu L} + g_3\ \nu_{\tau L}^T C^{-1}\nu_{\tau L}\right)\rho_L\Bigg] \quad \text{(neutrino Type II seesaw mass)} \\
&+ \frac{1}{2}\left(\left[k_1 N_{2R}^T C^{-1}N_{2R} + k_2 N_{3R}^T C^{-1}N_{3R}\right]\chi + k_3 N_{2R}^T C^{-1}N_{3R}\gamma\right) \\
&+ \frac{1}{2}\left(k_4 N_{1R}^T C^{-1}N_{2R}\tilde{\chi} + k_5 N_{1R}^T C^{-1}N_{3R}\tilde{\gamma}\right) \quad \text{(rh neutrino mass)} + h.c.\ .
\end{aligned}
\tag{5.8}
$$

Here, $\tilde{\chi}$ and $\tilde{\gamma}$ are charge conjugated fields which transform under Z_3 as $\omega^* = \omega^2$. For each term in the Lagrangian the fermion masses which arise therefrom have been indicated. Both Type I and Type II seesaw contributions for neutrino masses are present.

The above Lagrangian gives rise to the mass matrices in Eqs. (5.1) - (5.6) through the Yukawa couplings and the *vev*s in Table 5.3. Before turning to these let us note how the quantum number assignments of the fermion and scalar fields force certain entries in the mass matrices to be vanishing. For example, the mass term $\bar{\tau}_L e_R$ is zero in Eq. (5.5) because there is no $SU(2)_L$ doublet field which transforms as a $1'$ under $S3$. Similarly the diagonal nature of the left-handed neutrino Majorana mass matrix in Eq. (5.1) is ensured by the absence of an $SU(2)_L$ triplet field which transforms either as (i) a $1'$ under $S3$ or (ii) as ω^2 under Z_3. The neutrino Dirac mass matrix in Eq. (5.6) arises from the Yukawa couplings[85] of the $SU(2)_L$ doublet scalar β. Since it transforms as 1 under both $S3$ and $Z3$ it can be seen from the left-handed and right-handed neutrino quantum numbers in Table 5.2 that only diagonal terms are allowed. Finally, the $N_{1R}^T N_{1R}$ term is absent in the right-handed neutrino Majorana mass matrix in Eq. (5.6) since there is no $Z3$ singlet among the $SU(2)_L$ singlet scalars.

Before proceeding further it may be useful to comment on the sizes of the various vacuum expectation values in Table 5.3. The $SU(2)_L$ doublets acquire *vev*s $v_{\eta,a,b,\alpha,\beta}$ which are $\mathcal{O}(M_W)$ while the triplet *vev*s $v_{\Delta,\rho}$ are several orders of magnitude smaller. This is in consonance with the smallness of the neutrino masses as also the ρ parameter of electroweak symmetry breaking. Needless to say, the $SU(2)_L$ singlet fields χ and γ can acquire *vev*s well above the electroweak scale.

The non-vanishing entries in the mass matrices in Eqs. (5.1) - (5.6) which arise from the Yukawa couplings entail the following relationships:

[85] As the N_{iR} carry $L = 0$, conservation of lepton number forbids any contribution to the Dirac mass from the $SU(2)_L$ scalar doublets which generate the charged lepton masses.

1. Charged lepton masses – On matching the Lagrangian in Eq. (5.8), the scalar doublet *vev*s in Table 5.3 and the charged lepton mass matrix in Eq. (5.5) one gets:

$$f_1\langle\phi_1^0\rangle = -\frac{m_\tau}{\sqrt{2}}\sin\theta_{12}^0 \;\;,\;\; f_1\langle\phi_2^0\rangle = -\frac{m_\mu}{\sqrt{2}}\sin\theta_{12}^0 \;\;, \tag{5.9}$$

$$f_2\langle\phi_3^0\rangle = \frac{m_\tau}{\sqrt{2}}\cos\theta_{12}^0 \;\;,\;\; f_2\langle\phi_4^0\rangle = \frac{m_\mu}{\sqrt{2}}\cos\theta_{12}^0 \;\;,\;\; f_3\langle\phi_3^0\rangle = \frac{m_\tau}{\sqrt{2}} \;\;,\;\; f_3\langle\phi_4^0\rangle = \frac{m_\mu}{\sqrt{2}} \;\;, \tag{5.10}$$

and

$$f_4\langle\alpha^0\rangle = m_e\sin\theta_{12}^0 \;\;,\;\; f_5\langle\eta^0\rangle = m_e\cos\theta_{12}^0 \;\;. \tag{5.11}$$

Notice that Eqs. (5.9) and (5.10) imply

$$\frac{w_2}{w_1} = \frac{w_4}{w_3} = \frac{m_\mu}{m_\tau} \;\;. \tag{5.12}$$

2. Left-handed neutrino Majorana mass – Similarly, the mass matrix in Eq. (5.1) is obtained when

$$g_1\langle\Delta_L^0\rangle = m_1^0 = g_2\langle\rho_L^0\rangle \;\;,\;\; g_3\langle\rho_L^0\rangle = m_3^0 \;\;. \tag{5.13}$$

The first equation above requires a matching between two sets of Yukawa couplings and *vev*s. This is to ensure degeneracy of two neutrino states, implying the vanishing of the solar mass splitting at this stage. Notice that the relatively large size of the atmospheric mass splitting requires g_2 and g_3 to be of different order.

3. Neutrino Dirac mass – The Dirac mass matrix in Eq. (5.6) is due to the relations:

$$h_1 = h_2 = h_3 = h \;\text{ and }\; h\langle\beta^0\rangle = m_D \;\;. \tag{5.14}$$

The equality of the three Yukawa couplings, h_i, above is only a simplified choice. We have checked that deviations from this relation, i.e., a diagonal Dirac mass matrix but not proportional to the identity, can also readily lead to the results which we discuss in this chapter.

4. Right-handed neutrino Majorana mass – Finally, the right-handed neutrino Majorana mass matrix follows from:

$$k_1\langle\chi^0\rangle = \frac{m_R e^{-i\phi_2}}{2\sqrt{2}x} = k_2\langle\chi^0\rangle \;\;,\;\; k_3\langle\gamma^0\rangle = -\frac{m_R e^{-i\phi_2}}{2\sqrt{2}x} \;\;,\;\; k_4\langle\tilde{\chi}^0\rangle = \frac{m_R e^{-i\phi_1}}{2y} = k_5\langle\tilde{\gamma}^0\rangle \;\;. \tag{5.15}$$

We show in Appendix 5.B how from a minimisation of the scalar potential the required scalar *vev*s may be obtained.

5.2.1 Type I seesaw contribution

In the previous section we have shown that the $S3$ model results in a diagonal left-handed neutrino mass matrix given in Eq. (5.1) through a Type II seesaw.

The charged lepton mass matrix as given in Eq. (5.5) is not diagonal and induces a mixing in the lepton sector. This mixing, Eq. (5.4), receives further corrections from a smaller Type I seesaw contribution to the neutrino mass matrix as we discuss.

The Type I seesaw arising from the Dirac and right-handed neutrino mass matrices in Eq. (5.6) is

$$M' = \left[M_D^T (M_R)^{-1} M_D\right] = \frac{m_D^2}{m_R} \begin{pmatrix} 0 & y\ e^{i\phi_1} & y\ e^{i\phi_1} \\ y\ e^{i\phi_1} & \frac{x\ e^{i\phi_2}}{\sqrt{2}} & \frac{-x\ e^{i\phi_2}}{\sqrt{2}} \\ y\ e^{i\phi_1} & \frac{-x\ e^{i\phi_2}}{\sqrt{2}} & \frac{x\ e^{i\phi_2}}{\sqrt{2}} \end{pmatrix} \quad . \tag{5.16}$$

5.3 Results

We have given above the contributions to the neutrino mass matrix from the Type I and Type II seesaw. Of these, the former is taken to be significantly smaller than the latter. As we have noted, in the absence of the Type I seesaw the leptonic mixing matrix in this model is determined entirely by the charged lepton mass matrix. It has $\theta_{13} = 0$, $\theta_{23} = \pi/4$, and θ_{12} arbitrary. We will be considering four mixing patterns which fall within this scheme and in each of which the value of θ_{12}^0 is specified, namely, the TBM, BM, GR, and NSM cases. In addition, in this model the Type II seesaw sets the solar mass splitting to be zero. The Type I seesaw, whose effect we incorporate perturbatively, brings all the above leptonic parameters into agreement with their values preferred by the data. Before we proceed further with this discussion it will be useful to mention that we have used the 3σ global fit ranges of the neutrino mixing parameters furnished in Eq. (1.24). Later, we also remark about the compatibility of this model with the recent T2K and NOνA hints [10, 11] of δ being near -$\pi/2$.

5.3.1 Real M_R ($\phi_1 = 0$ or $\pi, \phi_2 = 0$ or π)

A limiting case, with less complications, corresponds to no CP violation. This happens when M_R is real, i.e., the phases $\phi_{1,2}$ in Eq. (5.16) are 0 or π. These cases can be compactly considered by keeping x and y real but allowing them to be of either sign, i.e., four alternatives. We show below how the experimental data picks out one out of these.

Without the phases $\phi_{1,2}$, i.e., for real M_R, one gets

$$M' = \frac{m_D^2}{m_R} \begin{pmatrix} 0 & y & y \\ y & \frac{x}{\sqrt{2}} & -\frac{x}{\sqrt{2}} \\ y & -\frac{x}{\sqrt{2}} & \frac{x}{\sqrt{2}} \end{pmatrix} \quad . \tag{5.17}$$

The equality of two neutrino masses from the Type II seesaw requires the use of degenerate perturbation theory to obtain corrections to the solar mixing parameters.

The 2×2 submatrix of M' relevant for this is:

$$M'_{2\times 2} = \frac{m_D^2}{m_R} \begin{pmatrix} 0 & y \\ y & x/\sqrt{2} \end{pmatrix} \ . \tag{5.18}$$

This results in:

$$\theta_{12} = \theta_{12}^0 + \zeta \ \ , \ \ \tan 2\zeta = 2\sqrt{2}\left(\frac{y}{x}\right) \ . \tag{5.19}$$

A related quantity, ϵ, which is found useful later is given by

$$\sin\epsilon = \frac{y}{\sqrt{y^2 + x^2/2}} \ \text{ and } \ \cos\epsilon = \frac{x/\sqrt{2}}{\sqrt{y^2 + x^2/2}} \ \ , \ \text{ i.e., } \ \tan\epsilon = \frac{1}{2}\tan 2\zeta \ . \tag{5.20}$$

Model (θ_{12}^0)	TBM (35.3°)	BM (45.0°)	GR (31.7°)	NSM (0.0°)
ζ	-4.0° $\leftrightarrow$ 0.6°	-13.7° $\leftrightarrow$ -9.1°	-0.4° $\leftrightarrow$ 4.2°	31.3° $\leftrightarrow$ 35.9°
ϵ	-4.0° $\leftrightarrow$ 0.6°	-14.5° $\leftrightarrow$ -9.3°	-0.4° $\leftrightarrow$ 4.2°	44.0° $\leftrightarrow$ 56.7°
$\epsilon - \theta_{12}^0$	-39.2° $\leftrightarrow$ -34.6°	-59.5° $\leftrightarrow$ -54.4°	-39.2° $\leftrightarrow$ -30.0°	44.0° $\leftrightarrow$ 56.7°

Table 5.4: The ranges of ζ (Eq. (5.19)), ϵ (Eq. (5.20)), and $(\epsilon - \theta_{12}^0)$ allowed by the data for the different popular mixing patterns.

Once a mixing pattern is chosen, i.e., θ_{12}^0 fixed, the experimental limits on θ_{12} as given in Eq. (1.24) set bounds on the range of ζ and also from Eq. (5.20) on ϵ. These are displayed for the four mixing patterns in Table 5.4. If ζ is positive (negative) then the ratio (y/x) will also be positive (negative). In addition, from Eq. (5.20) the sign of y is fixed by the value of ϵ. Taking these points into account one can conclude that x is always positive, i.e., ϕ_2 has to be 0. On the other hand, y must be positive, $\phi_1 = 0$ (negative, $\phi_1 = \pi$) for NSM (BM). For the other mixing patterns, i.e., TBM and GR, both signs of y are possible.

The solar mass splitting arising from the Type I seesaw is also obtained from Eq. (5.18).

$$\Delta m^2_{solar} = \frac{\sqrt{2}m_D^2}{m_R}\ m_1^{(0)}\sqrt{x^2 + 8y^2} = \frac{\sqrt{2}m_D^2}{m_R}\ m_1^{(0)}\frac{x}{\cos 2\zeta} \ . \tag{5.21}$$

Furthermore, incorporating the leading order corrections to neutrino mixing from Eq. (5.17) one gets from Eq. (5.3):

$$U = U^0 U_\nu \text{ with } U_\nu = \begin{pmatrix} \cos\zeta & -\sin\zeta & \kappa_r \sin\epsilon \\ \sin\zeta & \cos\zeta & -\kappa_r\cos\epsilon \\ \kappa_r \sin(\zeta - \epsilon) & \kappa_r \cos(\zeta - \epsilon) & 1 \end{pmatrix} \ , \tag{5.22}$$

with

$$\kappa_r \equiv \frac{m_D^2}{m_R m^-}\sqrt{y^2 + x^2/2} = \frac{m_D^2}{m_R m^-}\frac{x}{\sqrt{2}\cos\epsilon} \ . \tag{5.23}$$

The third column of the leptonic mixing matrix becomes:

$$|\psi_3\rangle = \begin{pmatrix} \kappa_r \sin(\epsilon - \theta_{12}^0) \\ \frac{1}{\sqrt{2}}[1 - \kappa_r \cos(\epsilon - \theta_{12}^0)] \\ \frac{1}{\sqrt{2}}[1 + \kappa_r \cos(\epsilon - \theta_{12}^0)] \end{pmatrix} \quad . \tag{5.24}$$

Since, as noted, x is always positive, κ_r is positive (negative) for normal (inverted) ordering.

The right-hand-side of Eq. (5.24) has to be matched with the third column of Eq. (1.15). This yields:

$$\sin\theta_{13}\cos\delta = \kappa_r \sin(\epsilon - \theta_{12}^0) \quad , \tag{5.25}$$

and

$$\tan(\pi/4 - \theta_{23}) \equiv \tan\omega = \kappa_r \cos(\epsilon - \theta_{12}^0) \; . \tag{5.26}$$

For ready reference the ranges of $(\epsilon - \theta_{12}^0)$ allowed for the different mixing patterns are presented in Table 5.4. For normal ordering[86] the CP phase δ is 0 (π) when $\sin(\epsilon - \theta_{12}^0)$ is positive (negative). From Table 5.4 one can then observe that $\delta = 0$ for the NSM mixing pattern and is π for the three other cases. Needless to say, both correspond to CP conservation.

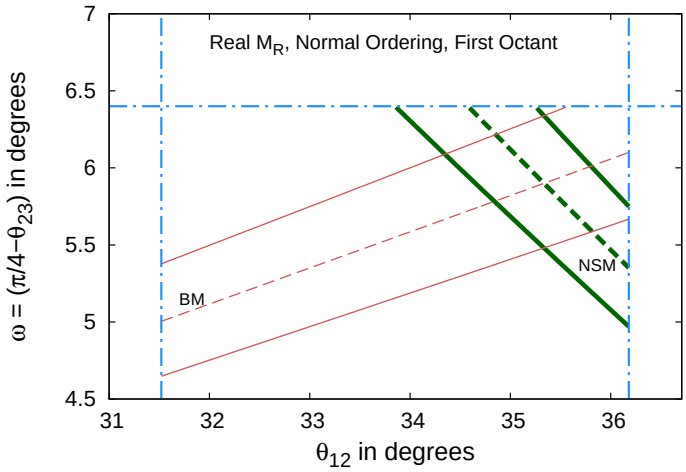

Figure 5.1: $\omega = (\pi/4 - \theta_{23})$ as a function of θ_{12} for normal ordering. The solid lines indicate the range for the 3σ allowed variation of $\sin\theta_{13}$ while the dashed line corresponds to the best-fit value. Thick green (thin pink) lines are for the NSM (BM) case. The horizontal and vertical blue dot-dashed lines delimit the 3σ allowed range from data. Note that ω is always positive, i.e., the first octant of θ_{23} is preferred. For the TBM and GR mixing patterns ω, still positive, lies beyond the 3σ range. Best-fit values of the solar and atmospheric splittings are used. For M_R real there is no allowed solution for inverted ordering.

Combining Eqs. (5.21), (5.23), and (5.25) one can write:

$$\Delta m^2_{solar} = 2\; m^- m_1^{(0)} \; \frac{\sin\theta_{13}\cos\delta\cos\epsilon}{\cos 2\zeta \;\; \sin(\epsilon - \theta_{12}^0)} \quad . \tag{5.27}$$

[86] We show in the following that inverted ordering is not consistent with real M_R.

Eq. (5.27) leads to the conclusion that inverted ordering is not allowed for this case of real M_R. To establish this property one can define:

$$z \equiv m^- m_1^{(0)}/\Delta m^2_{atmos} \;\; \text{and} \;\; \tan\xi \equiv m_0/\sqrt{|\Delta m^2_{atmos}|} \;\; , \tag{5.28}$$

where z is positive for both mass orderings. From Eq. (5.27) one has

$$z = \left(\frac{\Delta m^2_{solar}}{|\Delta m^2_{atmos}|}\right)\left(\frac{\cos 2\zeta \;\; \sin(\epsilon - \theta^0_{12})}{2\sin\theta_{13}|\cos\delta|\cos\epsilon}\right) \;\; . \tag{5.29}$$

It is easy to verify from Eq. (5.28) that

$$\begin{aligned} z &= \sin\xi/(1+\sin\xi) \;\; \text{i.e.,} \;\; 0 \leq z \leq \frac{1}{2} \;\; \text{(for normal ordering)}, \\ z &= 1/(1+\sin\xi) \;\; \text{i.e.,} \;\; \frac{1}{2} \leq z \leq 1 \;\; \text{(for inverted ordering)} \;\; . \end{aligned} \tag{5.30}$$

There is a one-to-one correspondence of z with the lightest neutrino mass m_0. The quasidegeneracy limit, i.e., $m_0 \to$ large, is approached as $z \to \frac{1}{2}$ for both mass orderings.

In Eq. (5.29) $|\cos\delta| = 1$ for real M_R. Using the global fit mass splittings and mixing angles given in Eq. (1.24) and Table 5.4 one finds $z \sim 10^{-2}$ or smaller for all four mixing patterns. This excludes the inverted mass ordering option for real M_R.

From Eqs. (5.25) and (5.26) one has

$$\tan\omega = \frac{\sin\theta_{13}\cos\delta}{\tan(\epsilon - \theta^0_{12})} \;\; . \tag{5.31}$$

The noteworthy point is that for normal ordering Eq. (5.26) implies that ω is always positive irrespective of the mixing pattern. So, in this model θ_{23} is restricted to the first octant for real M_R.

Eqs. (5.19) and (5.20) can be used to express ϵ in terms of θ_{12} and thereby put ω in Eq. (5.31) as a function of θ_{12} and θ_{13} only. In Fig. 5.1, ω is shown as a function of θ_{12} for the NSM (thick green lines) and BM (thin pink lines) mixing patterns. The ranges of θ_{12} and ω have been kept within their 3σ allowed limits from global fits as given in Eq. (1.24). The TBM and GR cases are excluded because for the allowed values of θ_{12} they predict θ_{23} beyond the 3σ range. The solid lines in the figure correspond to the 3σ limiting values of θ_{13} and the dashed line is for its best-fit value. The blue dot-dashed horizontal and vertical lines display the 3σ experimental bounds on θ_{23} and θ_{12}.

Using Eq. (5.29) any allowed point in the $\omega - \theta_{12}$ plane and the associated θ_{13} can be translated to a value of z or equivalently m_0, provided the solar and atmospheric mass splittings are given. We find that for both the allowed mixing patterns the range of variation of m_0 is very small. For the NSM (BM) case this range is 2.13 meV $\leq m_0 \leq$ 3.10 meV (3.20 meV $\leq m_0 \leq$ 4.42 meV) when both neutrino mass splittings and all mixing angles are varied over their full 3σ ranges.

To summarise the real M_R case:

1. Only the normal mass ordering is allowed.

2. θ_{23} can lie only in the first octant.

3. The TBM and GR alternatives are inconsistent with the allowed ranges of the neutrino mixing angles even after including the Type I seesaw corrections.

4. For the NSM and BM mixing patterns real M_R can give consistent solutions for the neutrino masses and mixings. The ranges of allowed lightest neutrino masses are very tiny.

5.3.2 Complex M_R

Keeping M_R real eliminates CP violation. Further, inverted ordering is disallowed. Also, the TBM and GR mixing patterns cannot be accommodated. These restrictions can be ameliorated by taking M_R in its general complex form giving rise to the Type I seesaw contribution M' as given in Eq. (5.16). Recall that this introduces the phases $\phi_{1,2}$ and x and y take only positive values.

With its complex entries, M' is now not hermitian any more. To address this we consider the combination $(M^0 + M')^\dagger (M^0 + M')$, and treat $M^{0\dagger} M^0$ as the leading term with $(M^{0\dagger} M' + M'^\dagger M^0)$ acting as a perturbation at the lowest order, both hermitian by construction. The unperturbed eigenvalues are thus $(m_i^{(0)})^2$. The perturbation matrix is

$$(M^{0\dagger} M' + M'^\dagger M^0) = \frac{m_D^2}{m_R} \begin{pmatrix} 0 & 2y m_1^{(0)} \cos\phi_1 & y f(\phi_1) \\ 2y m_1^{(0)} \cos\phi_1 & \sqrt{2} x m_1^{(0)} \cos\phi_2 & -\frac{x}{\sqrt{2}} f(\phi_2) \\ y f^*(\phi_1) & -\frac{x}{\sqrt{2}} f^*(\phi_2) & \sqrt{2} x m_3^{(0)} \cos\phi_2 \end{pmatrix} . \tag{5.32}$$

In the above

$$f(\varphi) = m^+ \cos\varphi - i m^- \sin\varphi \ . \tag{5.33}$$

The remaining calculation proceeds in much the same manner as for real M_R while keeping the distinctive features of Eq. (5.32) in mind.

In place of Eqs. (5.19) and (5.20) for the real M_R case, we get from (5.32)

$$\theta_{12} = \theta_{12}^0 + \zeta \ , \ \ \tan 2\zeta = 2\sqrt{2}\, \frac{y}{x}\, \frac{\cos\phi_1}{\cos\phi_2} \ , \tag{5.34}$$

and

$$\sin\epsilon = \frac{y \cos\phi_1}{\sqrt{y^2 \cos^2\phi_1 + x^2 \cos^2\phi_2/2}} \ , \ \ \cos\epsilon = \frac{x \cos\phi_2/\sqrt{2}}{\sqrt{y^2 \cos^2\phi_1 + x^2 \cos^2\phi_2/2}} \ ,$$

$$\tan\epsilon = \frac{1}{2} \tan 2\zeta \ . \tag{5.35}$$

Mixing Pattern	Normal Ordering		Inverted Ordering	
	δ quadrant	θ_{23} octant	δ quadrant	θ_{23} octant
NSM	First/Fourth	First	Second/Third	Second
BM, TBM, GR	Second/Third	First	First/Fourth	Second

Table 5.5: Quadrants of the leptonic CP phase δ and the octant of θ_{23} for both mass orderings for different mixing patterns.

The allowed ranges of ζ and ϵ depend on the mixing pattern and are given in Table 5.4. It is seen that for all patterns $\cos\epsilon$ is positive. Therefore, from Eq. (5.35) we can immediately conclude that ϕ_2 must be always in the first or fourth quadrants. The possible quadrants of ϕ_1 are also determined from the range of ϵ for the different mixing patterns. From the first relation in Eq. (5.35) we find that ϕ_1 has to be in the first or fourth (second or third) quadrants if ϵ is positive (negative). Using the results in Table 5.4 we conclude that the first (second) option is valid for the NSM (BM) patterns. For TBM and GR cases ϵ spans a range over positive and negative values and so both options are included.

The solar mass splitting is induced entirely through the Type I seesaw contribution. From Eq. (5.32) one finds:

$$\begin{aligned}\Delta m^2_{solar} &= \sqrt{2}m_1^{(0)}\ \frac{m_D^2}{m_R}\sqrt{x^2\cos^2\phi_2+8y^2\cos^2\phi_1} = \sqrt{2}m_1^{(0)}\ \frac{m_D^2}{m_R}\ \frac{x\cos\phi_2}{\cos 2\zeta} \\ &= \sqrt{2}m_1^{(0)}\ \frac{m_D^2}{m_R}\frac{2\sqrt{2}y\cos\phi_1}{\sin 2\zeta}\ . \end{aligned} \tag{5.36}$$

Eq. (5.24) is now replaced by:

$$|\psi_3\rangle = \begin{pmatrix} \kappa_c[\frac{\sin\epsilon}{\cos\phi_1}f(\phi_1)\cos\theta_{12}^0 - \frac{\cos\epsilon}{\cos\phi_2}f(\phi_2)\sin\theta_{12}^0]/m^+ \\ \frac{1}{\sqrt{2}}\{1-\kappa_c[\frac{\sin\epsilon}{\cos\phi_1}f(\phi_1)\sin\theta_{12}^0 + \frac{\cos\epsilon}{\cos\phi_2}f(\phi_2)\cos\theta_{12}^0]/m^+\} \\ \frac{1}{\sqrt{2}}\{1+\kappa_c[\frac{\sin\epsilon}{\cos\phi_1}f(\phi_1)\sin\theta_{12}^0 + \frac{\cos\epsilon}{\cos\phi_2}f(\phi_2)\cos\theta_{12}^0]/m^+\} \end{pmatrix}\ , \tag{5.37}$$

where

$$\kappa_c = \frac{m_D^2}{m_R m^-}\ \sqrt{y^2\cos^2\phi_1 + x^2\cos^2\phi_2/2}\ , \tag{5.38}$$

Eq. (5.35) has been used, and the complex function $f(\phi_{1,2})$ is defined in Eq. (5.33).

κ_c is positive (negative) for normal (inverted) ordering. Comparing the right-hand-side of Eq. (5.37) with the third column of Eq. (1.15) we find

$$\sin\theta_{13}\cos\delta = \kappa_c\ \sin(\epsilon-\theta_{12}^0)\ , \tag{5.39}$$

$$\sin\theta_{13}\sin\delta = \kappa_c\,\frac{m^-}{m^+\cos\phi_1\cos\phi_2}\left[\sin\epsilon\sin\phi_1\cos\phi_2\cos\theta_{12}^0 - \cos\epsilon\cos\phi_1\sin\phi_2\sin\theta_{12}^0\right]\ . \tag{5.40}$$

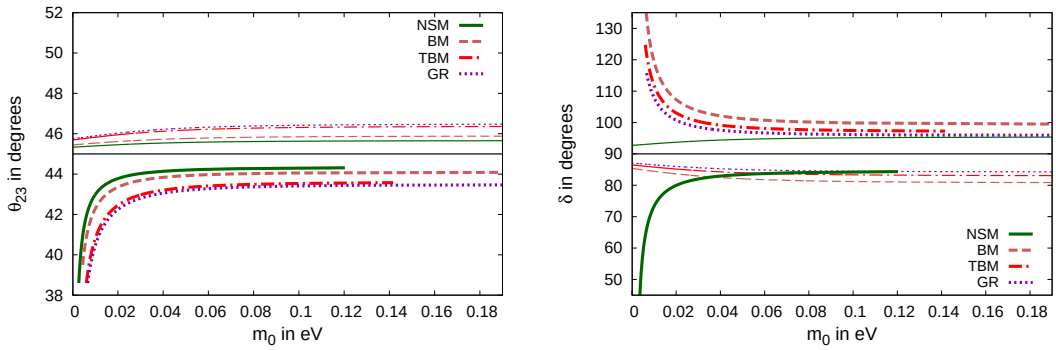

Figure 5.2: θ_{23} (left) and the CP phase δ (right) as a function of m_0 from this model for different mixing patterns when the best-fit values of the input data are used. The NSM, BM, TBM and GR cases correspond to the green solid, pink dashed, red dot-dashed, and violet dotted curves respectively. Thick (thin) curves of each type indicate normal (inverted) mass orderings.

As indicated in Table 5.4, $(\epsilon - \theta_{12}^0)$ always remains in the first (fourth) quadrant for the NSM (BM, TBM, and GR) mixing pattern. For normal ordering Eq. (5.39) then implies that for the NSM (BM, TBM, and GR) case(s) δ lies in the first or fourth (second or third) quadrants. For inverted ordering of masses, κ_c changes sign and so the quadrants are accordingly modified. The different possibilities are indicated in Table 5.5. For any mixing pattern and mass ordering there are two allowed quadrants of δ which have $\sin\delta$ of opposite sign. Which of these is chosen is determined by the phases $\phi_{1,2}$ through the sign of the right-hand-side of Eq. (5.40). As noted above, ϕ_2 can be in either the first or fourth quadrants and the quadrant of ϕ_1 is determined by the mixing pattern in such a way that $\sin\phi_1$ can be of either sign. Thus the the phases ϕ_1 and ϕ_2 can always be chosen such that $\sin\delta$ can be of any particular sign. Therefore the two alternate quadrants of δ for every case in Table 5.5 are equally viable in this model.

The perturbative Type I seesaw contribution to θ_{23} can also be extracted from Eq. (5.37). One finds:

$$\tan\omega = \frac{\sin\theta_{13}\cos\delta}{\tan(\epsilon - \theta_{12}^0)} \ . \tag{5.41}$$

Recalling that Eq. (5.39) correlates δ and $(\epsilon - \theta_{12}^0)$ through κ_c one can readily conclude that for all mixing patterns θ_{23} always lies in the first (second) octant for normal (inverted) ordering. This important conclusion from these models is shown in Table 5.5.

In the expression for the solar mass splitting in Eq. (5.36) one can trade the factor m_D^2/m_R in terms of κ_c and use Eq. (5.39) to get

$$\Delta m^2_{solar} = \frac{2m^- m_1^{(0)}\sin\theta_{13}\cos\delta\cos\epsilon}{\sin(\epsilon - \theta_{12}^0)\ cos2\zeta} \ . \tag{5.42}$$

The strategy that we have followed to extract the predictions of this model relies on utilising Eqs. (5.41) and (5.42). We take the three mixing angles θ_{13}, θ_{12}, and θ_{23} as inputs. With these at hand Eq. (5.41) fixes a value of the CP phase δ. Using these and the experimentally determined solar mass splitting one can calculate from Eq. (5.42) the combination $m_1^{(0)}m^-$, or equivalently the variable z, which fixes the lightest neutrino mass m_0. It might appear that arbitrarily large values of m_0, and hence $m_1^{(0)}m^-$, may be admitted by taking $\cos\delta$ to smaller and smaller values. However, this is not the case. Experimental data require $\omega = (\pi/4 - \theta_{23})$ to lie within determined limits. Since all other factors have experimentally allowed ranges, Eq. (5.41) also gives lower and upper bounds on δ. Consequently, for any mixing pattern m_0 lies within a fixed range.

In the left (right) panel of Fig. 5.2 we show the mixing angle θ_{23} (the CP phase δ) as a function of the lightest neutrino mass m_0 as obtained from this model for different mixing patterns when the best-fit values of the various measured angles and mass splittings are used. The NSM, BM, TBM and GR correspond to the green solid, pink dashed, red dot-dashed, and violet dotted curves respectively. The thick (thin) curves of each type indicate normal (inverted) mass orderings. Note that normal and inverted orderings are always associated with the first and second octants of θ_{23} respectively. For normal (inverted) ordering with the NSM mixing pattern δ lies in the first (second) quadrant while for the other cases it is in the second (first) quadrant. As expected, for inverted ordering $|\delta|$ stays close to $\pi/2$ for the entire range of m_0. For normal ordering δ is near $\pi/2$ for m_0 larger than around 0.05 eV.

Of course, as indicated in Table 5.5 if δ is a solution for some m_0 then by suitably picking alternate values of the phases $\phi_{1,2}$ which appear in M_R one can also get a second solution with the phase $-\delta$. We have not shown this mirror set of solutions in Fig. 5.2. The T2K [10] and NOνA [11] experiments have presented data which may be taken as a preliminary hint of normal ordering associated with $\delta \sim -\pi/2$. As seen from Fig. 5.2 this is consistent with our model, with $\delta \sim -\pi/2$ favouring m_0 in the quasidegenerate regime, i.e., $m_0 \geq \mathcal{O}(0.05\text{ eV})$. If this result is confirmed by further analysis then the model will require neutrino masses to be in a range to which ongoing experiments will be sensitive [19, 86].

The correlation between the octant of θ_{23}, the quadrant of the CP phase δ, and the ordering of neutrino masses is a smoking-gun signal of this $S3 \times Z3$ based model.

5.4 Conclusions

In this chapter we have put forward an $S3 \times Z3$ model for neutrino mass and mixing. After assigning the flavour quantum numbers to the leptons and the scalars we write down the most general Lagrangian consistent with the symmetry. Once the symmetry is broken, the Yukawa couplings give rise to the charged lepton masses as well as the Dirac and Majorana masses for the left- and right-handed neutrinos.

Neutrino masses originate from both Type I and Type II seesaw terms of which the former can be treated as a small correction. The dominant Type II seesaw results in the atmospheric mass splitting, no solar splitting, keeps $\theta_{23} = \pi/4$, and $\theta_{13} = 0$. By a choice of the Yukawa couplings θ_{12} can be given any preferred value. Thus, at this level this model can accommodate any of the much-studied Tribimaximal, Bimaximal, Golden Ratio, and no solar mixing patterns. The smaller Type I seesaw contribution acting as a perturbation generates the solar mass splitting and nudges the mixing angles to values consistent with the global fits. The octants of θ_{23} are correlated with the neutrino mass ordering – first (second) octant is allowed for normal (inverted) ordering. The model is testable through its predictions for the CP phase δ and from the relationships between mixing angles and mass splittings that it entails. Further, inverted mass ordering is correlated with a near-maximal CP phase δ and arbitrarily small neutrino masses are permitted. For normal mass ordering δ can vary over a wider range and maximality is realised in the quasi-degenerate limit. The lightest neutrino mass must be at least a few meV in this case.

5.A Appendix: Essentials of the $S3$ group

$S3$ is a discrete group of order 6 which consists of all permutations of three objects. It can be generated by two elements A and B satisfying $A^2 = I = B^3$ and $(AB)\,(AB) = I$. The group table is given below.

	I	A	B	C	D	F
I	I	A	B	C	D	F
A	A	I	C	B	F	D
F	F	C	I	D	A	B
C	C	F	D	I	B	A
D	D	B	A	F	I	C
B	B	D	F	A	C	I

Table 5.6: The group table for $S3$.

The group has two 1-dimensional representations denoted by 1 and $1'$, and a 2-dimensional representation. 1 is inert under the group while $1'$ changes sign under the action of A. For the 2-dimensional representation a suitable choice of matrices with the specified properties can be readily obtained. We choose

$$I = \begin{pmatrix} 1 & 0 \\ 0 & 1 \end{pmatrix} \;\; , \;\; A = \begin{pmatrix} 0 & 1 \\ 1 & 0 \end{pmatrix} \;\; , \;\; B = \begin{pmatrix} \omega & 0 \\ 0 & \omega^2 \end{pmatrix} \;\; , \tag{5.A.1}$$

where ω is a cube root of unity, i.e., $\omega = e^{2\pi i/3}$. For this choice of A and B the remaining matrices of the representation are:

$$C = \begin{pmatrix} 0 & \omega^2 \\ \omega & 0 \end{pmatrix} \;\; , \;\; D = \begin{pmatrix} 0 & \omega \\ \omega^2 & 0 \end{pmatrix} \;\; , \;\; F = \begin{pmatrix} \omega^2 & 0 \\ 0 & \omega \end{pmatrix} \;\; . \tag{5.A.2}$$

The product rules for the different representations are:

$$1 \times 1' = 1',\ 1' \times 1' = 1,\ \text{and}\ 2 \times 2 = 2 + 1 + 1' \ . \tag{5.A.3}$$

One can see that each of the 2×2 matrices M_{ij} in Eqs. (5.A.1) and (5.A.2) satisfies:

$$\sum_{j,l\ =1,2} \alpha_{jl}\ M_{ij}\ M_{kl} = \alpha_{ik}\ \ , \tag{5.A.4}$$

where $\alpha_{ij} = 0$ for $i = j$ and $\alpha_{ij} = 1$ for $i \neq j$.

If $\Phi \equiv \begin{pmatrix} \phi_1 \\ \phi_2 \end{pmatrix}$ and $\Psi \equiv \begin{pmatrix} \psi_1 \\ \psi_2 \end{pmatrix}$ are two field multiplets transforming under $S3$ as doublets then using Eqs. (5.A.1) and (5.A.4):

$$\phi_1\psi_2 + \phi_2\psi_1 \equiv 1\ \ ,\ \ \phi_1\psi_2 - \phi_2\psi_1 \equiv 1'\ \text{and}\ \ \begin{pmatrix} \phi_2\psi_2 \\ \phi_1\psi_1 \end{pmatrix} \equiv 2\ \ . \tag{5.A.5}$$

Sometimes we have to deal with hermitian conjugate fields. Noting the nature of the complex representation (see, for example, B in Eq. (5.A.1)) the conjugate $S3$ doublet is $\Phi^\dagger \equiv \begin{pmatrix} \phi_2^\dagger \\ \phi_1^\dagger \end{pmatrix}$. As a result, one has in place of (5.A.5)

$$\phi_2^\dagger\psi_2 + \phi_1^\dagger\psi_1 \equiv 1\ \ ,\ \ \phi_2^\dagger\psi_2 - \phi_1^\dagger\psi_1 \equiv 1'\ \text{and}\ \ \begin{pmatrix} \phi_1^\dagger\psi_2 \\ \phi_2^\dagger\psi_1 \end{pmatrix} \equiv 2\ \ . \tag{5.A.6}$$

Eqs. (5.A.5) and (5.A.6) are essential in writing down the fermion mass matrices in Sec. 5.2.

5.B Appendix: The scalar potential and its minimum

As seen in Table 5.3 this model has a rich scalar field content. In this Appendix we write down the scalar potential of the model keeping all these fields and derive conditions which must be met by the coefficients of the various terms so that the desired *vev*s can be achieved. These conditions ensure that the potential is locally minimized by this choice.

Table 5.3 displays the behaviour of the scalar fields under $S3 \times Z3$ besides the gauged electroweak $SU(2)_L \times U(1)_Y$. The fields also carry a lepton number. The scalar potential is the most general polynomial in these fields with up to quartic terms. Our first step will be to write down the explicit form of this potential. Here we do not exclude any term permitted by the symmetries. $SU(2)_L \times U(1)_Y$ invariance of the terms as well as the abelian lepton number and $Z3$ conservation are readily verified. It is only the $S3$ behaviour which merits special attention.

There are a variety of scalar fields in this model, e.g., $SU(2)_L$ singlets, doublets, and triplets. Therefore, the scalar potential has a large number of terms. For simplicity we choose all couplings in the potential to be real. In this Appendix we list the potential in separate parts: (a) those belonging to any one $SU(2)_L$ sector, and (b) inter-sector couplings of scalars. The $SU(2)_L$ singlet *vev*s, which are responsible for the right-handed neutrino mass, are significantly larger than those of other scalars. So, in the second category we retain only those terms which couple the singlet fields to either the doublet or the triplet sectors.

5.B.1 $SU(2)_L$ Singlet Sector:

The $SU(2)_L$ singlet sector comprises of two fields χ and γ transforming as $1(\omega)$ and $1'(\omega)$ of $S3$ (Z_3) respectively. They have $L = 0$. The scalar potential arising out of these is:

$$\begin{aligned} V_{singlet} &= m_\chi^2 \chi^\dagger \chi + m_\gamma^2 \gamma^\dagger \gamma + \Lambda_1^s \left\{ \gamma^2 \chi + h.c. \right\} + \frac{\lambda_1^s}{2} \left[\chi^\dagger \chi \right]^2 + \frac{\lambda_2^s}{2} \left[\gamma^\dagger \gamma \right]^2 \\ &+ \frac{\lambda_3^s}{2} (\chi^\dagger \chi)(\gamma^\dagger \gamma) + \lambda_4^s \left\{ (\gamma^\dagger \chi)(\gamma^\dagger \chi) + h.c. \right\} \quad , \end{aligned} \tag{5.B.1}$$

where the coefficient of the cubic term, Λ_1^s, carries the same dimension as mass while the λ_i^s are dimensionless.

5.B.2 $SU(2)_L$ Doublet Sector:

The $SU(2)_L$ doublet sector of the model has two fields $\Phi_{a,b}$ that are doublets of $S3$, in addition to α, β, and η which are $S3$ singlets. Among them, all fields except Φ_b and α ($\in \omega$ of Z_3) are invariant under Z_3.

$$\begin{aligned} V_{doublet} &= m_{\Phi_a}^2 \Phi_a^\dagger \Phi_a + m_{\Phi_b}^2 \Phi_b^\dagger \Phi_b + m_\eta^2 \eta^\dagger \eta + m_\alpha^2 \alpha^\dagger \alpha + m_\beta^2 \beta^\dagger \beta \\ &+ \frac{\lambda_1^d}{2} \left(\Phi_a^\dagger \Phi_a \right)^2 + \frac{\lambda_2^d}{2} \left(\Phi_b^\dagger \Phi_b \right)^2 + \frac{\lambda_3^d}{2} (\Phi_a^\dagger \Phi_a)(\Phi_b^\dagger \Phi_b) + \frac{\lambda_4^d}{2} (\Phi_a^\dagger \Phi_b)(\Phi_b^\dagger \Phi_a) \\ &+ \frac{\lambda_5^d}{2} (\Phi_a^\dagger \Phi_a)(\eta^\dagger \eta) + \frac{\lambda_6^d}{2} (\Phi_a^\dagger \Phi_a)(\alpha^\dagger \alpha) + \frac{\lambda_7^d}{2} (\Phi_a^\dagger \Phi_a)(\beta^\dagger \beta) + \frac{\lambda_8^d}{2} (\Phi_b^\dagger \Phi_b)(\alpha^\dagger \alpha) \\ &+ \frac{\lambda_9^d}{2} (\Phi_b^\dagger \Phi_b)(\beta^\dagger \beta) + \frac{\lambda_{10}^d}{2} (\Phi_b^\dagger \Phi_b)(\eta^\dagger \eta) + \frac{\lambda_{11}^d}{2} \left(\alpha^\dagger \alpha \right)^2 + \frac{\lambda_{12}^d}{2} (\alpha^\dagger \alpha)(\eta^\dagger \eta) \\ &+ \frac{\lambda_{13}^d}{2} (\alpha^\dagger \eta)(\eta^\dagger \alpha) + \frac{\lambda_{14}^d}{2} (\alpha^\dagger \alpha)(\beta^\dagger \beta) + \frac{\lambda_{15}^d}{2} \left(\eta^\dagger \eta \right)^2 + \frac{\lambda_{16}^d}{2} (\eta^\dagger \eta)(\beta^\dagger \beta) \\ &+ \lambda_{17}^d \left\{ (\Phi_a^\dagger \Phi_b)(\alpha^\dagger \eta) + h.c. \right\} + \frac{\lambda_{18}^d}{2} \left(\beta^\dagger \beta \right)^2 \quad . \end{aligned} \tag{5.B.2}$$

Leaving aside $S3$ properties for the moment, to which we return below, out of any $SU(2)$ doublet Φ one can construct two quartic invariants $(\Phi^\dagger \Phi)(\Phi^\dagger \Phi)$ and $(\Phi^\dagger \vec{\tau} \Phi)(\Phi^\dagger \vec{\tau} \Phi)$. Needless to say, this can be generalised to the case where several distinct $SU(2)$ doublets are involved. In order to avoid cluttering, in Eq. (5.B.2) we have displayed only the first combination for all quartic terms.

The quartic terms involving λ_1 to λ_4 in Eq. (5.B.2) are combinations of two pairs of $S3$ doublets. Each pair can combine in accordance to $2\times 2 = 1+1'+2$ resulting in three terms. The $S3$ invariant in the potential arises from a combination of the $1,\ 1',$ or 2 from one pair with the corresponding term from the other pair. Thus, for each such term of four $S3$ doublets, three possible singlet combinations exist (recall, Eq. (5.A.3)) and we have to keep an account of all of them. We elaborate on this using as an example the λ_1^d term which actually stands for a set of terms:

$$\begin{aligned}\frac{\lambda_1^d}{2}\left(\Phi_a^\dagger\Phi_a\right)^2 \;&\to\; \lambda_{1_1}^d\left[(\Phi_1^\dagger\Phi_1)+(\Phi_2^\dagger\Phi_2)\right]^2+\lambda_{1_{1'}}^d\left[(\Phi_1^\dagger\Phi_1)-(\Phi_2^\dagger\Phi_2)\right]^2\\ &+\; \lambda_{1_2}^d\left[(\Phi_1^\dagger\Phi_2)(\Phi_2^\dagger\Phi_1)+(\Phi_2^\dagger\Phi_1)(\Phi_1^\dagger\Phi_2)\right]. \qquad (5.B.3)\end{aligned}$$

Substituting *vevs*, $\langle\Phi_1\rangle = v_1$ and $\langle\Phi_2\rangle = v_2$ and defining $\lambda_{1_1}^d + \lambda_{1_{1'}}^d = \frac{\lambda_{a_1}^d}{2}$ and $2(\lambda_{1_1}^d - \lambda_{1_{1'}}^d + \lambda_{1_2}^d) = \frac{\lambda_{a_2}^d}{2}$ we get:

$$\frac{\lambda_1^d}{2}\left(\Phi_a^\dagger\Phi_a\right)^2 \longrightarrow \frac{\lambda_{a_1}^d}{2}\left[(v_1^*v_1)^2+(v_2^*v_2)^2\right]+\frac{\lambda_{a_2}^d}{2}(v_1^*v_1)(v_2^*v_2). \qquad (5.B.4)$$

Similarly,

$$\frac{\lambda_2^d}{2}\left(\Phi_b^\dagger\Phi_b\right)^2 \longrightarrow \frac{\lambda_{b_1}^d}{2}\left[(v_3^*v_3)^2+(v_4^*v_4)^2\right]+\frac{\lambda_{b_2}^d}{2}(v_3^*v_3)(v_4^*v_4) \qquad (5.B.5)$$

where, $\langle\Phi_3\rangle = v_3$ and $\langle\Phi_4\rangle = v_4$. Further,

$$\begin{aligned}\frac{\lambda_3^d}{2}\left[(\Phi_a^\dagger\Phi_a)(\Phi_b^\dagger\Phi_b)\right] \;&\to\; \lambda_{3_1}^d\left[(\Phi_1^\dagger\Phi_1+\Phi_2^\dagger\Phi_2)(\Phi_3^\dagger\Phi_3+\Phi_4^\dagger\Phi_4)\right]\\ &+\; \lambda_{3_{1'}}^d\left[(\Phi_1^\dagger\Phi_1-\Phi_2^\dagger\Phi_2)(\Phi_3^\dagger\Phi_3-\Phi_4^\dagger\Phi_4)\right]\\ &+\; \lambda_{3_2}^d\left[(\Phi_1^\dagger\Phi_2)(\Phi_4^\dagger\Phi_3)+(\Phi_2^\dagger\Phi_1)(\Phi_3^\dagger\Phi_4)\right]. \qquad (5.B.6)\end{aligned}$$

Substituting the respective *vevs* and defining $\lambda_{3_1}^d + \lambda_{3_{1'}}^d = \frac{\lambda_{ab_1}^d}{2}$, $\lambda_{3_1}^d - \lambda_{3_{1'}}^d = \frac{\lambda_{ab_2}^d}{2}$ and $\lambda_{3_2}^d = \lambda_{ab_3}^d$ we get;

$$\begin{aligned}\frac{\lambda_3^d}{2}\left[(\Phi_a^\dagger\Phi_a)(\Phi_b^\dagger\Phi_b)\right] \;&\longrightarrow\; \frac{\lambda_{ab_1}^d}{2}\left[(v_1^*v_1)(v_3^*v_3)+(v_2^*v_2)(v_4^*v_4)\right]\\ &+\; \frac{\lambda_{ab_2}^d}{2}\left[(v_1^*v_1)(v_4^*v_4)+(v_2^*v_2)(v_3^*v_3)\right]\\ &+\; \lambda_{ab_3}^d\left[(v_1^*v_2)(v_4^*v_3)+(v_2^*v_1)(v_3^*v_4)\right]. \qquad (5.B.7)\end{aligned}$$

In a similar fashion the λ_4^d term when expanded will lead to

$$\begin{aligned}\frac{\lambda_4^d}{2}\left[(\Phi_a^\dagger\Phi_b)(\Phi_b^\dagger\Phi_a)\right] \;&\longrightarrow\; \frac{\tilde\lambda_{ab_1}^d}{2}\left[(v_1^*v_3)(v_3^*v_1)+(v_2^*v_4)(v_4^*v_2)\right]\\ &+\; \frac{\tilde\lambda_{ab_2}^d}{2}\left[(v_1^*v_3)(v_4^*v_2)+(v_2^*v_4)(v_3^*v_1)\right]\\ &+\; \tilde\lambda_{ab_3}^d\left[(v_1^*v_4)(v_4^*v_1)+(v_2^*v_3)(v_3^*v_2)\right]. \qquad (5.B.8)\end{aligned}$$

Adding Eqs. (5.B.7) and Eq. (5.B.8) we get:

$$\begin{aligned}\frac{\lambda_3^d}{2}\left[(\Phi_a^\dagger\Phi_a)(\Phi_b^\dagger\Phi_b)\right]+\frac{\lambda_4^d}{2}\left[(\Phi_a^\dagger\Phi_b)(\Phi_b^\dagger\Phi_a)\right] &= \frac{\hat{\lambda}_{ab_1}^d}{2}\left[(v_1^*v_1)(v_3^*v_3)+(v_2^*v_2)(v_4^*v_4)\right]\\ &+ \frac{\hat{\lambda}_{ab_2}^d}{2}\left[(v_1^*v_1)(v_4^*v_4)+(v_2^*v_2)(v_3^*v_3)\right]\\ &+ \hat{\lambda}_{ab_3}^d\left[(v_1^*v_2)(v_4^*v_3)+(v_2^*v_1)(v_3^*v_4)\right];\end{aligned} \tag{5.B.9}$$

where, $\frac{\hat{\lambda}_{ab_1}^d}{2}\equiv\frac{\tilde{\lambda}_{ab_1}^d}{2}+\frac{\lambda_{ab_1}^d}{2}$, $\frac{\hat{\lambda}_{ab_2}^d}{2}\equiv\tilde{\lambda}_{ab_3}^d+\frac{\lambda_{ab_2}^d}{2}$ and $\hat{\lambda}_{ab_3}^d\equiv\frac{\tilde{\lambda}_{ab_2}^d}{2}+\lambda_{ab_3}^d$. Also, summing up the λ_{12}^d and λ_{13}^d terms lead to $\frac{\hat{\lambda}_{123}^d}{2}(v_\alpha^*v_\alpha)(v_\eta^*v_\eta)$, where $\hat{\lambda}_{123}^d\equiv\lambda_{12}^d+\lambda_{13}^d$.

5.B.3 $SU(2)_L$ Triplet Sector:

Both the $SU(2)_L$ triplets present in our model (Δ_L, ρ_L) that are responsible for Majorana mass generation of the left handed neutrinos happen to be $S3$ invariants and differ only in their Z_3 properties i.e., $\Delta_L(1)$ and $\rho_L(\omega)$.

$$\begin{aligned}V_{triplet} &= m_{\Delta_L}^2\Delta_L^\dagger\Delta_L+m_{\rho_L}^2\rho_L^\dagger\rho_L+\frac{\lambda_1^t}{2}\left[\Delta_L^\dagger\Delta_L\right]^2+\frac{\lambda_2^t}{2}\left[\rho_L^\dagger\rho_L\right]^2+\frac{\lambda_3^t}{2}(\Delta_L^\dagger\Delta_L)(\rho_L^\dagger\rho_L)\\ &+ \frac{\lambda_4^t}{2}(\Delta_L^\dagger\rho_L)(\rho_L^\dagger\Delta_L)+\frac{\lambda_5^t}{2}(\Delta_L\rho_L)(\Delta_L\rho_L)^\dagger\ .\end{aligned} \tag{5.B.10}$$

It is noteworthy that when we write the minimized potential in terms of the vacuum expectation values, the λ_3^t, λ_4^t and λ_5^t terms will be providing the same contribution as far as potential minimization is concerned. Thus we can club these couplings together as $\lambda_{345}^t\equiv\lambda_3^t+\lambda_4^t+\lambda_5^t$.

5.B.4 Inter-sector terms:

So far we have listed those terms in the potential which arise from scalars of any specific $SU(2)_L$ behaviour – singlets, doublets, or triplets. In addition, there can be terms which couple one of these sectors to another. Since the vacuum expectation values of the singlet scalars are the largest we only consider here the couplings of this sector to the others. The $SU(2)_L$ triplet sector vev is very small and we drop the doublet-triplet cross-sector couplings.

$SU(2)_L$ Singlet-Doublet cross-sector:

Couplings between the $SU(2)_L$ singlet and doublet scalars in the potential give rise to the terms:

$$V_{ds} = \Lambda_1^{ds}\left[(\Phi_b^\dagger\Phi_a)_{1'}\gamma+h.c.\right]+\Lambda_2^{ds}\left[(\Phi_b^\dagger\Phi_a)_1\chi+h.c.\right]+\Lambda_3^{ds}\left[(\alpha^\dagger\eta)\chi+h.c.\right]$$

$$
\begin{aligned}
&+ \quad \frac{\lambda_1^{ds}}{2}(\Phi_a^\dagger\Phi_a)(\chi^\dagger\chi) + \frac{\lambda_2^{ds}}{2}(\Phi_a^\dagger\Phi_a)(\gamma^\dagger\gamma) + \frac{\lambda_3^{ds}}{2}(\Phi_b^\dagger\Phi_b)(\chi^\dagger\chi) + \frac{\lambda_4^{ds}}{2}(\Phi_b^\dagger\Phi_b)(\gamma^\dagger\gamma) \\
&+ \quad \frac{\lambda_5^{ds}}{2}(\alpha^\dagger\alpha)(\chi^\dagger\chi) + \frac{\lambda_6^{ds}}{2}(\alpha^\dagger\alpha)(\gamma^\dagger\gamma) + \frac{\lambda_7^{ds}}{2}(\eta^\dagger\eta)(\chi^\dagger\chi) + \frac{\lambda_8^{ds}}{2}(\eta^\dagger\eta)(\gamma^\dagger\gamma) \\
&+ \quad \lambda_9^{ds}\left[(\Phi_a^\dagger\Phi_b)\chi^2 + h.c.\right] + \lambda_{10}^{ds}\left[(\Phi_a^\dagger\Phi_b)\gamma^2 + h.c.\right] + \lambda_{11}^{ds}\left[(\eta^\dagger\alpha)\chi^2 + h.c.\right] \\
&+ \quad \lambda_{12}^{ds}\left[(\eta^\dagger\alpha)\gamma^2 + h.c.\right] + \lambda_{13}^{ds}\left[(\Phi_a^\dagger\Phi_b)_{1'}(\chi\gamma) + h.c.\right] + \frac{\lambda_{14}^{ds}}{2}(\beta^\dagger\beta)(\chi^\dagger\chi) \\
&+ \quad \frac{\lambda_{15}^{ds}}{2}(\beta^\dagger\beta)(\gamma^\dagger\gamma) \quad . \qquad (5.B.11)
\end{aligned}
$$

$SU(2)_L$ **Singlet-Triplet cross-sector:**

The terms in the potential which arise from couplings between the $SU(2)_L$ singlet and triplet scalars are:

$$
\begin{aligned}
V_{ts} \quad &= \quad \Lambda_1^{ts}\left[(\rho_L^\dagger\Delta_L)\chi + h.c.\right] + \frac{\lambda_1^{ts}}{2}(\Delta_L^\dagger\Delta_L)(\chi^\dagger\chi) + \frac{\lambda_2^{ts}}{2}(\Delta_L^\dagger\Delta_L)(\gamma^\dagger\gamma) \\
&+ \quad \frac{\lambda_3^{ts}}{2}(\rho_L^\dagger\rho_L)(\chi^\dagger\chi) + \frac{\lambda_4^{ts}}{2}(\rho_L^\dagger\rho_L)(\gamma^\dagger\gamma) + \lambda_5^{ts}\left\{(\Delta_L^\dagger\rho_L)\chi^2 + h.c.\right\} \\
&+ \quad \lambda_6^{ts}\left\{(\Delta_L^\dagger\rho_L)\gamma^2 + h.c.\right\} \quad . \qquad (5.B.12)
\end{aligned}
$$

5.B.5 The minimization conditions:

The vevs of the scalar fields are given in Table 5.3. Using these:

$SU(2)_L$ singlets: $\langle\gamma^0\rangle = u_\gamma$ and $\langle\chi^0\rangle = u_\chi$.

$SU(2)_L$ doublets: $\langle\Phi_a\rangle = \begin{pmatrix} 0 & v_1 \\ 0 & v_2 \end{pmatrix}$, $\langle\Phi_b\rangle = \begin{pmatrix} 0 & v_3 \\ 0 & v_4 \end{pmatrix}$, $\langle\eta\rangle = v_\eta\,(\,0 \quad 1\,)$, $\langle\alpha\rangle = v_\alpha\,(\,0 \quad 1\,)$ and $\langle\beta\rangle = v_\beta\,(\,1 \quad 0\,)$.

Recall that from the structure of the charged lepton mass matrix Eq. (5.12) requires $v_2/v_1 = v_4/v_3 = A$ where the real quantity $A = m_\mu/m_\tau$. We often also need $B \equiv (1 + A^2)$.

$SU(2)_L$ triplets: $\langle\rho_L^0\rangle = v_\rho$ and $\langle\Delta_L^0\rangle = v_\Delta$.

$SU(2)_L$ **Singlet sector:**

$$
\frac{\partial V_{singlet}|_{min}}{\partial u_\chi^*} = 0 \Rightarrow u_\chi\left[m_\chi^2 + \lambda_1^s u_\chi^* u_\chi\right] + \Lambda_1^s\left(u_\gamma^*\right)^2 + u_\gamma\left[\frac{\lambda_3^s}{2}u_\chi u_\gamma^* + 2\lambda_4^s u_\chi^* u_\gamma\right] = 0 \quad , \qquad (5.B.13)
$$

and

$$\frac{\partial V_{singlet}|_{min}}{\partial u_\gamma^*} = 0 \Rightarrow u_\gamma \left[m_\gamma^2 + \lambda_2^s u_\gamma^* u_\gamma\right] + 2\Lambda_1^s \left(u_\gamma^* u_\chi^*\right) + u_\chi \left[\frac{\lambda_3^s}{2} u_\gamma u_\chi^* + 2\lambda_4^s u_\gamma^* u_\chi\right] = 0 \ . \tag{5.B.14}$$

$SU(2)_L$ **Doublet sector:**

Define $V_{\mathscr{D}} = V_{doublet} + V_{ds}$.

$$\begin{aligned}\frac{\partial V_{\mathscr{D}}|_{min}}{\partial v_\alpha^*} &= v_\alpha \left[m_\alpha^2 + \frac{\lambda_6^d}{2}(v_1^* v_1)B + \frac{\lambda_8^d}{2}(v_3^* v_3)B\right] \\ &+ v_\alpha \left[\lambda_{11}^d (v_\alpha^* v_\alpha) + \frac{\hat{\lambda}_{123}^d}{2}(v_\eta^* v_\eta) + \lambda_{14}^d (v_\beta^* v_\beta) + \frac{\lambda_5^{ds}}{2}(u_\chi^* u_\chi) + \frac{\lambda_6^{ds}}{2}(u_\gamma^* u_\gamma)\right] \\ &+ v_\eta \left[\lambda_{17}^d (v_1^* v_3)B + \Lambda_3^{ds} u_\chi + \lambda_{11}^{ds}(u_\chi^*)^2 + \lambda_{12}^{ds}(u_\gamma^*)^2\right] = 0.\end{aligned} \tag{5.B.15}$$

$$\begin{aligned}\frac{\partial V_{\mathscr{D}}|_{min}}{\partial v_\beta^*} &= v_\beta \left[m_\beta^2 + \frac{\lambda_7^d}{2}(v_1^* v_1)B + \frac{\lambda_9^d}{2}(v_3^* v_3)B + \frac{\lambda_{14}^d}{2}(v_\alpha^* v_\alpha) + \frac{\lambda_{16}^d}{2}(v_\eta^* v_\eta)\right] \\ &+ v_\beta \left[\lambda_{18}^d (v_\beta^* v_\beta) + \frac{\lambda_{14}^{ds}}{2}(u_\chi^* u_\chi) + \frac{\lambda_{15}^{ds}}{2}(u_\gamma^* u_\gamma)\right] = 0.\end{aligned} \tag{5.B.16}$$

$$\begin{aligned}\frac{\partial V_{\mathscr{D}}|_{min}}{\partial v_\eta^*} &= v_\eta \left[m_\eta^2 + \frac{\lambda_5^d}{2}(v_1^* v_1)B + \frac{\lambda_{10}^d}{2}(v_3^* v_3)B + \frac{\hat{\lambda}_{123}^d}{2}(v_\alpha^* v_\alpha) + \lambda_{15}^d (v_\eta^* v_\eta)\right] \\ &+ v_\eta \left[\frac{\lambda_{16}^d}{2}(v_\beta^* v_\beta) + \frac{\lambda_7^{ds}}{2}(u_\chi^* u_\chi) + \frac{\lambda_8^{ds}}{2}(u_\gamma^* u_\gamma)\right] \\ &+ v_\alpha \left[\lambda_{17}^d (v_3^* v_1)B + \Lambda_3^{ds} u_\chi^* + \lambda_{11}^{ds}(u_\chi)^2 + \lambda_{12}^{ds}(u_\gamma)^2\right] \\ &= 0.\end{aligned} \tag{5.B.17}$$

$$\begin{aligned}\frac{\partial V_{\mathscr{D}}|_{min}}{\partial v_1^*} &= v_1 \left[m_{\Phi_a}^2 + (v_1^* v_1)\left(\lambda_{a_1}^d + A^2 \frac{\lambda_{a_2}^d}{2}\right)\right] \\ &+ v_1 \left[(v_3^* v_3)\left(\frac{\hat{\lambda}_{ab_1}^d}{2} + A^2 \frac{\hat{\lambda}_{ab_2}^d}{2} + A^2 \hat{\lambda}_{ab_3}^d\right)\right]\end{aligned}$$

$$
\begin{aligned}
&+ \quad v_1\left[\left\{\frac{\lambda_5^d}{2}(v_\eta^* v_\eta)+\frac{\lambda_6^d}{2}(v_\alpha^* v_\alpha)+\frac{\lambda_7^d}{2}(v_\beta^* v_\beta)\right\}\right]\\
&+ \quad v_1\left[\left\{\frac{\lambda_1^{ds}}{2}(u_\chi^* u_\chi)+\frac{\lambda_2^{ds}}{2}(u_\gamma^* u_\gamma)\right\}\right]+v_3\left[\left\{\lambda_{17}^d(v_\alpha^* v_\eta)\right\}\right]\\
&+ \quad v_3\left[\left\{\Lambda_1^{ds}u_\gamma^*+\Lambda_2^{ds}u_\chi^*+\lambda_9^{ds}(u_\chi)^2+\lambda_{10}^{ds}(u_\gamma)^2+\lambda_{13}^{ds}(u_\chi u_\gamma)\right\}\right]\\
&= \quad 0. \qquad (5.B.18)
\end{aligned}
$$

$$
\begin{aligned}
\frac{\partial V_{\mathscr{D}}|_{min}}{\partial v_2^*} &= Av_1\left[m_{\Phi_a}^2+(v_1^* v_1)\left(A^2\lambda_{a_1}^d+\frac{\lambda_{a_2}^d}{2}\right)\right]\\
&+ Av_1\left[(v_3^* v_3)\left(A^2\frac{\hat\lambda_{ab_1}^d}{2}+\frac{\hat\lambda_{ab_2}^d}{2}+\hat\lambda_{ab_3}^d\right)\right]\\
&+ Av_1\left[\left\{\frac{\lambda_5^d}{2}(v_\eta^* v_\eta)+\frac{\lambda_6^d}{2}(v_\alpha^* v_\alpha)+\frac{\lambda_7^d}{2}(v_\beta^* v_\beta)\right\}\right]\\
&+ Av_1\left[\left\{\frac{\lambda_1^{ds}}{2}(u_\chi^* u_\chi)+\frac{\lambda_2^{ds}}{2}(u_\gamma^* u_\gamma)\right\}\right]+Av_3\left[\left\{\lambda_{17}^d(v_\alpha^* v_\eta)\right\}\right]\\
&+ Av_3\left[\left\{-\Lambda_1^{ds}u_\gamma^*+\Lambda_2^{ds}u_\chi^*+\lambda_9^{ds}(u_\chi)^2+\lambda_{10}^{ds}(u_\gamma)^2-\lambda_{13}^{ds}(u_\chi u_\gamma)\right\}\right]\\
&= 0. \qquad (5.B.19)
\end{aligned}
$$

$$
\begin{aligned}
\frac{\partial V_{\mathscr{D}}|_{min}}{\partial v_3^*} &= v_3\left[m_{\Phi_b}^2+(v_3^* v_3)\left(\lambda_{b_1}^d+A^2\frac{\lambda_{b_2}^d}{2}\right)\right]\\
&+ v_3\left[(v_1^* v_1)\left(\frac{\hat\lambda_{ab_1}^d}{2}+A^2\frac{\hat\lambda_{ab_2}^d}{2}+A^2\hat\lambda_{ab_3}^d\right)\right]\\
&+ v_3\left[\left\{\frac{\lambda_8^d}{2}(v_\alpha^* v_\alpha)+\frac{\lambda_9^d}{2}(v_\beta^* v_\beta)+\frac{\lambda_{10}^d}{2}(v_\eta^* v_\eta)\right\}\right]\\
&+ v_3\left[\left\{\frac{\lambda_3^{ds}}{2}(u_\chi^* u_\chi)+\frac{\lambda_4^{ds}}{2}(u_\gamma^* u_\gamma)\right\}\right]+v_1\left[\left\{\lambda_{17}^d(v_\eta^* v_\alpha)\right\}\right]\\
&+ v_1\left[\left\{\Lambda_1^{ds}u_\gamma+\Lambda_2^{ds}u_\chi+\lambda_9^{ds}(u_\chi^*)^2+\lambda_{10}^{ds}(u_\gamma^*)^2+\lambda_{13}^{ds}(u_\chi^* u_\gamma^*)\right\}\right]\\
&= 0.
\end{aligned}
\qquad (5.B.20)
$$

$$
\begin{aligned}
\frac{\partial V_{\mathscr{D}}|_{min}}{\partial v_4^*} &= Av_3\left[m_{\Phi_b}^2+(v_3^* v_3)\left(A^2\lambda_{b_1}^d+\frac{\lambda_{b_2}^d}{2}\right)\right]\\
&+ Av_3\left[(v_1^* v_1)\left(A^2\frac{\hat\lambda_{ab_1}^d}{2}+\frac{\hat\lambda_{ab_2}^d}{2}+\hat\lambda_{ab_3}^d\right)\right]\\
&+ Av_3\left[\left\{\frac{\lambda_8^d}{2}(v_\alpha^* v_\alpha)+\frac{\lambda_9^d}{2}(v_\beta^* v_\beta)+\frac{\lambda_{10}^d}{2}(v_\eta^* v_\eta)\right\}\right]
\end{aligned}
$$

$$
\begin{aligned}
&+ \quad Av_3\left[\left\{\frac{\lambda_3^{ds}}{2}(u_\chi^* u_\chi)+\frac{\lambda_4^{ds}}{2}(u_\gamma^* u_\gamma)\right\}\right]+Av_1\left[\left\{\lambda_{17}^{d}(v_\eta^* v_\alpha)\right\}\right]\\
&+ \quad Av_1\left[+\left\{-\Lambda_1^{ds}u_\gamma+\Lambda_2^{ds}u_\chi+\lambda_9^{ds}(u_\chi^*)^2+\lambda_{10}^{ds}(u_\gamma^*)^2-\lambda_{13}^{ds}(u_\chi^* u_\gamma^*)\right\}\right]\\
&= \quad 0. \qquad (5.B.21)
\end{aligned}
$$

$SU(2)_L$ **Triplet sector:**

Define $V_{\mathscr{T}} = V_{triplet} + V_{ts}$.

$$
\begin{aligned}
\frac{\partial V_{\mathscr{T}}|_{min}}{\partial v_\Delta^*} &= v_\Delta\left[\left\{m_{\Delta_L}^2+\lambda_1^t(v_\Delta^* v_\Delta)+\frac{\lambda_{345}^t}{2}(v_\rho^* v_\rho)\right\}\right]\\
&+ v_\Delta\left[+\left\{\frac{\lambda_1^{ts}}{2}(u_\chi^* u_\chi)+\frac{\lambda_2^{ts}}{2}(u_\gamma^* u_\gamma)\right\}\right]\\
&+ v_\rho\left[\Lambda_1^{ts}u_\chi^*+\lambda_5^{ts}u_\chi^2+\lambda_6^{ts}u_\gamma^2\right]=0. \qquad (5.B.22)
\end{aligned}
$$

$$
\begin{aligned}
\frac{\partial V_{\mathscr{T}}|_{min}}{\partial v_\rho^*} &= v_\rho\left[\left\{m_{\rho_L}^2+\lambda_2^t(v_\rho^* v_\rho)+\frac{\lambda_{345}^t}{2}(v_\Delta^* v_\Delta)\right\}\right]\\
&+ v_\rho\left[\left\{\frac{\lambda_3^{ts}}{2}(u_\chi^* u_\chi)+\frac{\lambda_4^{ts}}{2}(u_\gamma^* u_\gamma)\right\}\right]\\
&+ v_\Delta\left[\Lambda_1^{ts}u_\chi+\lambda_5^{ts}(u_\chi^*)^2+\lambda_6^{ts}(u_\gamma^*)^2\right]=0. \qquad (5.B.23)
\end{aligned}
$$

Chapter 6

Summary and Conclusions

Neutrino mass and mixing have been subjects of intensive exploration as they shed light on the physics beyond the standard model. The three-neutrino oscillation scenario is completely characterised by the three mixing angles (θ_{12}, θ_{13}, θ_{23}), two independent mass square splittings (Δm^2_{solar}, Δm^2_{atm}) and the CP phase δ. Oscillation experiments over vastly different baselines and a range of neutrino energies have filled up a vast portion of the mass and mixing jigsaw of the neutrino sector. Atmospheric and solar neutrinos indicate two very different scales of neutrino mass splitting – $\Delta m^2_{solar}/|\Delta m^2_{atm}| \sim 10^{-2}$ – which are confirmed in accelerator and reactor experiments. Yet, we still remain in the dark with regard to CP violation in the lepton sector. Neither do we know the mass ordering – whether it is normal or inverted. Further open issues are the absolute mass scale of neutrinos and whether they are of Majorana or Dirac nature. While we await experimental guidance for each of the above unknowns, there have been many attempts to build models of lepton mass which capture much of what is known which is the prime intent of my doctoral research as well.

The thematic flow of the thesis has been to consider a two-component procedure such that from the dominant contribution we could achieve any of the popular lepton mixings viz. TBM, BM, GR and the NSM, each of which requires $\theta_{13} = 0$ and $\theta_{23} = \frac{\pi}{4}$. Needless to say that these mixing patterns are in sharp contrast with the current status of the neutrino oscillation data. The role played by the sub-dominant contribution had been to tweak the dominant component so as the obtain the oscillation parameters within the observed range.

After a summary of the essential background of neutrino physics and the Standard Model of particle physics, in Chapter 2 and Chapter 3 model independent implementations of this mechanism were undertaken. The dominant contribution in Chapter 2 had $\Delta m^2_{solar} = 0$ with the data allowed value of Δm^2_{atm}. The mixing angles were that of the popular lepton mixing type studied case by case. Summing up, all the dominant contributions were characterised by $\Delta m^2_{solar} = 0$ and $\theta_{13} = 0$ that were ameliorated by the sub-dominant contribution to produce non-zero values of these quantities. CP phase δ was predicted for all the four mixing

patterns. We restricted ourselves to the NSM scheme in Chapter 3. Thus the dominant component had $\Delta m^2_{solar} = 0, \quad \theta_{13} = 0, \quad \theta_{23} = \frac{\pi}{4}, \quad \theta_{12} = 0$. The origin of it can be derived from a Type II seesaw mechanism. The corrections offered by a Type I seesaw sub-dominant contribution tuned these oscillations parameters in to the allowed range. Predictions for the octant of θ_{23}, CP phase δ and the effective mass for neutrinoless double beta decay in terms of the lightest neutrino mass were presented. As a result these unknowns of the neutrino sector get correlated in our model. Chapter 4 comprises of a model for the scheme discussed in Chapter 3 based on the discrete flavour symmetry $A4$. All the four mixing patterns were amended by this two-component formalism in Chapter 5 where the mass matrices derived their origin from an underlying $S3 \times Z3$ symmetry of the Lagrangian.

Both the models depicted in Chapter 4 and Chapter 5 had an opulent scalar sector. All the lepton mass matrices – charged leptons, left- and right-handed Majorana and Dirac masses of the neutrinos – were generated through these scalars via spontaneous symmetry breaking. All terms consistent with the symmetry were retained. No soft symmetry breaking terms were entertained. The scalar potential was extensively studied with all the terms allowed by the particular flavour symmetries under consideration to the extent of local minimization.

Several predictions were obtained including the octant of θ_{23}, CP phase δ and the effective mass for neutrinoless double beta decay which if found to be in contrast with the experimental observations in future can rule out our model. An interesting inference of our enterprise was the interrelationships between the octant of θ_{23} and the ordering of neutrino mass. Normal ordering always was predicted to be associated with the first octant of θ_{23} whereas inverted ordering got correlated to the second octant of θ_{23}. Thus the models are amenable to testing in the near future.

Bibliography

[1] W. Pauli, *the letter that he sent to the Tubingen conference* on December 4, 1930.

[2] F. Reines and C. L. Cowan, Phys. Rev. **113**, 273 (1959).

[3] Z. Maki, M. Nakagawa and S. Sakata, Prog. Theor. Phys. **28**, 870 (1962).

[4] B. Pontecorvo, Sov. Phys. JETP **6**, 429 (1957) [Zh. Eksp. Teor. Fiz. **33**, 549 (1957)]; Sov. Phys. JETP **7**, 172 (1958) [Zh. Eksp. Teor. Fiz. **34**, 247 (1957)].

[5] L. L. Chau and W. Y. Keung, Phys. Rev. Lett. **53**, 1802 (1984); C. Jarlskog, Z. Phys. C **29**, 491 (1985); C. Jarlskog, Phys. Rev. D **35**, 1685 (1987).

[6] A. Kumar *et al.*, Pramana **88**, 79 (2017).

[7] L. Wolfenstein, Phys. Rev. D **17**, 2369 (1978); L. Wolfenstein, Phys. Rev. D **20**, 2634 (1979); S. P. Mikheev and A. Y. Smirnov, Sov. J. Nucl. Phys. **42**, 913 (1985) [Yad. Fiz. **42**, 1441 (1985)]; S. P. Mikheev and A. Y. Smirnov, Nuovo Cim. C **9**, 17 (1986).

[8] M. C. Gonzalez-Garcia, M. Maltoni, J. Salvado and T. Schwetz, JHEP **1212**, 123 (2012) [arXiv:1209.3023v3 [hep-ph]], NuFIT 2.1 (2016).

[9] C. Bronner on behalf of the T2K collaboration, Talk at the International Conference on Massive Neutrinos, Nanyang Technological University, Singapore, February 2015.

[10] K. Abe et al. (T2K collaboration), arXiv:1502.01550v2 [hep-ex].

[11] P. Adamson et al. (NOVA collaboration), arXiv:1601.05022v2 [hep-ex]; Ryan Patterson [for the NOνA Collaboration], Joint Experimental and Theoretical Seminar, Fermilab, August 06, 2015.

[12] For the current status of θ_{13} see presentations from Double Chooz, RENO, Daya Bay, and T2K at Neutrino 2016 (http://neutrino2016.iopconfs.org/programme).

[13] M. Bass, D. Cherdack and R. J. Wilson, arXiv:1310.6812 [hep-ex];

R. Acciarri *et al.* [DUNE Collaboration], arXiv:1601.05471 [physics.ins-det].

[14] F. P. An *et al.* [Daya Bay Collaboration], Phys. Rev. Lett. **108**, 171803 (2012) [arXiv:1203.1669 [hep-ex]].

[15] J. K. Ahn *et al.* [RENO Collaboration], Phys. Rev. Lett. **108**, 191802 (2012) [arXiv:1204.0626 [hep-ex]].

[16] R. Henning, Rev. Phys. **1**, 29 (2016).

[17] C. Arnaboldi *et al.* [CUORE Collaboration], Nucl. Instrum. Meth. A **518**, 775 (2004) [hep-ex/0212053]; K. Alfonso *et al.* [CUORE Collaboration], Phys. Rev. Lett. **115**, 102502 (2015) [arXiv:1504.02454 [nucl-ex]].

[18] M. Agostini *et al.* [GERDA Collaboration], Phys. Rev. Lett. **111**, 122503 (2013) [arXiv:1307.4720 [nucl-ex]]; K. H. Ackermann *et al.* [GERDA Collaboration], Eur. Phys. J. C **73**, 2330 (2013) [arXiv:1212.4067 [physics.ins-det]]; M. Agostini *et al.* [GERDA Collaboration], Eur. Phys. J. C **74**, 2764 (2014) [arXiv:1306.5084 [physics.ins-det]]; K. T. Knpfle [GERDA Collaboration], PoS TIPP **2014**, 109 (2014).

[19] M. Haag [KATRIN Collaboration], PoS EPS **-HEP2013**, 518 (2013).

[20] M. G. Aartsen *et al.*, Nucl. Phys. B **908**, 161 (2016).

[21] See, for example, P.F. Harrison, D.H. Perkins and W.G. Scott, Phys. Lett. B **530**, 167 (2002); Z. -z. Xing, Phys. Lett. B **533**, 85 (2002); X. He and A. Zee, Phys. Lett. B **560**, 87 (2003).

[22] See, for example, F. Vissani, hep-ph/9708483; V. D. Barger, S. Pakvasa, T. J. Weiler and K. Whisnant, Phys. Lett. B **437**, 107 (1998) [hep-ph/9806387]; R. N. Mohapatra and S. Nussinov, Phys. Rev. D **60**, 013002 (1999) [hep-ph/9809415].

[23] See, for example, A. Datta, F. -S. Ling and P. Ramond, Nucl. Phys. B **671**, 383 (2003) [hep-ph/0306002]; Y. Kajiyama, M. Raidal and A. Strumia, Phys. Rev. D **76**, 117301 (2007) [arXiv:0705.4559 [hep-ph]]; G. -J. Ding, L. L. Everett and A. J. Stuart, Nucl. Phys. B **857**, 219 (2012) [arXiv:1110.1688 [hep-ph]].

[24] S. Pramanick and A. Raychaudhuri, Phys. Rev. D **88**, 093009 (2013) [arXiv:1308.1445 [hep-ph]].

[25] Ta-Pei Cheng and Ling-Fong Li, *'Gauge theory of elementary particle physics'*, Oxford University Press(1984); David Griffiths, *'Introduction to elementary particles'*, Wiley VCH, Second Revised edition (2008); Francis Halzen and Alan D. Martin, *'Quarks and Leptons: An Introductory Course in Modern Particle Physics'*, John Wiley and Sons (1984).

[26] B. W. Lee, C. Quigg and H. B. Thacker, Phys. Rev. D **16**, 1519 (1977).

[27] G. Bhattacharyya, Rept. Prog. Phys. **74**, 026201 (2011) [arXiv:0910.5095 [hep-ph]].

[28] P. W. Higgs, Phys. Lett. **12**, 132 (1964); Phys. Rev. Lett. **13**, 508 (1964); F. Englert and R. Brout, Phys. Rev. Lett. **13**, 321 (1964); G. S. Guralnik, C. R. Hagen and T. W. B. Kibble, Phys. Rev. Lett. **13**, 585 (1964); T. W. B. Kibble, Phys. Rev. **155**, 1554 (1967).

[29] John Gunion, Howard Haber, Gordon Kane and Sally Dawson, *'The Higgs Hunter's Guide'*, Basic Books (1990); S. Dawson, hep-ph/9901280.

[30] G. Aad *et al.* [ATLAS Collaboration], Phys. Lett. B **716**, 1 (2012) [arXiv:1207.7214 [hep-ex]].

[31] S. Chatrchyan *et al.* [CMS Collaboration], Phys. Lett. B **716**, 30 (2012) [arXiv:1207.7235 [hep-ex]].

[32] S. Pramanick and A. Raychaudhuri, Pramana **86**, 407 (2016).

[33] S. Pramanick and A. Raychaudhuri, Phys. Lett. B **746**, 237 (2015) [arXiv:1411.0320 [hep-ph]].

[34] S. Pramanick and A. Raychaudhuri, Int. J. Mod. Phys. A **30**, 1530036 (2015) [arXiv:1504.01555 [hep-ph]].

[35] S. Pramanick and A. Raychaudhuri, Adv. Ser. Direct. High Energy Phys. **25**, 59 (2015).

[36] S. Pramanick and A. Raychaudhuri, Springer Proc. Phys. **174**, 395 (2016).

[37] S. Pramanick and A. Raychaudhuri, Phys. Rev. D **93**, 033007 (2016) [arXiv:1508.02330 [hep-ph]].

[38] S. Pramanick and A. Raychaudhuri, Phys. Rev. D **94**, 115028 (2016) [arXiv:1609.06103 [hep-ph]].

[39] D. A. Dwyer [Daya Bay Collaboration], Nucl. Phys. Proc. Suppl. **235-236**, 30 (2013) [arXiv:1303.3863 [hep-ex]]. F. P. An *et al.* [DAYA-BAY Collaboration], Phys. Rev. Lett. **108**, 171803 (2012) [arXiv:1203.1669 [hep-ex]].

[40] J. K. Ahn *et al.* [RENO Collaboration], Phys. Rev. Lett. **108**, 191802 (2012) [arXiv:1204.0626 [hep-ex]].

[41] Y. Abe *et al.* [DOUBLE-CHOOZ Collaboration], Phys. Rev. Lett. **108**, 131801 (2012) [arXiv:1112.6353 [hep-ex]]; Phys. Lett. B **723**, 66 (2013) [arXiv:1301.2948 [hep-ex]].

[42] P. Adamson *et al.* [MINOS Collaboration], Phys. Rev. Lett. [arXiv:1301.4581 [hep-ex]].

[43] The Review of Particle Physics, K. Nakamura et al. (Particle Data Group), J. Phys. G **37**, 075021 (2010).

[44] M. C. Gonzalez-Garcia, M. Maltoni, J. Salvado and T. Schwetz, JHEP **1212**, 123 (2012) [arXiv:1209.3023v3 [hep-ph]].

[45] D. V. Forero, M. Tortola and J. W. F. Valle, Phys. Rev. D **86**, 073012 (2012) [arXiv:1205.4018 [hep-ph]].

[46] J. Liao, D. Marfatia and K. Whisnant, Phys. Rev. D **87**, 013003 (2013) [arXiv:1205.6860 [hep-ph]]; S. Gupta, A. S. Joshipura and K. M. Patel, arXiv:1301.7130 [hep-ph]; A. Damanik, arXiv:1305.6900 [hep-ph].

[47] B. Grinstein and M. Trott, JHEP **1209**, 005 (2012) [arXiv:1203.4410 [hep-ph]]; D. Borah and M. K. Das, Nuclear Physics B 870, **461** (2013) [arXiv:1210.5074 [hep-ph]].

[48] D. Meloni, F. Plentinger and W. Winter, Phys. Lett. B **699**, 354 (2011) [arXiv:1012.1618 [hep-ph]]; D. Marzocca, S. T. Petcov, A. Romanino and M. Spinrath, JHEP **1111**, 009 (2011) [arXiv:1108.0614 [hep-ph]]; C. Duarah, A. Das and N. N. Singh, Phys. Lett. B **718**, 147 (2012) [arXiv:1207.5225 [hep-ph]]; S. Gollu, K. N. Deepthi and R. Mohanta, arXiv:1303.3393 [hep-ph].

[49] S. Boudjemaa and S. F. King, Phys. Rev. D **79**, 033001 (2009) [arXiv:0808.2782 [hep-ph]]; S. Goswami, S. T. Petcov, S. Ray and W. Rodejohann, Phys. Rev. D **80**, 053013 (2009) [arXiv:0907.2869 [hep-ph]].

[50] D. Aristizabal Sierra, I. de Medeiros Varzielas and E. Houet, Phys. Rev. D **87**, 093009 (2013) [arXiv:1302.6499 [hep-ph]]; R. Dutta, U. Ch, A. K. Giri and N. Sahu, arXiv:1303.3357 [hep-ph]; L. J. Hall and G. G. Ross, arXiv:1303.6962 [hep-ph]; B. Adhikary, A. Ghosal and P. Roy, arXiv:1210.5328 [hep-ph].

[51] G. Altarelli and F. Feruglio, Nucl. Phys. B **741**, 215 (2006) [hep-ph/0512103]; E. Ma and D. Wegman, Phys. Rev. Lett. **107**, 061803 (2011) [arXiv:1106.4269 [hep-ph]]; S. Gupta, A. S. Joshipura and K. M. Patel, Phys. Rev. D **85**, 031903 (2012) [arXiv:1112.6113 [hep-ph]]; S. Dev, R. R. Gautam and L. Singh, Phys. Lett. B **708**, 284 (2012) [arXiv:1201.3755 [hep-ph]]. G. C. Branco, R. Gonzalez Felipe, F. R. Joaquim and H. Serodio, Phys. Rev. D **86**, 076008 (2012) [arXiv:1203.2646 [hep-ph]]; E. Ma, Phys. Lett. B **660**, 505 (2008) [arXiv:0709.0507 [hep-ph]]. F. Plentinger, G. Seidl and W. Winter, JHEP **0804**, 077 (2008) [arXiv:0802.1718 [hep-ph]]; N. Haba, R. Takahashi, M. Tanimoto and K. Yoshioka, Phys. Rev. D **78**, 113002 (2008) [arXiv:0804.4055 [hep-ph]]; S. -F. Ge, D. A. Dicus and W. W. Repko, Phys. Rev. Lett. **108**, 041801 (2012) [arXiv:1108.0964 [hep-ph]]; T. Araki and Y. F. Li, Phys. Rev. D **85**, 065016 (2012) [arXiv:1112.5819 [hep-ph]]; Z. -z. Xing, Chin. Phys. C **36**, 281 (2012) [arXiv:1203.1672 [hep-ph]]; Phys. Lett. B **696**, 232 (2011) [arXiv:1011.2954 [hep-ph]]; P. S. Bhupal Dev, B. Dutta, R. N. Mohapatra and M. Severson, Phys. Rev. D **86**, 035002 (2012).

[52] B. Adhikary, B. Brahmachari, A. Ghosal, E. Ma and M. K. Parida, Phys. Lett. B **638**, 345 (2006) [hep-ph/0603059].

[53] J. Heeck and W. Rodejohann, JHEP **1202**, 094 (2012)

[54] B. Brahmachari and A. Raychaudhuri, Phys. Rev. D **86**, 051302 (2012) [arXiv:1204.5619 [hep-ph]].

[55] Evgeny K. Akhmedov, G.C. Branco, M.N. Rebelo, Phys. Rev. Lett. **84**, 3535 (2000) [hep-ph/9912205].

[56] I. Stancu and D. V. Ahluwalia, Phys. Lett. B **460**, 431 (1999).

[57] C. Jarlskog, Phys. Rev. Lett. **55**, 1039 (1985); O. W. Greenberg, Phys. Rev. D **32**, 1841 (1985).

[58] A. Zee, Phys. Lett. B **93**, 389 (1980), Erratum-ibid. **95**, 461 (1980).

[59] X. -G. He and S. K. Majee, JHEP **1203**, 023 (2012) [arXiv:1111.2293 [hep-ph]].

[60] M. Borah, B. Sharma and M. K. Das, Nucl. Phys. B **885**, 76 (2014) [arXiv:1304.0164 [hep-ph]].

[61] T. Araki, arXiv:1305.0248 [hep-ph]; M. -C. Chen, J. Huang, K. T. Mahanthappa and A. M. Wijangco, arXiv:1307.7711 [hep-ph].

[62] P. Minkowski, Phys. Lett. B **67**, 421 (1977); M. Gell-Mann, P. Ramond and R. Slansky, in *Supergravity*, p. 315, edited by F. van Nieuwenhuizen and D. Freedman, North Holland, Amsterdam, (1979); T. Yanagida, Proc. of the *Workshop on Unified Theory and the Baryon Number of the Universe*, KEK, Japan, (1979); S.L. Glashow, NATO Sci. Ser. B **59**, 687 (1980); R.N. Mohapatra and G. Senjanović, Phys. Rev. D **23**, 165 (1981).

[63] Earlier work on neutrino mass models in which a few elements dominate over others can be traced to F. Vissani, JHEP **9811**, 025 (1998) [hep-ph/9810435]. Models with somewhat similar points of view as those espoused here are E. K. Akhmedov, Phys. Lett. B **467**, 95 (1999) [hep-ph/9909217], and M. Lindner and W. Rodejohann, JHEP **0705**, 089 (2007) [hep-ph/0703171].

[64] For more recent work after the determination of θ_{13} see, for example, B. Brahmachari and A. Raychaudhuri, Phys. Rev. D **86**, 051302 (2012) [arXiv:1204.5619 [hep-ph]]; B. Adhikary, A. Ghosal and P. Roy, Int. J. Mod. Phys. A **28**, 1350118 (2013) arXiv:1210.5328 [hep-ph]; D. Aristizabal Sierra, I. de Medeiros Varzielas and E. Houet, Phys. Rev. D **87**, 093009 (2013) [arXiv:1302.6499 [hep-ph]]; R. Dutta, U. Ch, A. K. Giri and N. Sahu, Int. J. Mod. Phys. A **29**, 1450113 (2014) arXiv:1303.3357 [hep-ph]; L. J. Hall and G. G. Ross, JHEP **1311**, 091 (2013) arXiv:1303.6962 [hep-ph]; T. Araki, PTEP **2013**, 103B02 (2013) arXiv:1305.0248 [hep-ph]; M. -C. Chen, J. Huang, K. T. Mahanthappa and A. M. Wijangco, JHEP **1310**, 112 (2013) [arXiv:1307.7711] [hep-ph]. S. Pramanick and A. Raychaudhuri, Phys. Rev. D **88**, 093009 (2013) [arXiv:1308.1445 [hep-ph]]; B. Brahmachari and P. Roy, JHEP **1502**, 135 (2015) arXiv:1407.5293 [hep-ph].

[65] W. Rodejohann, Int. J. Mod. Phys. E **20**, 1833 (2011) [arXiv:1106.1334 [hep-ph]].

[66] For the present status of θ_{13} see presentations from Double Chooz, RENO, Daya Bay, MINOS/MINOS+ and T2K at Neutrino 2014. https://indico.fnal.gov/conferenceOtherViews.py?view=standard&confId=8022.

[67] For other recent work after the determination of θ_{13} see S. Antusch, S. F. King, C. Luhn and M. Spinrath, Nucl. Phys. B **856**, 328 (2012) [arXiv:1108.4278 [hep-ph]]; B. Adhikary, A. Ghosal and P. Roy, Int. J. Mod. Phys. A **28**, 1350118 (2013) arXiv:1210.5328 [hep-ph]; D. Aristizabal Sierra, I. de Medeiros Varzielas and E. Houet, Phys. Rev. D **87**, 093009 (2013) [arXiv:1302.6499 [hep-ph]]; R. Dutta, U. Ch, A. K. Giri and N. Sahu, Int. J. Mod. Phys. A **29**, 1450113 (2014) arXiv:1303.3357 [hep-ph]; L. J. Hall and G. G. Ross, JHEP **1311**, 091 (2013) arXiv:1303.6962 [hep-ph]; T. Araki, PTEP **2013**, 103B02 (2013) arXiv:1305.0248 [hep-ph]; A. E. Carcamo Hernandez, I. de Medeiros Varzielas, S. G. Kovalenko, H. Päs and I. Schmidt, Phys. Rev. D **88**, 076014 (2013) [arXiv:1307.6499 [hep-ph]]; M. -C. Chen, J. Huang, K. T. Mahanthappa and A. M. Wijangco, JHEP **1310**, 112 (2013) [arXiv:1307.7711] [hep-ph]; B. Brahmachari and P. Roy, JHEP **1502**, 135 (2015) [arXiv:1407.5293 [hep-ph]].

[68] For a review see, for example, S. F. King and C. Luhn, Rept. Prog. Phys. **76**, 056201 (2013) [arXiv:1301.1340 [hep-ph]].

[69] E. Ma and G. Rajasekaran, Phys. Rev. D **64**, 113012 (2001) [hep-ph/0106291].

[70] G. Altarelli and F. Feruglio, Nucl. Phys. B **741**, 215 (2006) [hep-ph/0512103]; H. Ishimori, T. Kobayashi, H. Ohki, Y. Shimizu, H. Okada and M. Tanimoto, Prog. Theor. Phys. Suppl. **183**, 1 (2010) [arXiv:1003.3552 [hep-th]].

[71] For a sampling see, for example, F. Bazzocchi, S. Morisi and M. Picariello, Phys. Lett. B **659**, 628 (2008) [arXiv:0710.2928 [hep-ph]]; E. Ma, Phys. Rev. D **73**, 057304 (2006) [hep-ph/0511133]; P. Ciafaloni, M. Picariello, E. Torrente-Lujan and A. Urbano, Phys. Rev. D **79**, 116010 (2009) [arXiv:0901.2236 [hep-ph]].

[72] E. Ma and D. Wegman, Phys. Rev. Lett. **107**, 061803 (2011) [arXiv:1106.4269 [hep-ph]]; S. Gupta, A. S. Joshipura and K. M. Patel, Phys. Rev. D **85**, 031903 (2012) [arXiv:1112.6113 [hep-ph]]; G. C. Branco, R. G. Felipe, F. R. Joaquim and H. Serodio, arXiv:1203.2646 [hep-ph]; B. Adhikary, B. Brahmachari, A. Ghosal, E. Ma and M. K. Parida, Phys. Lett. B **638**, 345 (2006) [hep-ph/0603059]; B. Karmakar and A. Sil, Phys. Rev. D **91**, 013004 (2015) [arXiv:1407.5826 [hep-ph]]; E. Ma, Phys. Lett. B **752**, 198 (2016) [arXiv:1510.02501 [hep-ph]].

[73] S. K. Kang and M. Tanimoto, Phys. Rev. D **91**, 073010 (2015) [arXiv:1501.07428 [hep-ph]].

[74] J. Barry and W. Rodejohann, Phys. Rev. D **81**, 093002 (2010) [arXiv:1003.2385 [hep-ph]]; J. Barry, W. Rodejohann and H. Zhang, JHEP **1107**, 091 (2011) [arXiv:1105.3911 [hep-ph]]; A. Adulpravitchai and R. Takahashi, JHEP **1109**, 127 (2011) [arXiv:1107.3829 [hep-ph]].

[75] R. Gonzalez Felipe, H. Serodio and J. P. Silva, Phys. Rev. D **87**, 055010 (2013) [arXiv:1302.0861 [hep-ph]].

[76] S. F. King and M. Malinsky, Phys. Lett. B **645**, 351 (2007) [hep-ph/0610250]; E. Ma, H. Sawanaka and M. Tanimoto, Phys. Lett. B **641**, 301 (2006) [hep-ph/0606103]; S. Morisi, M. Nebot, K. M. Patel, E. Peinado and J. W. F. Valle, Phys. Rev. D **88**, 036001 (2013) [arXiv:1303.4394 [hep-ph]]; S. Morisi, E. Peinado, Y. Shimizu and J. W. F. Valle, Phys. Rev. D **84**, 036003 (2011) [arXiv:1104.1633 [hep-ph]].

[77] A. Degee, I. P. Ivanov and V. Keus, JHEP **1302**, 125 (2013) [arXiv:1211.4989 [hep-ph]].

[78] R. Gonzalez Felipe, H. Serodio and J. P. Silva, Phys. Rev. D **88**, 015015 (2013) [arXiv:1304.3468 [hep-ph]].

[79] See, for example, P. F. Harrison and W. G. Scott, Phys. Lett. B **557**, 76 (2003) [hep-ph/0302025].

[80] S. L. Chen, M. Frigerio and E. Ma, Phys. Rev. D **70**, 073008 (2004) Erratum: [Phys. Rev. D **70**, 079905 (2004)] [hep-ph/0404084]; E. Ma, Phys. Rev. D **61**, 033012 (2000) [hep-ph/9909249].

[81] A sampling is W. Grimus and L. Lavoura, JHEP **0508**, 013 (2005) [hep-ph/0504153]; R. Jora, J. Schechter and M. Naeem Shahid, Phys. Rev. D **80**, 093007 (2009) Erratum: [Phys. Rev. D **82**, 079902 (2010)] [arXiv:0909.4414 [hep-ph]]; Z. z. Xing, D. Yang and S. Zhou, Phys. Lett. B **690**, 304 (2010) [arXiv:1004.4234 [hep-ph]]; T. Teshima and Y. Okumura, Phys. Rev. D **84**, 016003 (2011) [arXiv:1103.6127 [hep-ph]]; S. Dev, S. Gupta and R. R. Gautam, Phys. Lett. B **702**, 28 (2011) [arXiv:1106.3873 [hep-ph]]; S. Zhou, Phys. Lett. B **704**, 291 (2011) [arXiv:1106.4808 [hep-ph]]; R. Jora, J. Schechter and M. N. Shahid, Int. J. Mod. Phys. A **28**, 1350028 (2013) [arXiv:1210.6755 [hep-ph]]; H. B. Benaoum, Phys. Rev. D **87**, 073010 (2013) [arXiv:1302.0950 [hep-ph]].

[82] S. Morisi, hep-ph/0605167; M. Tanimoto and T. Yanagida, Phys. Lett. B **633**, 567 (2006) [hep-ph/0511336]; S. Gupta, C. S. Kim and P. Sharma, Phys. Lett. B **740**, 353 (2015) [arXiv:1408.0172 [hep-ph]].

[83] A. E. C. Hernandez, E. C. Mur and R. Martinez, Phys. Rev. D **90**, 073001 (2014) [arXiv:1407.5217 [hep-ph]]; V. V. Vien and H. N. Long, Zh. Eksp. Teor. Fiz. **145**, 991 (2014) J. Exp. Theor. Phys. **118**, 869 (2014) [arXiv:1404.6119 [hep-ph]]; E. Ma and R. Srivastava, Phys. Lett. B **741**, 217 (2015) [arXiv:1411.5042 [hep-ph]]; D. Meloni, S. Morisi and E. Peinado,

J. Phys. G **38**, 015003 (2011) [arXiv:1005.3482 [hep-ph]]; A. E. Carcamo Hernandez, I. de Medeiros Varzielas and E. Schumacher, Phys. Rev. D **93**, 016003 (2016) [arXiv:1509.02083 [hep-ph]]; A. E. Carcamo Hernandez, I. de Medeiros Varzielas and N. A. Neill, Phys. Rev. D **94**, 033011 (2016) [arXiv:1511.07420 [hep-ph]]; D. Das, U. K. Dey and P. B. Pal, Phys. Lett. B **753**, 315 (2016) [arXiv:1507.06509 [hep-ph]]; R. N. Mohapatra, S. Nasri and H. B. Yu, Phys. Lett. B **639**, 318 (2006) [hep-ph/0605020].

[84] F. Feruglio and Y. Lin, Nucl. Phys. B **800**, 77 (2008) [arXiv:0712.1528 [hep-ph]].

[85] J. Kubo, A. Mondragon, M. Mondragon and E. Rodriguez-Jauregui, Prog. Theor. Phys. **109**, 795 (2003) Erratum: [Prog. Theor. Phys. **114**, 287 (2005)] [hep-ph/0302196]; S. Kaneko, H. Sawanaka, T. Shingai, M. Tanimoto and K. Yoshioka, Prog. Theor. Phys. **117**, 161 (2007) [hep-ph/0609220].

[86] See, for example, G. Drexlin, V. Hannen, S. Mertens and C. Weinheimer, Adv. High Energy Phys. **2013**, 293986 (2013) [arXiv:1307.0101 [physics.ins-det]].

List of Publications

Journal Publications:

1. **Smallness of θ_{13} and the size of the solar mass splitting: Are they related?**,
   Soumita Pramanick and Amitava Raychaudhuri,
   Phys. Rev. D **88**, 093009 (2013), [arXiv:1308.1445 [hep-ph]].

2. **Relating the small parameters of neutrino oscillations**,
   Soumita Pramanick and Amitava Raychaudhuri,
   Phys. Lett. B **746**, 237 (2015), [arXiv:1411.0320 [hep-ph]].

3. **Relating small neutrino masses and mixing**,
   Soumita Pramanick and Amitava Raychaudhuri,
   Int. J. Mod. Phys. A **30**, 1530036 (2015), [arXiv:1504.01555 [hep-ph]].

4. **$A4$-based seesaw model for realistic neutrino masses and mixing**,
   Soumita Pramanick and Amitava Raychaudhuri,
   Phys. Rev. D **93**, 033007 (2016), [arXiv:1508.02330 [hep-ph]].

5. **Neutrino mass model with S_3 symmetry and seesaw interplay**,
   Soumita Pramanick and Amitava Raychaudhuri,
   Phys. Rev. D **94**, 115028 (2016), [arXiv:1609.06103 [hep-ph]].

Conference Publications:

1. **Relating Small Neutrino Masses and Mixing**,
   Soumita Pramanick and Amitava Raychaudhuri,
   Adv. Ser. Direct. High Energy Phys. **25**, 59 (2015).

2. **Is the size of θ_{13} related to the smallness of the solar mass splitting?**,
   Soumita Pramanick and Amitava Raychaudhuri,
   Pramana **86**, 407 (2016).

3. **Is It All in a Perturbation?**,
   Soumita Pramanick and Amitava Raychaudhuri,
   Springer Proc. Phys. **174**, 395 (2016).